Tunable Delivery of siRNA from a Biodegradable Scaffold for Regenerative Medicine

By

Christopher Edward Nelson

Dissertation

Submitted to the Faculty of the

Graduate School of Vanderbilt University

in partial fulfillment of the requirements

for the degree of

DOCTOR OF PHILOSOPHY

in

Biomedical Engineering

May, 2014

Nashville, Tennessee

Approved:

Craig L. Duvall, Ph.D.

Todd D. Giorgio, Ph.D.

Hak-Joon Sung, Ph.D.

Scott A. Gulecher, Ph.D.

Jeffrey M. Davidson, Ph.D.

This work is dedicated to my wife Heather Marie Nelson

whose patience and support made this work possible.

Acknowledgments

I would like to thank first, my Ph.D. advisor, Professor Craig Duvall for the guidance he has provided in the development of this project and my career. I would also like to thank the members of my committee, Professors Jeffrey Davidson, Todd Giorgio, Scott Guelcher, and Hak-Joon Sung for their insight, experience, and time. I would like to thank my fellow graduate students and the undergraduate students who contributed to the research and supported the laboratory that we shared. I would also like to thank Garrett Rettig (IDT) for advice on designing dsiRNAs.

I would like to acknowledge the funding agencies for the financial support including a Vanderbilt Discovery Grant, NIH R21EB012750, and NIH 1R01AR056138-01A2. Finally, I would also like to acknowledge the members of the core laboratories for their support and advice: Confocal Imaging was performed using a Zeiss LSM 510 Inverted Confocal Microscope in part through the use of the VUMC Cell Imaging Shared Resources, (supported by NIH Grants CA68485, DK20593, DK58404, HD15052, DK59637, and Ey008126). Dynamic light scattering, TEM, and SEM were conducted through the use of the core facilities of the Vanderbilt Institute of Nanoscale Sciences and Engineering (VINSE). qRT-PCR was conducted at the Vanderbilt University Molecular Cell Biology Resource Core. Fluorescence and bioluminescence readings were performed through the Vanderbilt University Institute for Imaging Science (VUIIS). Histology sections were prepared through the use of Translation Pathology Shared Resource (TPSR).

Table of Contents

Page

List of Tables

List of Figures

List of Equations

Chapter 1

Introduction and Significance

Text partially adapted from:

Nelson CE, Gupta MK, Adolph EJ, Guelcher SA, Duvall CL. siRNA Delivery from an Injectable Scaffold for Wound Therapy. Advances in Wound Care. 2013; 2(3):93-99

1.1 Motivation

Impaired wound healing is a significant healthcare problem, and the primary risk group is patients with diabetes, a disease that is a prevalent and rapidly growing public health issue in the United States and worldwide. Approximately 8% of individuals the US or 23.6 million people have diabetes [1]. A global epidemic as well, many developed countries and developing countries alike are seeing dramatic increases in the prevalence of diabetes, and these increases threaten to reverse economic gains in these countries [2]. Furthermore, the incidence of diabetes has tripled from 1980-2006 in the US and the Center for Disease Control predicts that if this trend continues, one in three of today's children will develop diabetes in their lifetime [3].

Patients with diabetes are more susceptible to impaired wound healing which results in 25% of diabetics developing chronic ulcers [4]. For this reason, diabetics suffer increased morbidity and mortality having 10 times the rate of lower-limb amputation of non-diabetics [1]. Morbidity and mortality after lower-limb amputation is high with about one quarter receiving additional amputations, and about one third die after one year [5].

In addition to the morbidity and mortality associated with chronic wounds, treatment is now a $25 billion annual cost to health care and is been described as a "snowballing threat to public health", where the incidence of chronic wounds will grow with the increasing prevalence of comorbidities [4]. These statistics highlight the deleterious impact of diabetes in the United States today and clearly define a tremendous clinical need for improved therapeutic strategies to reduce wound related morbidity and mortality in diabetic patients.

1.2 Molecular Basis for Non-Healing Wounds

Diabetes mellitus (type 2) is characterized by insulin resistance and will result in periods of sustained hyperglycemia. Currently, diabetes is managed with lifestyle modification followed by administration of pharmaceuticals including insulin, metformin, and others which can improve the quality of life for these patients. However, in many patients, unmanaged hyperglycemia leads to a number of pathologies, notably cardiovascular defects and poor collateral vessel formation [6]. As a result, simple skin wounds and pressure ulcers may develop into chronic non-healing wounds. Procedures have been developed to improve wound healing and decrease the associated morbidity (good wound care). Biologic drugs have recently been sought to correct the molecular dysfunction including platelet derived growth factor (PDGF in Regranex®); however, 50% of wounds still remain unclosed [7].

Recent evidence points to an impairment in the activation of HIF-1α as a result of prolonged hyperglycemia [6] and correcting this abnormality may restore normal wound healing. Prolyl hydroxylase domain protein 2 (PHD2) is a negative regulator of HIF-1α [8] and represents a logical target for improving HIF-1α activity, stability, and resulting angiogenesis and tissue regeneration [9]. This is discussed in more detail in section 2.7.

As an engineering approach for inhibiting PHD2, small molecule inhibitors, antisense oligonucleotides (ODNs), and small interfering RNA (siRNA) have been used. Small molecule inhibitors have shown some promise and are a good proof of principle, however, lack specificity for PHDs or specific isoforms of PHD and as a result, have undesired non-target effects [10]. ODNs, and siRNA are much more specific and can be engineered to have a local effect instead of a widespread systemic effect. From these antisense approaches, siRNA is the most potent capable of 100-1000 times more silencing than ODNs [11]. This motivates the use of PHD2 siRNA as a molecular based therapy for treating chronic wounds.

1.3 siRNA as a Molecular Therapy for Wound Healing

Since the discovery of RNA interference in gene regulation, a large volume of research has been directed into rapidly developing siRNA for clinical use [12]. siRNA are short (~21-22 base pairs) double stranded RNA, where the guide strand of the molecule is loaded onto the RNA induced silencing complex (RISC), a cohort of proteins intrinsic to mammalian cells. The activated RISC identifies the targeted mRNA through complementary base pairing and cleaves the mRNA. The guide strand and activated RISC are conserved and may reinitiate degradation of additional mRNA molecules [13], making the process catalytic and thus more potent than stoichiometric (i.e. protein or small molecule) inhibitors. These favorable properties of siRNA have led to rapid advancement into clinical tests for a variety of conditions including respiratory syncytial virus infection, macular degeneration, hepatitis B, renal failure, macular oedema, pachyonychia congenital, and solid tumors [14-16].

siRNA is regarded to have untapped clinical potential, but one of the major challenges to harnessing RNA interference pharmaceutically is efficient cytoplasmic delivery of the siRNA biomacromolecules into target cells. “Naked” siRNA has a very short half-life *in vivo* due to rapid degradation by nucleases and clearance through kidney filtration. siRNA is also relatively large in molecular weight, anionic, and polar, making it impermeable to cell membranes. This is problematic for initial cellular internalization and for escape from endo-lysosomal vesicles following uptake by endocytosis. Thus, siRNA carriers are required to package and protect the siRNA and deliver siRNA into the cytoplasm of the cell where the RISC machinery is located. Polycations have been heavily studied as an approach to package and protect siRNA and enable endosome escape via the proton sponge effect. However, most polycations are characterized by cytotoxicity and instability *in vivo*, and recent efforts have aimed to overcome these limitations.

Although siRNA activity is catalytic, it does have a finite half-life in the cell. Previous reports generally note maximum silencing at around two days post-transfection [17] with normal gene expression restored by approximately one week in rapidly dividing cells [18]. One approach

to extend silencing may be to achieve sustained, local release from scaffolds injected or transplanted onto the wound. Mostly natural materials such as alginate, collagen, and agarose have been pursued for biomaterial-based siRNA delivery to this point [19-22]. Recently, key proof-of-concept studies were published describing effective topical siRNA gene silencing in vivo using agarose scaffolds loaded with siRNA packaged into the commercial reagent Lipofectamine 2000. This particular approach represents a significant breakthrough, though it did suffer from the potential limitation of siRNA diffusing from the scaffold in a relatively rapid "burst" release that required removal and re-application of siRNA-loaded scaffolds to achieve better and more sustained siRNA activity [21, 22]. It may be possible to achieve more optimal wound therapies with delivery systems that integrate efficient, nontoxic siRNA carriers into an injectable delivery matrix that can achieve sustained and tunable rates of siRNA release for greater than 1 week.

1.4 Approach

Our work has focused on the combination of two complementary biomaterials that enable efficient, sustained siRNA intracellular delivery to skin wounds (**Fig. 1.1**).The first class is a pH-responsive micelle, referred to here as the smart polymer nanoparticle (NP). The NP is capable of electrostatic loading and nuclease protection of siRNA in addition to pH-dependent membrane disruptive activity that can mediate escape from endo-lysosomal vesicles. This NP is self-assembled from a reversible addition fragmentation chain transfer (RAFT) synthesized diblock copolymer recently described [23]. This diblock polymer (see structure in **Fig. 1.1A)** is composed of siRNA condensing block consisting of 2-dimethylaminoethyl methacrylate (DMAEMA). This block is the relatively hydrophilic block and forms the corona of the micelle. It has pendant tertiary amines that are approximately 50% protonated at physiologic pH, which enables electrostatic loading of siRNA into the "shell" of the si-NP (**Fig. 1.1B**). The second block is a more hydrophobic and approximately charge neutral terpolymer block. This terpolymer contains approximately equimolar quantities of 2-propyl acrylic acid (PAA) and DMAEMA in order to maintain charge

neutrality at physiologic pH. Butyl methacrylate (BMA) is the third monomer and is incorporated to increase the hydrophobic character and drive micelle self-assembly in aqueous solution. Importantly, both the PAA and DMAEMA monomers are pH-responsive (i.e. environmental pH dictates their protonation state and affects their physical properties), and it is this characteristic that mediates escape from endo-lysosomes upon acidification of these vesicles following cellular internalization of the carrier (**Fig. 1.1D**).

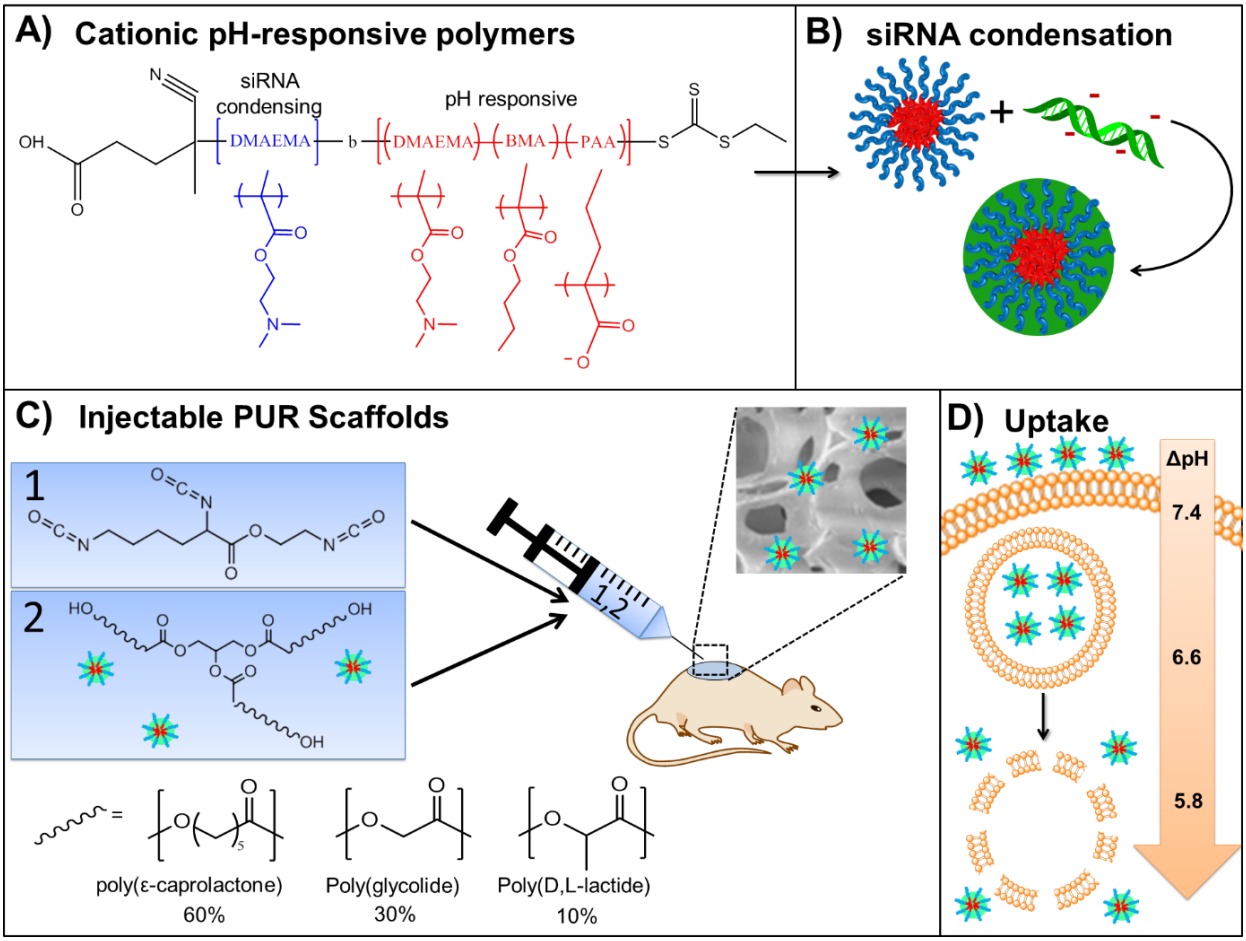

Figure 1.1 – **Schematic illustrating the approach used in this study. A)** RAFT-synthesized diblock co-polymer with the siRNA condensing block shown in blue and the pH responsive block in red **B)** In aqueous solutions, the diblock copolymer self-assembles into micellar nanoparticles with a positive surface charge that can be used to electrostatically condense siRNA. **C)** Lyophilized si-NPs are mixed into the polyol component and then added to the LTI and water to form a porous PUR scaffold containing embedded si-NPs. **D)** The si-NPs can diffuse out of the PUR scaffold, and, upon release, si-NPs can be internalized and efficiently delivered in a bioactive form into the cytoplasm of cells.

The second biomaterial is an injectable polyurethane (PUR) scaffold composed of a polyol component that is 60% poly(ε-caprolactone), 30% poly(glycolide), and 10% poly(D,L-lactide), and a hardening component, lysine triisocyanate (LTI). The polyol and the LTI react to form urethane bonds, and water is added to the reaction to produce CO_2 that creates scaffold porosity (Figure 1C). PUR-based scaffolds are desirable because components can be mixed and injected into a wound site where it quickly cures *in situ*, thus enhancing its flexibility and potential for clinical use. Also, the PUR adheres to underlying tissue, does not elicit significant inflammation [24], and biodegrades at tunable rates into biocompatible products [25]. Furthermore, the scaffold morphology is highly porous, which allows for ingrowth of granulation tissue and promotes tissue remodeling. The PURs have been previously used for controlled delivery of growth factors but have not been previously employed for release of carriers for intracellular-acting biologic drugs.

1.5 Innovation

Currently, there are no commonly utilized clinical applications of intracellular-acting biomacro-molecular drugs (growth factors act on extracellular receptors). The delivery requirements for intracellular-acting biomolecules like siRNA are more rigorous because they cannot cross cellular membranes, and when endocytosed, the predominant fate is enzymatic degradation in lysosomes or recycling and extracellular clearance. Here, we describe a “smart” polymer carrier that “recognizes” environmental changes to become membrane disruptive in the lower pH environment of endosomes. This innovative approach to gene inhibition may enable a new level of pharmaceutical breadth and specificity that would overcome many of the shortcomings of small molecule drugs and also allow manipulation of intracellular targets that were previously considered “undruggable”. The majority of recent applications of siRNA have focused on *in vitro* validation, systemic *in vivo* delivery, or *in vivo* applications where siRNA formulations have been injected locally in saline with no regard for persistence of sustained bioactivity (i.e. intraocular or intratumoral injection, lung inhalation). The use of siRNA for regenerative applications could be

tremendously enhanced by means of sustained, local delivery from scaffolds that serve as porous tissue templates. The innovative combination of si-NPs and PUR scaffolds provides a porous scaffold template for cell in-growth, ease of delivery for clinical applications (injectability), multiple levels of tunability for release kinetics, and ultimately, the ability to optimize siRNA activity for specific target genes and pathological applications. Finally, targeting PHD2 to increase angiogenesis and improve wound healing in tissue regenerative scaffolds is a novel and potentially a highly rewarding pursuit.

1.6 Specific Aims

The central hypothesis of this study is that efficient and temporally controlled administration of siRNA can be used to improve tissue regeneration, specifically through targeting PHD2. This hypothesis will be evaluated through the completion of the following four specific aims:

Specific Aim 1: Synthesize and characterize a novel siRNA delivery platform *in vitro*: PUR based delivery of endosomolytic NPs carrying siRNA will be validated *in vitro* for controlled release and knockdown efficiency.

Specific Aim 2: Asses the *in vivo* activity and biocompatibility of the siRNA delivery platform: The delivery platform will be validated *in vivo* using subcutaneous implants in mice. Dicer substrate siRNA against model genes luciferase and cyclophilin B (PPIB) will be used to optimize and validate the delivery system *in vivo.* The result of this aim will be a thoroughly validated tissue-engineering scaffold based siRNA delivery platform with precise temporal control for gene silencing *in vivo*.

Specific Aim 3: Improve *in vivo* angiogenesis through the delivery of siRNA against PHD2: Validated dicer substrate siRNA against PHD2 will be delivered using the validated platform developed in Specific Aim 2. Therapeutic response in subcutaneous implants will be evaluated by monitoring gene expression with qRT-PCR. Blood vessel growth will be evaluated post-mortem with microCT and immunohistochemistry.

Specific Aim 4: Investigate sustained PHD2 knockdown for improved wound healing in diabetic rats: The therapeutic effect of PHD2 silencing will be tested with polyester urethanes implanted in excisional wounds in streptozotocin (STZ) induced diabetic rats. Gene expression will be monitored by qRT-PCR and blood vessel growth will be evaluated by histology.

1.7 Outline

Herein, a thorough description of the development of a powerful platform for temporally controlled local gene silencing is given. Chapter 2 will provide a concise and targeted review of the previous work in local RNA delivery. Chapter 3 will detail the initial development of the platform and *in vitro* confirmation of bioactivity and biocompatibility. Chapter 4 will describe the *in vivo* testing of the platform and application of the platform for PHD2 gene silencing. In Chapter 5, an additional application of siRNA will be considered utilizing endosomolytic NPs for intravenous gene silencing. Finally, a summary with regard to broader impacts, challenges, and continuing work will conclude this writing. Each of the research chapters (3-5) will contain a concise introduction and methods with their own discussion and conclusions.

Chapter 2

Background: Local RNAi for Regenerative Medicine

Text partially adapted from:

Li HM*, Nelson CE*, Evans BC*, Duvall CL. "Delivery of Intracellular-acting Biologics in Pro-Apoptotic Therapies". For a special issue entitled "Development of drugs interfering with apoptosis" in the journal Current Pharmaceutical Design. 2011; 17(3): 293-319. *Equally Contributing 1st authors.

Nelson CE, Gupta MK, Adolph EJ, Guelcher SA, Duvall CL. siRNA Delivery from an Injectable Scaffold for Wound Therapy. Advances in Wound Care. 2013; 2(3):93-99

Nelson CE, Gulecher SA, Duvall CL. Local RNAi for Regenerative Medicine. In preparation.

2.1 Introduction

Since the discovery of RNA interference (RNAi) 16 years ago, researchers have rushed to develop therapeutics to treat a broad range of conditions by powerfully and specifically down regulating target genes. Regenerative medicine is among the diverse fields of research that RNAi may benefit by allowing precise control over genes that prohibit tissue regeneration. The clinical potential of successful strategies includes chronic wound healing, critical bone defect formation, organ/tissue replacement, and others. The primary barrier for utilizing RNAi for any application is the extraordinary delivery barriers that prevent RNAi therapies from reaching the target location (i.e. the cytoplasm of target cells). In addition to the delivery barriers of intravenous RNAi applications, additional considerations should be taken for regenerative medicine including local delivery, sustaining the delivery to target tissues, providing biocompatible and tissue inductive materials for regrowth, and controlling spatial and temporal availability of small interfering RNA (siRNA).

This review is focused on the material development for local administration of therapeutic siRNA for regenerative medicine. The review will begin with a description of siRNA and its mechanism. Strategies for siRNA modification, intracellular delivery, and sustained local delivery

will be described with discussion on advantages and disadvantages of the systems. Finally, gene targets of interest will be discussed for improving regenerative medicine.

A rapidly growing area of research, RNAi has several very thorough recent reviews on topics related to this review. The reader is referred elsewhere on the following subjects: other antisense strategies in regenerative medicine [26], molecular modifications [27], detailed reviews on materials for intracellular delivery [27, 28], targeted delivery [29], siRNA-conjugate systems [30], physical methods for local/topical delivery [31], and finally, a most recent clinical update [28].

2.2 SIRNA Discovery and Mechanism

Controlled manipulation of gene expression using RNAi has been rigorously pursued for almost two decades now, and thorough elucidation of this mechanism combined with recent breakthroughs in RNA delivery technologies have RNAi poised to make a tremendous clinical impact. RNAi is an especially promising therapeutic approach for inhibition of genes related to tissue regeneration (inflammation, cell cycle control, etc), or other relevant targets because it allows for optimal therapeutic specificity and breadth (i.e., in theory, any desired gene target can be efficiently silenced). The initial discovery of RNAi came in 1990 when Napoli *et al*. observed an unexpected reduction in expression when delivering RNA in an attempt to overexpress chalcone synthase in Petunias [32]. Others elucidated and applied this finding by delivering antisense oligodeoxynucleotides (ODN), complementary sequences of DNA, which yielded modest reduction in gene expression in C. elegans [33]. In 1998, Fire *et al*. showed that intracellular-acting double stranded RNA (dsRNA) was more effective than either the sense or anti-sense strand alone [12]. In fact, dsRNA has been shown to be 100 to 1000 times more effective than ODNs due to a longer half-life and greater potency [11]. Over the next few years, researchers proved that endogenous RNAi, known as microRNA (miRNA), exists and that it serves as a natural, post-transcriptional controller of gene expression where cellular machinery selectively degrades complementary mRNA in an enzymatic manner [13]. The elucidation of

similar machinery for RNAi in mammalian cells further heightened the interest in therapeutically harnessing these pathways [34].

Since these early findings, the mechanisms of ODN and that of miRNA, dsRNA, siRNA, and short hairpin RNA (shRNA) have been more clearly elucidated (**Fig. 2.1**). Single-stranded antisense ODN are thought to function by multiple mechanisms including translational arrest due to steric blockage of ribosomes by ODN-mRNA Watson-Crick base pairing and also through RNase-H-mediated cleavage of both the ODN and mRNA strands [35]. Endogenous RNAi molecules in the form of miRNA enter the cytoplasm after transcription, or alternatively, functionally-similar dsRNA can be exogenously delivered. shRNA that more closely mimic the structure of endogenous miRNA have also been exogenously delivered [36]. In each of these cases, the RNase III family enzyme Dicer cleaves the miRNA/dsRNA/shRNA to produce guide RNA, more commonly known as siRNA. siRNA are double-stranded RNA 19-21 base pairs in length with 3' nucleotide overhangs [37], these molecules can assemble into the RNA induced silencing complex (RISC), a nuclease complex that degrades complementary mRNA in a sequence specific, enzymatic manner [13]. Traditional siRNAs have been 19-21 nucleotides that bypass the initial dicer processing and are loaded into the RISC. Recent work has suggested that dsRNAs that contain a 27mer antisense strand and a 25mer sense strand may have an increased potency of 10X or more when compared with their 21mer siRNA counterparts [38]. This "dicer substrate siRNA" (DsiRNA) is now being used as a more potent siRNA to lower the required dose which minimizes dose-dependent off target effects. Further, siRNA prediction tools are improving through the use of predicative algorithms and automated neural networks [27].

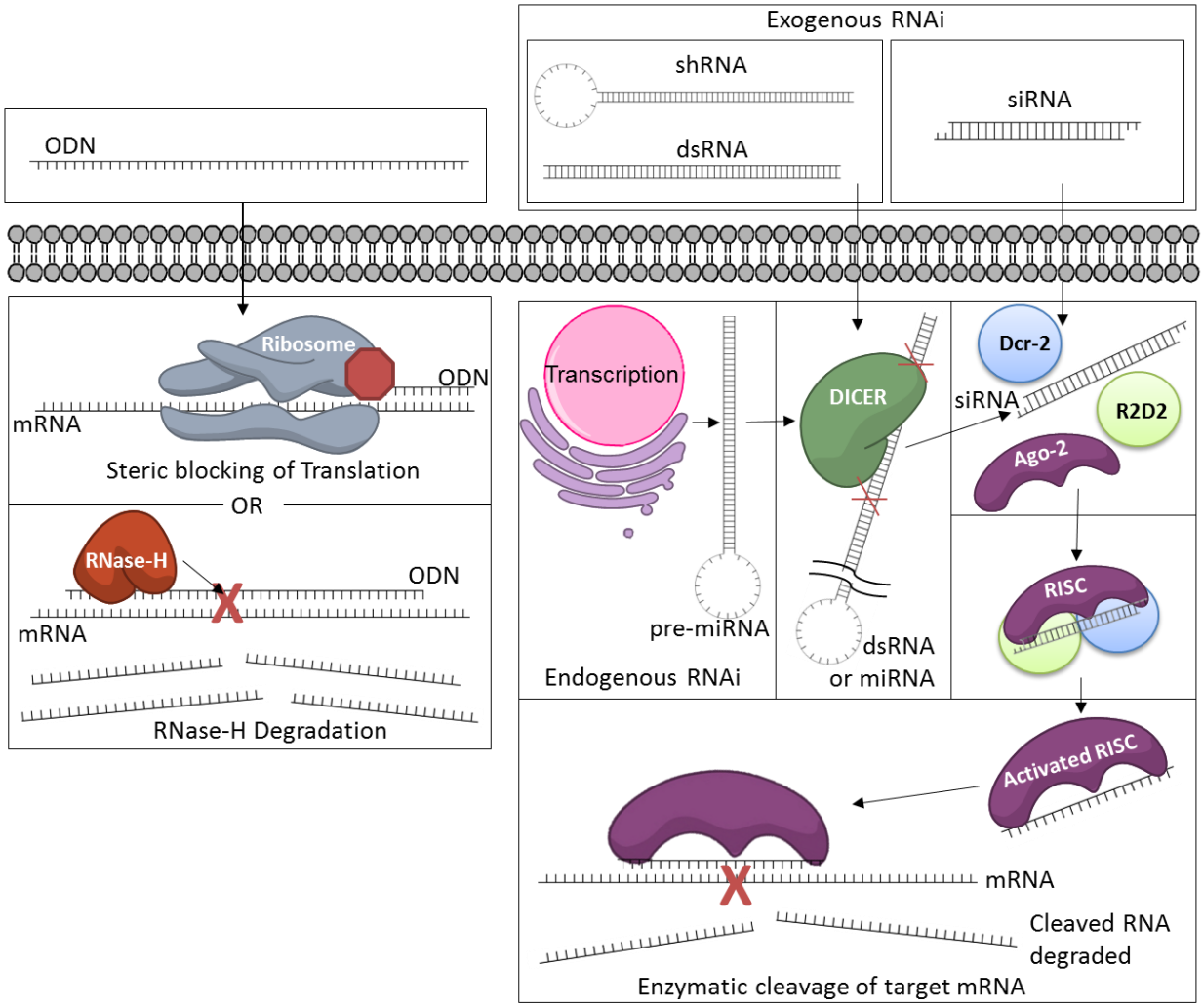

Figure 2.1. Mechanisms of RNA interference (A) ODN silencing is believed to be induced by stericly blocking translation through hybridization with mRNA and RNAse-H mediated degradation of both the ODN and mRNA (B) Proposed mechanisms for RNA interference by miRNA, shRNA, dsRNA, and siRNA. Endogenous miRNA, which is made transcriptionally, and exogenously delivered shRNA/dsRNA must all be first processed into siRNA, double stranded RNA molecules around 20 base pairs in size. siRNA is loaded onto the RISC complex and mediates degradation of mRNA complementary to the antisense siRNA strand. For each type of therapeutic RNAi, the exogenous RNA must reach the cytoplasm to interact with mRNA and other intracellular machinery required for gene silencing.

Because of the tremendous promise of siRNA to be used therapeutically (i.e., for silencing pro-inflammatory genes in wound healing), RNAi has been pursued rigorously in many applications. The main issue with using RNAi clinically is with the delivery barriers that must be addressed between the initial application of siRNA (either intravenously or topically) and the target RISC machinery.

2.3 Barriers

Based on the mechanism of siRNA in **Fig. 2.1**, cytoplasmic delivery is required for RNAi to occur. In order to achieve cytoplasmic delivery, an array of barriers must be navigated that depends on the delivery route and the target tissue of interest. As a result, clinical translation of siRNA rests in solving the delivery barriers.

Delivery Barriers for Systemic Administration

Systemic administration of siRNA presents several significant delivery barriers that must be addressed for clinical translation. These barriers are summarized in **Fig 2.2**. (1) siRNA is rapidly degraded in the *in vivo* environment by nucleases [39], and carriers may be opsonized or cleared from the circulation [40, 41]. (2) siRNA or carriers must exit the vasculature at the target tissue either by the EPR in tumors or through some active targeting mechanism. (3) siRNA or carriers must provide some active uptake mechanism to facilitate uptake as siRNA does not readily diffuse across cellular membranes. (4) In many cases, siRNA or carriers are taken into endosomes leading to lysosomes for degradation or exocytosed (5) If endocytosed, siRNA or carriers must provide some endosome escape mechanism to reach the cytoplasm. (6) Finally, siRNA must be released from the carrier in the cytoplasm to begin RNAi [42-45]. Stability of biologics is a primary concern considering the harsh environment encountered *in vivo*.

Delivery Barriers for Local Administration and Regenerative Medicine

By delivering siRNA with local drug delivery depots, some of the drug delivery barriers of systemic application are avoided including stabilization for the intravenous environment and tissue targeting. However, in some local delivery applications, the skin or other tissues may present an additional barrier to delivery and must be addressed. The delivery barriers associated with topical delivery are discussed in detail by elsewhere [31] with regards to delivery to the skin, lung, eye, nervous system, digestive system, and vagina. For regenerative medicine applications,

the target cells are ideally in direct contact with the material. For example, in wound healing applications the skin barrier is absent and infiltrating cells are the main target.

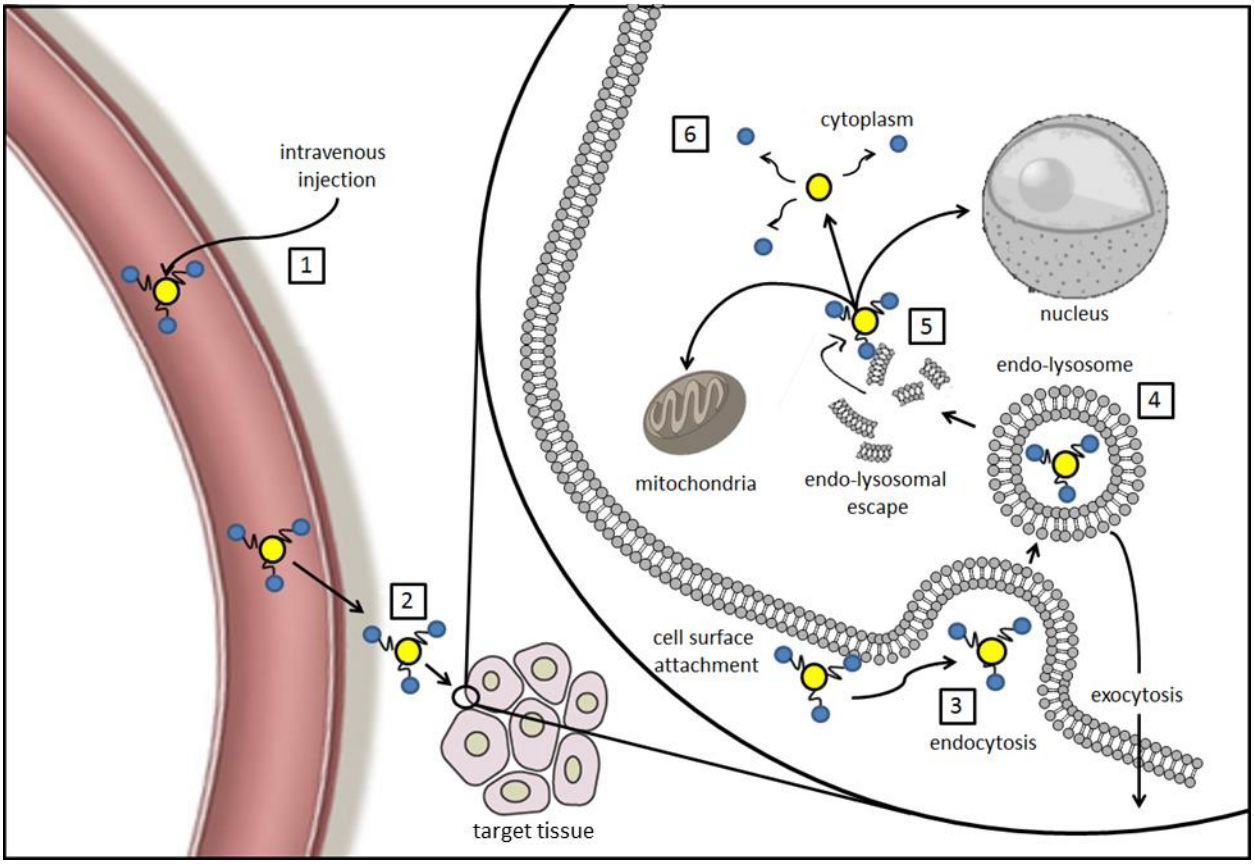

Figure 2.2. Intracellular delivery barriers. 1) Upon entering systemic circulation, the drug formulation must protect the biomacromolecule from enzymatic degradation and serum protein destabilization and/or opsonization. 2) Drug circulation half-life needs to be long enough such that the drug persists in the vasculature until it accumulates (through specific targeting or nonspecifically thorough the enhanced permeation and retention effect) in the target tissue. 3) The drug must interact with the cell membrane to initiate internalization, which can result in uptake into an endosomal (or pinocytic) vesicle. 4) If no endosomal escape mechanism is present, the drug can be degraded in the lysosome, remain in the late endosome, or undergo trafficking for exocytosis. 5) If the drug is able to escape the endo-lysosomal pathway, it is released where it can diffuse to molecular targets in the cytoplasm. 6) If attached to a carrier or loaded within a nanoparticle such as a liposome, polyplex, etc., the drug may need to be released from this formulation to become bioavailable.

Another consideration for local administration of siRNA is to create a drug delivery depot for sustained release. Though the enzymatic action of siRNA generates potent gene silencing, the activity has a finite half-life. In rapidly dividing cells (e.g. a healing wound), a maximum silencing effect is noted near two days post-transfection [17] with gene silencing nearly absent in

one week [18]. It may be beneficial to create platforms with tunable release profiles in order to allow gene silencing platforms to be tailored to specific pathological applications.

Finally, local drug delivery depots must be biocompatible, non-toxic, and have well-characterized degradation and clearance mechanisms. To serve in a regenerative medicine capacity, it may also be beneficial for the platform to serve as a tissue template for *de novo* tissue formation [46]. A careful balance of the above considerations may create the idealized platform for regenerative medicine.

2.4 siRNA biochemistry

A major effort in adapting siRNA for therapeutic use is the advanced chemistry and modifications to create more stable siRNAs, bioconjugates of siRNA, or novel nucleic acid nanoparticles. This body of work may result in siRNAs that are more stable *in vivo,* provide intrinsic cellular uptake, and in some cases, may provide a means for using no additional carrier. Some of the most recent and notable examples are outlined below.

siRNA Design

Many of the characteristics of idealized siRNA sequences were initially identified by Elbashir and authors. For example they discovered that duplexes made of 21 base pairs with 3' overhangs two nucleotides in length are optimal, and they also determined that mismatches between the antisense siRNA and mRNA in the middle of the siRNA can abolish activity, while the 3' nucleotide has little effect on gene silencing [34, 47, 48]. Later work would identify that double stranded RNAs with a 25-mer sense and 27-mer antisense to be more ideal for gene silencing [27]. Reynolds and co-authors more recently completed a systematic, mass screening of siRNA sequences for two genes and identified low guanine/cytidine content, a low internal stability at the 3' end of the sense strand, and lack of inverted repeats as desirable siRNA characteristics in addition to uncovering sense strand base preferences at specific sites in the

sequence [49]. siRNA sequence optimization is a rapidly changing field and is covered in detail elsewhere [50, 51]. One common approach to silencing a new gene is to acquire several siRNA sequences that satisfy these design criteria and that target different loci on the mRNA. The sequences can be either pooled together or screened individually to identify an optimal sequence for further study. Off-target gene silencing and nonspecific immune responses mediated through toll-like receptors (TLRs) can also be triggered by suboptimal siRNA sequences, and instances have occurred where nonspecific effects have been misinterpreted as siRNA-driven phenotype modification resulting from silencing of a target gene [52]. However, siRNA therapeutic potential remains strong as chemical modifications and new rules for sequence identification are progressing in-step with the iterative improvements in delivery approaches. In preclinical studies, testing for immune activation and verifying phenotypes independently using different siRNA sequences against the gene of interest are desirable standards of practice [53].

Chemical Modifications

A major hurdle for the use of siRNA *in vivo* is the threat of nuclease degradation. siRNA carriers may protect siRNA from nucleases but for unprotected siRNA, modification patterns have been used to improve stability. The modifications are usually on the 2' position including 2'-O-methyl (2OME), 2'deoxy-2'-floro, 2'-O-(2-methoxyethyl), 2'-deoxoy-2'-floro-β-D-arabinonucleotide (FANA), and a methylene bridge connecting the 2'-O with the 4'-C (locked nucleic acid) [30]. One of the most common modifications is a 2'-O-Methyl modification, which is a naturally occurring nucleotide [27] that improves duplex stability (T_m) and nuclease resistance without hindering activity, causing toxicity, or being immunostimulatory [54].

As mentioned above, one potential concern is that the intracellular delivery of exogenous dsRNAs or siRNAs may lead to the recognition by TLRs. TLRs recognize the molecular pattern of dsRNA and respond as a defense mechanism toward a viral genome. This effect could result in pathological inflammation in clinical trials and has also led to the misinterpretation of pre-clinical

studies related to viral repression, oncology, angiogenesis, and inflammation [55]. TLRs recognition is thought to be sequence dependent [56] and carefully selected siRNA sequences may avoid recognition by TLRs. Further, chemical modification on the backbone of the dsRNA may eliminate TLR activation while having negligible effects on the potency of gene silencing [55]. In fact, only minimal modifications of 2-OMe are required to avoid an immune response [57].

Nucleic Acid Based Carriers

Several groups are working to harness genetics to create siRNA carriers entirely from nucleic acids. Interesting work is being done in creating self-assembled oligonucleotide-nanoparticles that are comprised entirely of DNA and siRNA that can be modified to present a targeting ligand on the surface [58]. Self-assembling microsponges comprised entirely of hairpin RNA have been created that carry more than 500,000 copies of siRNA per microsponge [59]. Also, RNA based aptamers conjugated to siRNA have demonstrated effectiveness *in vivo* suppressing HIV-1 [60].

Conjugates

Combined with the work to stabilize siRNA *in vivo* through chemical modifications, another approach to improve uptake of siRNA is to conjugate various biomolecules directly to the nucleic acid. These molecules include polymers, peptides, lipids, antibodies, and aptamers. Conjugate based siRNA delivery approaches have been reviewed extensively elsewhere [28, 30]. Notably, Cholesterol and α-tocopherol has demonstrated improved stability against nuclease degradation and increased cellular internalization [61-64]. Peptides have also been used to increase cell delivery. Some successful approaches using peptides is to conjugate siRNA with the RGD motif from integrin-binding peptides which has lowered the dose required for gene silencing [65]. Also, palmatic acid conjugated dicer substrate siRNAs have been shown to have enhanced effect in

gene silencing [66]. Conjugates may represent an exciting new approach for scaffold based delivery (section 2.6).

2.5 Intracellular Delivery Strategies

Another strategy for improving pharmacokinetics and cellular bioavailability of siRNA is to incorporate a carrier. Typically these carriers contain cationic moieties that allow electrostatic complexation of siRNA. These carriers may take many forms including nanoparticles, liposomes, lipids, and polymers. Intracellular delivery vectors have been reviewed extensively [27, 28, 67] but for the sake of this review, they are discussed in detail. For local delivery strategies (section 2.6) it is important to consider the compatibility of the intracellular delivery vehicle with the local delivery depot.

Physical Methods: Electroporation, Iontophoresis, Sonophoresis, Photochemical Internalization and Laser Irradiation

There are a variety of physical methods used for *in vitro* transfection or in some cases *in vivo* application to superficial pathologies but are generally considered to be too invasive for most therapies. These include electroporation, iontophoresis, sonophoresis, photochemical internalization and laser irradiation. Electroporation is a technique where high voltage pulses are applied to a tissue (or cell culture) triggering a voltage drop stimulating nano-pores in the cell membrane which allows larger molecules to diffuse across [68-71]. Iontophoresis utilizes the application of a constant current to move charge molecules (e.g. siRNA) through a tissue, typically the epidermis [72, 73]. This technique has been used for siRNA for ocular gene therapy [74]. Sonophoresis uses ultrasound to disrupt lipid structure in various tissues primarily for transdermal drug delivery [75]. Iontophoresis and sonophoresis do not always necessitate cellular internalization however, and may be limited in the uptake of siRNA. This leaves electroporation, which may negatively affect cell viability [76, 77].

Using photochemical internalization has also been explored where photosensitizing agents exposed to a light source generate singlet oxygen species that permeabilize membranes [78]. Photochemical internalization has been used to prolong siRNA-mediated gene silencing [79]. As a therapy, however, photochemical internalization is limited by the availability of the light source and possible toxicity. Laser irradiation is another technique that involves using a high-powered laser thought to disrupt intracellular connections allowing increased drug permeation [80]. This technique has been used to increase siRNA delivery transdermally [81]. Laser irradiation may improve siRNA transport through skin, but may still not overcome intracellular delivery barriers.

Cell-Penetrating and Fusogenic Peptides

Cell-Penetrating Peptides and fusogenic petides have been developed that mimic viral domains that allow intracellular localization of their genetic material. CPPs have been developed based on naturally occurring sequences (e.g. TAT of HIV-1) or synthetic sequences (e.g. Arginine-rich sequences) [70, 82-88]. Cell entry mechanisms are hypothesized to include membrane fusion via binding of CPPs to cell surface proteoglycans, the endocytosis pathway (caveolin-dependent, clathrin-dependent, or caveolin- and clathrin-dependent), and macropinocytosis [89-92]. An exhaustive list is given in Table 1 of the following review [67]. Many CPPs contain cationic peptides (poly(arginine)) which make these CPPs logical electrostatic complexing agents for siRNA.

Fusogenic peptides may overcome an additional intracellular barrier within the endo-lysosomal pathway. Peptides with fusogenic activity have an amphipathic structure but transition to lipophilic at lower pH environments characteristic of endosomes and lysosomes allowing membrane disruption. An exhaustive list is given in Table 2 in the following review [67]. One of the most widely utilized fusogenic peptides is the N-terminal sequence of the Influenza hemagglutinin subunit HA-2 and its derivatives [93-96].

It is important to consider that some CPPs have been shown to have cytotoxic effects depending on the synthetic route and CPP formulation used (e.g. some *retroinverso* cell penetrating peptides have been shown to result in severe cytotoxicity mediated through non-specific side effects) [97]. Other potential disadvantages of CPPs include poor serum and protease stability and their indiscriminate cell entry, which could be problematic for systemic delivery applications where specific cells are targeted.

Viral Transfection

Viral transfection may be a powerful means for incorporating DNA into cells *in vitro* or target tissues *in vivo*. DNA sequences can be engineered to generate expression for a missing or underexpressed gene or alternatively to code for a shRNA that is cleaved by dicer to an siRNA. Viral based gene therapy has been used extensively in research, however strong concerns have been raised about using viral transfection in human clinical trials [98]. Viral transfection is reviewed extensively elsewhere [99] and is considered out of the scope of this review

Lipids/Liposomes

One of the most common methods for nucleic acid transfection is formulation with lipids [100-102]. Lipid agents can form vesicles with a lipid bilayer membrane surrounding an aqueous interior where hydrophilic drugs can be encapsulated, or cationic lipids can be used to form lipoplexes with anionic nucleic acids. Lipids can either fuse to the cell membrane or enter the cell by endocytosis, eventually releasing their cargo into the cytoplasm [56, 103]. Information on liposome preparation, physicochemical properties, and applications can be found in more detail in a review of liposomal drug delivery systems by Samad *et al*. [103]. Lipids are commonly combined with other components to incorporate added functionality. For example, Morrissey *et al* used a cationic and fusogenic lipid (SNALP) delivery vesicle coated with a PEG-lipid layer to provide a neutral, hydrophilic exterior [104].

Polymers and Nanoparticles

One of the simplest ways to transfect cells with nucleic acid *in vitro* is with the electrostatic complexation with a linear cationic polymer which is best represented by linear polyethyleneimine (PEI). Cationic polymers are a logical approach for siRNA delivery because they electrostatically condense siRNA, protect from nuclease degradation, are attracted to the anionic cell membrane, and provide a mechanism for endosome escape through the proton sponge effect [105-109]. Examples include poly(L-lysine), linear and branched poly(ethylenimine) (PEI), poly(amidoamine) (PAMAM) dendrimers, poly(β-amino esters) (PBAE), and histidine and/or imidazole containing copolymers [110-116]. In addition, several natural polymers have been used to transfect siRNA including atelocollagen [117, 118] and chitosan [119]. Finally, several groups have combined cationic polymers with inorganic nanoparticles that provide dual functions including additional therapeutic functionalities or diagnostic capabilities. Noteworthy examples including gold nanoparticles (AuNPs) coated with cationic polymers [120] and quantum dot nanoparticles [121, 122].

Careful consideration into the use of cationic polymers *in vivo* must be taken. Cationic complexes also induce cellular toxicity at high concentrations, indiscriminately targets cell types, and may be unstable when exposed with competing ions *in vivo* particularly when exposed to the glomerular basement membrane in kidneys [123, 124]. Another concern is an irreducible complexation of polymer with siRNA in the cell cytoplasm preventing RISC uptake. Some approaches toward this problem have been to use a bioreducible disulfide linkage to connect siRNA to the polymeric carrier instead of electrostatic complexation [125, 126]. Another approach has been the use of hydrolytically degradable cationic moieties that results in a charge reversal of the polymer from a tertiary amine to an acrylic acid [127].

Polymer biodegradability can also be a significant advantage as exemplified by PBAE carriers, which decompose into cytocompatible, low molecular weight degradation products and are significantly less toxic than PEI and poly(L-lysine) [128, 129].

Stimuli-sensitive Polymers

Synthetic polymers can be used to mimic the activity of fusogenic peptides by responding to the low pH intracellular trafficking compartments to prevent lysosomal degradation or exocytotic recycling. These polymers are designed to be inert and membrane compatible at physiologic pH, but membrane disruptive at low pH. The primary class of polymers is represented by anionic acrylic acids including poly(ethylacrylic acid) and poly(propyl acrylic acid). These polymers become more hydrophobic in acidic environments, triggering adoption of a less solvated, compact globule conformation that partitions into and disrupts lipid bilayers [105, 107, 130, 131]. Polymers and copolymers of PPAA have been explored for siRNA delivery [132, 133].

Murthy et al. developed a related class of “encrypted” polymers that also have lipophilic activity that disrupts endo-lysosomal membranes. In the encrypted delivery system, PEG polymers attached via acid-labile acetal linkages “shield” a hydrophobic, endosomolytic polymer backbone until being shed upon exposure to acidic pH [134, 135].

PEGylation and Targeting

For intravenous applications, cationic shell materials have several major drawbacks. Cationic materials cause erythrocyte aggregation, opsonization, preferential distribution to the lungs, and possibly pulmonary emboli and mortality [136-139]. Modification with poly(ethylene glycol) (PEGylation) is the primary method used in improving pharmokinetics and minimize non-specific uptake and toxicity [140-145]. PEGylation has been used to improve the delivery of PEI, poly-L-lysine, PAMAM, PPI dendrimers, PDMAEMA, and BMA-DMAEMA complexes [124, 146-150]. Careful balance must be achieved because PEGylation can also reduce therapeutic efficacy by interfering with cellular uptake and endosomal escape [143]. One way to mitigate this loss in activity is to incorporate a mechanism for “shedability” or to have a PEG protecting layer be cleaved off by specific enzymes in the target tissue [151, 152].

In addition, cationic materials typically target cell membranes non-specifically and may require a targeting scheme to ensure desired biodistribution. PEGylated carriers have sacrificed cell uptake to improve biocompatibility and may require targeting molecules to improve uptake in the target tissue. Many of the targeting molecules created for this purpose are geared toward cancer applications with targeting molecules bombesin, the peptide EPPT, anisamide, folic acid, and transferrin representing only a small sampling of the available targeting molecules [145, 153-157].

For local delivery applications, PEGylation and tissue targeting may not be required as nanoparticles with condensed siRNA released from a local depot tend to have a primary effect in the local tissue without widespread effects [158].

2.6 Local Delivery Strategies

Local delivery of biologics has been pursued for tissue engineering and regenerative medicine with the goal to improve tissue regeneration by directing cellular responses. Biomacromolecules including growth factors [159] and plasmid DNA [160] have been delivered from tissue engineering matrices. Recently, several groups (including our own) have adapted tissue engineering matrices and drug delivery depots for the controlled delivery of siRNA. The choice of local delivery material is important as it may serve as dual functions as the siRNA depot maintaining a therapeutically relevant dose in the pathological environment and serve as a tissue engineering scaffold guiding cell infiltration and growth.

Regenerative Medicine Considerations

The choice of material for local delivery plays a large role in dictating biologic response. The materials alone may influence the regenerative potential of their surrounding tissue [161] and synergism may result between a properly designed material and carefully selected target gene (section 2.7). Natural extracellular matrix (ECM) may seem an ideal candidate for tissue

regeneration, however, other materials may be better suited that have more interconnected pore structure, better degradation rates, and other beneficial properties that accelerate tissue regeneration [46]. The material should provide the best possible environment for the target tissue and the material should be entirely resorbable and biodegradable as to avoid further surgical inteverentions and material removal [162]. The mechanical properties of the material are an important design consideration and should be matched carefully with the desired tissue which vary widely in mechanical properties (bone, myocardium, skin). The mechanical properties should provide an ideal environment for cell ingrowth and differentiation. Importantly, the degradation rate of the matrix should be matched to the rate of tissue in-growth to serve as an appropriate template [46, 163]. The pore size of the material can dictate cell fate and properly tuned porosity may benefit tissue regeneration [164]. Using biomaterials for tissue engineering is a complex topic dictated by a variety of factors including choice of material, mechanical properties, degradation rates, and porosity [161] and these factors should be weighted when selecting a material.

Our group has utilized polyester urethanes (PEUR), a promising class of synthetic biomaterials that have several of the above advantages including being injectable, tissue adherent, biocompatible, and biodegradable into biocompatible side products at rates dictated by the composition of the polyester triol and the isocyanate [24, 25]. PEURs provide mechanical support for tissue regeneration in excisional cutaneous wounds and bone defects [24, 165-167]. For clinical translatability, the use of lysine-derived polyisocyannates in the PEURs allow the scaffolds to be fabricated *in situ* with a reactive foaming process that has a rapid curing time filling unusual defects and allowing injectability [168, 169].

The choice of biomaterial scaffold is an important design consideration as the extracellular environment of neighboring and infiltrating cells may direct cell behavior and provide biologic cues. Further biologic direction may be forced through the incorporation of cells (e.g. stem cells) and biomacromolecules including siRNA.

Local Drug Depots for siRNA Delivery

Though the enzymatic action of siRNA generates potent gene silencing, the activity has a finite half-life. In rapidly dividing cells, a maximum silencing effect is noted near two days post-transfection [17] with gene silencing nearly absent in one week [18]. To address this issue in regenerative medicine, it has been proposed to sustain the delivery to a local environment from a tissue-engineering scaffold injected or implanted into a wound. **Table 2.1** summarizes recent efforts in the material based local delivery of siRNA.

One approach is to suspend siRNA transfection complexes within natural materials and hydrogels. The Alsberg group has developed injectable calcium crosslinked alginate, photocrosslinked alginate, and collagen based hydrogels and demonstrated strong GFP silencing in incorporated cells *in vitro* [19]. More recently, they used photocrosslinked dextran hydrogels and covalently incorporated cationic linear polyethyleneimine (LPEI) to achieve tunable and sustained siRNA release [170]. The Saadeh lab applied an agarose matrix system containing a liposomal siRNA transfection complex and have shown proof of principle *in vivo* with mapk1 and lamin A/C and have shown therapeutic potential delivering siRNA against PHD2, p53, and Smad3 [21, 22, 171].

Synthetic materials have been used for controlled delivery of siRNA to local environments with drug delivery depots. The Mikos group has used PLGA microspheres for controlled siRNA delivery to a model of temporomandibular joint inflammation and achieved sustained release over the course of two weeks [172, 173]. Song and co-authors have developed an injectable polyplex hydrogel comprised of poly(organophosphazene) and either PEI or a CPP as a transfection reagent [174, 175]. Importantly, they demonstrated sustained release to a local tumor environment *in vivo* and reduction in tumor volume. The Hammond group has been developing materials for sustained siRNA delivery to local wound environments by utilizing their layer-by-layer technology to electrostatically entrap calcium phosphate siRNA nanoparticles and deliver to a wound bed [176] .

Table 2.1 – Local delivery strategies for siRNA

	Local Delivery Strategy	Intracellular Delivery Strategy	Release Kinetics and Activity	Reference
Natural Materials	Agarose	Liposomal Complex	Fast release, requires reapplication, various gene silencing >50% *in vivo*	(J. W. Lee et al., 2010; P. D. Nguyen et al., 2010; Thanik et al., 2007; Wetterau et al., 2011) [21, 22, 171, 225]
	Alginate, Photoalginate, or collagen hydrogel	PEI or Chitosan	Release on the order of days tunable by the material. Gene silencing >90% *in vitro.*	(Krebs et al., 2009) [19]
	Photocrosslinked dextran Hydrogel	PEI	Tunable Release around 1 week. Gene silencing >90% *in vitro*	(K. Nguyen et al., 2013) [170]
	Collagen hydrogel	dPAMAM	Rapid release ~1 day. Gene silencing ~50% *in vitro.*	(Vinas-Castells, Holladay, di Luca, Diaz, & Pandit, 2009) [20]
	Chitosan hydrogel	Chitosan	Release not measured. Gene silencing >70% *in vivo.*	(Han et al., 2011) [226]
Synthetic Materials	PLA-DX-PEG pellets	PLA-DX-PEG	Release around 1 week. Gene silencing >70% *in vivo.*	(Manaka et al., 2011) [198]
	PCLEEP nanofibers	Transit TKO	Sustained release over 10-15 days. Gene silencing ~30% *in vitro.*	(Rujitanaroj, Wang, Wang, & Chew, 2011) [227]
	Nylon coated Layer-by-layer assembly	Calcium phosphate nanoparticles	Sustained release for 7-10 days. Gene silencing ~70% *in vitro.*	(Castleberry et al., 2013) [176]
	Polyurethane	Stimuli-sensitive Polymers	Controllable for 35 days, >90% silencing *in vivo.*	(C. E. Nelson et al., 2012; C. E. Nelson et al., 2014) [158, 181]
	PLGA Microspheres	PEI	Fast release (<1d) of complexes. Sustained siRNA release for 20d. Gene silencing 30-40%.	(Mountziaris et al., 2011; Mountziaris et al., 2012) [172, 173]
	PLGA Nanofibers	Chitosan	Sustained release for 30-35 days. Gene silencing ~50%.	(M. L. Chen et al., 2012) [228]
	PEI-poly(organophosphazene) Hydrogel	PEI	Sustained release for ~21 days. Gene silencing ~90% *in vitro.*	(Y. M. Kim et al., 2012, 2013) [174, 175]
	PEG Hydrogel	PEI	Dose requirement is too high for material	(Takahashi, Wang, & Grainger, 2010) [229]

Another promising approach is applying synthetic scaffold based matrices as a drug delivery depot and tissue template. Our group has adapted tissue engineering polyurethane as a local depot for siRNA delivery. The polyurethane materials were previously developed as a tissue engineering material and adapted for the sustained delivery of a variety of biomacromolecules including insulin-like growth factor-1 (IGF-1), hepatocyte growth factor (HGF), basic fibroblast growth factor (bFGF), recombinant human bone morphogenic protein 2 (rhBMP-2), platelet-derived growth factor (PDGF), and the antibiotic vancomycine [24, 165, 166, 177, 178]. We have demonstrated sustained silencing in mouse subcutaneous implants lasting at least 35 days (the

last time point measured with 90% silencing) and have shown therapeutic potential by silencing a regulator of angiogenesis, prolyl hydroxylase domain protein 2 (PHD2).

As section 2.5 discussed, siRNA requires an intracellular delivery scheme, so the compatibility of intracellular delivery scheme with the local delivery material must be taken into consideration. For example, PEI/DNA complexes have been shown to be unstable when incorporated into hydrogel scaffolds and require stabilizing agents to retain activity [179, 180]. Similarly, siRNA complexes were shown to have a 50% activity loss unless stabilized [158, 181].

Substrate Mediated Delivery

By immobilizing nucleic acids on a surface, the concentration of nucleic acid in the cellular microenvironment is increased leading to a 10-100 fold increase in transfection efficiency [182-184]. This concept termed 'substrate-mediated delivery' mimics the cellular internalization scheme of viruses that attach to extracellular matrix proteins to enhance cellular internalization [185, 186]. Immobilized nucleic acids are internalized through many modes of endocytosis, though caveolae-mediate endocytosis may play the largest role in substrate mediated plasmid delivery [187]. For comparison, substrate mediated delivery of a plasmid from a synthetic tissue-engineering scaffold generated expression for 28 weeks [188]. Sustained nucleic acid delivery has been investigated therapeutically in regenerative medicine with a VEGF plasmid that improved angiogenesis in mice [189]. The higher efficiency of substrate mediated transfection of plasmids and siRNA stands to benefit tissue engineering with long term modification of gene expression.

2.7 mRNA Targets

Due to the flexibility of siRNA against any gene target and the tunabiltiy of regenerative scaffolds, scaffold based RNAi may be widely applicable [196]. Several local applications for gene silencing have been covered in detail elsewhere including pathologies affecting the lungs, eye, nervous system, digestive system, and vagina [31]. Another potentially rewarding pursuit of local gene silencing is in primary tumor sites but is considered outside the scope for this review. There also may be potential for targeting genes related to infectious disease (e.g. herpes simplex virus 2 and respiratory syncytial virus) [197, 198]. Also, the differentiation of encapsulated stem cells may be guided by the inclusion of siRNA [199]. This discussion will be focused on gene silencing for tissue regeneration.

Table 2.2 Gene targets for regenerative medicine

Pathology	Gene	Reference
Inflammation	TNFα	(Jakobsen et al., 2009) (Y. Zhang et al., 2006)
	CD16	(Mountziaris et al., 2012)
Autoimmune	Tbox21	(M. Nakamura, et al., 2008)
	CD86	(Ritprajak, et al., 2008).
Fibrosis and Scarring	CTGF	(Abraham, 2008)
	mTOR	(H. Takahashi et al., 2010)
	Smad3	(J. W. Lee et al., 2010) (Z. Wang et al., 2007)
	erk2	(C. Zhang et al., 2014)
	TGFβ	(J. S. Huang et al., 2002) (H. Nakamura et al., 2004)
Cell Cycle	p53	(P. D. Nguyen et al., 2010)
	p21	(Bedelbaeva et al., 2010)
Bone Regeneration	Noggin	(Manaka et al., 2011)
Muscle Regeneration	Myostatin	(Kawakami et al., 2013)
Tendon Regeneration	Col5α1	(P. Lu et al., 2011)

Inflammation and Autoimmune Disorders

Genes that are pro-inflammatory represent possible targets for tissue regeneration, specifically for wound healing. Local TNFα silencing has been shown to improve psoriasis by reducing epidermal thickness and normalizing skin morphology [200]. Also, local TNFα silencing has been shown to improve a rodent model of inflammatory bowel disease [201]. These studies provide proof of principle that TNFα silencing may decrease chronic inflammation and restore regenerative capacity. In the same vein CD16 was used in a model for temporomandibular joint

(TMJ) inflammation and decreased TMJ induced changes in meal patterns and also decreased downstream interleukin-6 expression [173]. These studies suggest that TNFα or CD16 may be beneficial targets in regenerative medicine and wound healing. Immune recognition of synthetic or naturally derived materials may create serious complications. RNAi may be a high impact mediator of immune responses to materials. A few examples include T-box21 and CD86 silencing. Alopecia areata was treated with T-box21 siRNA conjugated to cationized gelatin in a mouse model resulting in hair shaft elongation [202]. CD86 siRNA applied topically reduced local inflammation and may be a potential strategy for treating allergic skin disease [203].

Tissue Specific Regeneration

Tissue specific regeneration may be encouraged by silencing genes that encourage differentiation of specific cell types. Bone formation has been encouraged using siRNA targeting Noggin mRNA [192] . In this study, bone morphogenic protein 2 (BMP-2) and siRNA against Noggin were included in poly-D,L-lactic acid-*p*-dioxanone-polyethylene glycol block co-polymer (PLA-DX-PEG) hydrogels which encouraged ectopic bone formation over controls [192]. It is feasible to use similar designs to assist bone regeneration and fill critical size bone defects. By injecting myostatin-siRNA nanoparticles with atelocollagen, skeletal muscles of a mouse model of muscular dystrophy were increased in size and electromyography indicated increased muscle activity [204]. This result motivates the use of myostatin siRNA in further studies to regenerate weak or absent muscle tissue. Collagen V has been shown to negatively regulate the size of type I collagen fibers and fibril diameter is inversely proportional to the collagen V concentration. By silencing Col5α1 mRNA in tenocytes and combining with normal tenocytes, collagen fibrils increased in size and improved tendon tissue regeneration [205].

Fibrosis and Scarring

Fibrosis and scarring to date have the largest number of genes studies to decrease the fibrotic response and improve the quality of the regenerated tissue. Connective tissue growth factor (CTGF) is a logical target that is overexpressed in scarred wounds. CTGF inhibition results in type I and III collagen decreases and attenuated liver fibrosis [206]. Though there are no studies using CTGF siRNA in scarless wound healing, it is a logical target to promote healing with less fibrotic wounds. Mammalian target of rapamycin (mTOR) is another potential target that when silenced *in vitro* decreases fibrotic markers. However, *in vivo* silencing in this study did not show significance. The authors expect this is due to low loading capacity of the hydrogel system [207]. TGF-β antagonists have been shown to reduce scarring and fibrosis and accelerate wound healing [208] so using RNAi to target TGF-β type II receptor resulted in inhibited fibronectin assembly and decreased cell migration. *In vivo,* TGF-β type II receptor inhibition reduced matrix deposition [209]. As an additional target, TGF-β may be dependent on Smad3 and when decreased with RNAi reveals a significant reduction in epidermal thickness and collage deposition in an ionizing radiation mouse model [22]. Another study has shown that Smad3 siRNA can decrease procollagen expression in keloid fibroblasts by interrupting TGF-β [210]. Finally, inhibition of ERK2 by siRNA reduced epidural fibrosis in a laminectomy model in rats by decreasing fibroblast proliferation preventing epidural scar adhesion [211].

Cell Cycle Control

The cell cycle regulator, p53, was silencing in diabetic mouse excisional wounds delivered from an agarose matrix which resulted in accelerated wound closure, an increase in CD31 cell staining, VEGF secretion, and SDF-1 expression [21]. To our knowledge, p21 silencing in regenerative medicine has not yet been performed. However, a p21 knockout mouse was able to regenerate ear holes suggesting a link between the cell cycle regulator p21 and appendage regeneration [212]. Though cell cycle regulators may be a dangerous target gene for systemic

silencing due to potential carcinogenic effects, they may prove to be an effective gene target for local and temporary silencing to improve tissue regeneration.

Angiogenesis (PHD2)

Angiogenesis is delayed or absent in pathological wound healing [213] and the increase of angiogenesis represents a logical approach for the improvement of diabetic wounds. PHD2 is an endogenous negative regulator of the transcription factor hypoxia-inducible factor-1α (HIF-1α), and PHD2 inhibition increases HIF-1α activity (**Fig. 2.3**) [214, 215]. This occurs through the hydroxylation of the proline residues Pro402 and Pro564 of HIF-1α [216]. It has been shown that PHD2 has a much higher impact than PHD1 or PHD3 in human cells [8] and the potent knockdown of PHD2 results in a large up-regulation of the transcription factor HIF-1α and its downstream genes VEGF, fibroblast growth factor 2 (FGF-2), endothelial nitric oxide synthase (eNOS), angiopoieten (ANGPT), and stromal cell-derived factor 1 (SDF-1) [217, 218]. These factors orchestrate both formation and maturation of vessels and, in the case of SDF-1, recruit endothelial progenitors that further promote local vasculogenesis [219]. Previous pro-angiogenic approaches have employed a single growth, factor, such as vascular endothelial growth factor (VEGF), which does not fully recapitulate the complex regulatory mechanisms involved in neovascularization and results in immature, leaky vasculature that is susceptible to rarefaction [220]. To compensate, a proof-of-concept material platform delivered multiple growth factors with precise temporal control resulting in angiogenesis, vessel maturation, and vascular remodeling [221]. However, growth factor delivery is expensive and the material platform to deliver such temporal control is cumbersome. Therefore, siRNAi-mediated silencing of PHD2 is a promising approach for pro-angiogenic therapy

Our Group and others have shown that PHD2 inhibition promotes therapeutic neovascularization of ischemic tissues and can promote tissue repair and tissue scaffold vascularization and integration [222-224]. Further, others have shown stabilization of HIF1α is

critical in wound healing and therapeutic intervention may reverse the negative effects of hyperglycemia in diabetes [225].

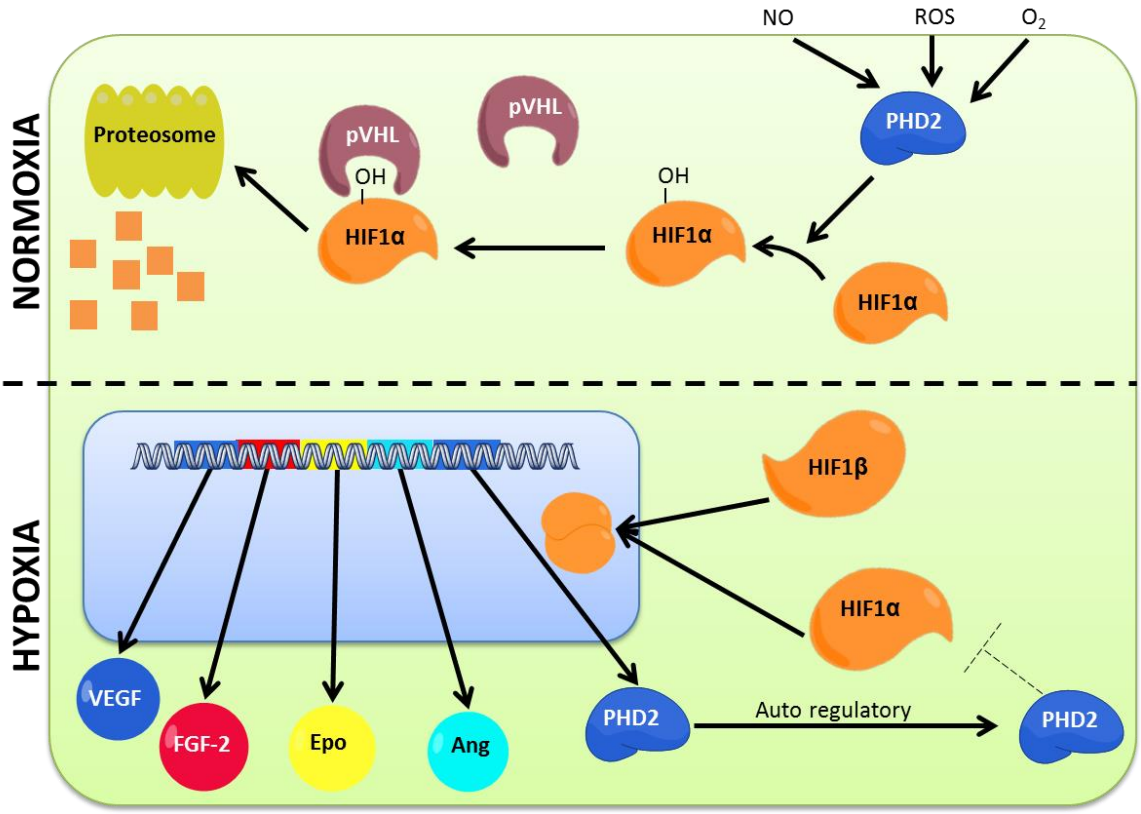

Figure 2.3 – **PHD2 Signaling in Normoxia and Hypoxia**. During normoxia, the oxygen dependent PHD2 hydroxylates proline residues in HIF-1α leading to its recognition by the Von Hippel-Lindau Tumor suppressor (pVHL) and results in the proteosomal degradation. Alternatively during hypoxia, PHD2 is inactive and HIF-1α is free to translocate to the nucleus with HIF-1β and begin transcription of pro-angiogenic genes.

2.8 Outlook

The promise of therapeutic siRNA has already been adapted for clinical trials in a variety of indications ranging from respiratory syncytial virus infection, macular degeneration, hepatitis B, renal failure, macular oedema [14], pachyonychia congenital [15], macular degeneration [226], skin disorders [227], and targeted delivery to melanoma [16, 228, 229]. There are 22 clinical trials in all when this review was compiled [28] and many more in the development pipeline. With properly designed material delivery platforms and new molecular based targets identified, powerful RNAi based therapies for regenerative medicine may be within reach.

Chapter 3

Aim 1 – *In vitro* Development of PEUR-NP Platform

Text for Chapter 3 taken from:

> Nelson CE, Gupta MK, Adolph EJ, Shannon JM, Guelcher SA, Duvall CL. "Sustained local delivery of siRNA from an injectable scaffold." Biomaterials. 2012; 33(4): 1154-61

3.1 Introduction

The discovery of RNA interference [12] motivated extensive efforts toward harnessing gene-silencing biomacromolecules for clinical therapeutic use. Small-interfering RNA (siRNA) has rapidly advanced into clinical trials for indications such as macular degeneration [226], skin disorders [227], and targeted delivery to melanoma [16, 228, 229]. The current work focuses on development of a platform technology to be used for the controlled, local delivery for regenerative medicine, which is a less mature but promising application area for siRNA [26].

Effective delivery has been the primary limitation to more rapid and widespread adoption of siRNA for clinical use due to its susceptibility to nucleases and poor intracellular cytosolic delivery [230]. A variety of strategies have been developed to protect siRNA and improve intracellular delivery including electrostatic complexation with cationic lipids, polymers, and polysacaccharides, as well as conjugation to cell-penetrating/fusogenic peptides, dendrimers, antibodies, vitamins, and nanoparticles [64, 231-240]. Controlled polymerization techniques such as reversible addition-fragmentation chain transfer (RAFT) polymerization offer a promising approach to designing synthetic polymers that are monodispersed, and contain spatially-defined functionalities [241, 242], and the current work employs a RAFT-synthesized, pH-responsive polymer-based micellar nanoparticle (si-NP) recently optimized for efficient and biocompatible intracellular siRNA delivery [23, 133].

The polyplex, bioconjugate, and nanoparticulate siRNA carriers that have advanced to *in vivo* preclinical testing have been primarily delivered intravenously or through local injection (i.e.,

intratumoral) in PBS. For tissue regeneration applications, it is anticipated that it will be desirable for siRNA activity to be locally sustained and mediated from a biocompatible and biodegradable tissue template. Because siRNA activity is typically transient and can be exhausted by one week in rapidly dividing cells [17, 18], natural materials including alginate, collagen and agarose have been applied for sustained delivery of siRNA [19-22]. Pre-fabricated synthetic scaffolds made from ε-caprolactone and ethyl ethylene phosphate copolymer (PCLEEP) nanofibers have also been pursued for the release of siRNA/transfection reagent (*TransIT*-TKO) complexes and have been shown to achieve sustained delivery of bioactive siRNA for 28 days [193].

Porous, biocompatible, and biodegradable polyester polyurethanes (PUR) comprise a promising class of synthetic injectable biomaterials that can provide both mechanical support and also controlled drug release to regenerating tissues [167]. Several drugs, including insulin-like growth factor-1 (IGF-1), hepatocyte growth factor (HGF), basic fibroblast growth factor (bFGF), recombinant human bone morphogenetic protein 2 (rhBMP-2), platelet-derived growth factor (PDGF), and the antibiotic vancomycin have been incorporated into and delivered from PUR scaffolds [24, 165, 166, 177, 178]. Additionally, PURs support the ingrowth of cells in excisional cutaneous wounds [24] and bone defects [165, 166]. Further advantages of PURs are that they adhere to tissue, do not stimulate inflammation [24], and biodegrade into biocompatible side products at rates that can be tuned based on the polyester triol and isocyanate precursor compositions [25]. Importantly, the use of lysine-derived polyisocyanates in the PUR scaffolds makes them more clinically translatable because they can be synthesized using a two-component foaming process that allows a short manipulation time for filling of any shape or size defect, followed by rapid curing *in situ* [168, 169].

The current study pursues a novel application of PURs to deliver pH-responsive micellar si-NPs designed for the intracellular delivery of siRNA. This investigation validates homogenous loading of siRNA nanocarriers within the PUR scaffold, sustained, diffusion-controlled release of intact nanoparticles, and maintenance of gene silencing bioactivity of the released si-NPs.

3.2. Methods

Materials

All chemicals were purchased from Sigma-Aldrich (Milwaukee, WI, USA) except the following. Purchase of siRNA was from Applied Biosciences (Ambion), LDH cytotoxicity kit from Roche, Hiperfect transfection reagent (positive control) from Qiagen, and PD10 desalting columns from GE healthcare. Lysine Triisocyanate (LTI) was purchased from Kyowa Hakko Kogyo Co., Ltd. (Tokyo, Japan). DMAEMA, and butyl methacrylate were vacuum distilled prior to use. 2,2'-Azobis(2-methylpropionitrile) (AIBN) was recrystallized twice with methanol.

Synthesis of 4-cyano-4{[(ethylsulfanyl)carbonthioyl]sulfanyl}pentanoic acid (ECT)

The RAFT chain transfer agent ECT was synthesized following protocols previously described by Convertine et al. [23] adapted from Moad et al. [243]. Briefly, Ethanethiol (76 mmol, 4.72 g) was reacted with carbon disulfide (79 mmol, 6.0 g) in the presence of sodium hydride (79 mmol, 3.15 g) in diethyl ether for 1h. The resulting sodium S-ethyl trithiocarbonate was further reacted with iodine (25 mmol, 6.3 g) to obtain bis(ethylfulfanythiocarbonyl) disulfide, which was further refluxed with 4,4'-azobis(4-cyanopentanoic acid) in ethylacetate for 18 h. The crude ECT was purified by column chromatography using silica gel as the stationary phase and ethyl acetate:hexane (50:50) as the mobile phase. ^{1}H NMR (400MHz, $CDCl_3$): δ 1.36 t ($SCH_2C\mathbf{H}_3$); δ 1.88 s ($CCNC\mathbf{H}_3$); δ 2.3–2.65 m ($C\mathbf{H}_2C\mathbf{H}_2$); δ 3.35 q ($SC\mathbf{H}_2CH_3$).

Synthesis of 2-propyl acrylic acid (PAA)

The synthesis of PAA was adapted from existing methods [244]. In brief, diethyl propylmalonate (200 mmol, 40.45 g) was stirred in 1M KOH in 95% ethanol and acifidied with HCl to yield 2-carbopropoxybutyric acid, which was reacted with diethylamine (200 mmol, 14.62 g) and formalin (200 mmol, 16.11 g) at room temperature for 24h, followed by reflux at 60°C for 8

hours. After acidification, the resulting 2 propylacrylate was refluxed in 2M KOH for 20 h to yield 2-propyl acrylic acid, which was extracted, dried, and vacuum distilled under vacuum to yield a colorless oil. ^{1}H NMR (400 MHz, $CDCl_3$) δ 0.97 t (CH_3CH_2); δ 1.55 m ($CH_3CH_2CH_2$); δ 2.31 t ($CH_3CH_2CH_2$); δ 5.69-6.32 q (CH_2=C); δ 12 s (CCOOH) .

Synthesis and characterization of pDMAEMA macro CTA

The synthesis of the poly[2-(diethylamino)ethyl methacrylate] pDMAEMA macro chain transfer agent (mCTA) was conducted by RAFT polymerization using conditions adapted from [23]. Based on a polymerization kinetics experiments (**Appendix Fig. A1**), the RAFT polymerization was conducted at 70 °C under a nitrogen atmosphere for eight hours with 1,4-dioxane as the solvent (70% by weight), an initial monomer to CTA ratio of 100, and a CTA to initiator ratio of 10. The pDMAEMA mCTA was isolated by precipitation into n-hexane (x3) and dried overnight. The polymer was analyzed by gel permeation chromatography (GPC, Shimadzu Crop., Kyoto, Japan) with an inline Wyatt miniDAWN TREOS light scattering detector (Wyatt Technology Corp., Santa Barabara, CA) and ^{1}H nuclear magnetic resonance spectroscopy (NMR, Bruker 400Mhz Spectrometer equipped with 9.4 Tesla Oxford magnet) for molecular weight and polydispersity.

Synthesis and characterization of DMAEMA-b-(PAA-co-BMA-co-DMAEMA)

RAFT polymerization was utilized to synthesize the second block as previously described [23]. Additional monomers butyl methacrylate (BMA), PAA, and DMAEMA were added to the pDMAEMA mCTA chain with an initial monomer to mCTA ratio of 250 in stoichiometric quantities of 50% BMA, 25% PAA, and 25% DMAEMA. The initiator AIBN was used with a mCTA to initiator ratio of 5. The polymerization was conducted for 18 hours under a nitrogen atmosphere at 70^{o}C. The resulting polymer was isolated by precipitation into chilled 50:50 ether:pentane, redissolved

in acetone and precipitated into chilled pentane twice, and vacuum dried overnight. The polymer was then dissolved in a minimal amount of ethanol, diluted into dH_2O, and further purified using PD10 desalting columns (GE Healthcare). The eluent was frozen and lyophilized yielding a pure polymer powder. The polymer was analyzed by GPC for number average molecular weight (M_n) and polydispersity. NMR in $CDCl_3$ and D_2O was used to determine composition and verify the formation of micelles with a DMAEMA corona. Transmission Electron Microscopy (TEM, Philips CM20 Transmission Electron Microscope, EO, Netherlands) and Dynamic Light Scattering (DLS, Zetasizer nano-ZS Malvern Instruments Ltd, Worcestershire, U.K.) were used to confirm presence and size of micelles, to determine the critical micelle concentration, and to characterize micelle pH-responsiveness. Carbon TEM grids (Ted Pella Inc. Redding, CA) were spotted with 5uL of polymer solution (~50ug/mL) and dried under vacuum for 24 hours.

Formation and Characterization of siRNA-loaded Micellar Nanoparticles

siRNA was dissolved in nuclease free water, and si-NPs were formed by injecting siRNA in nuclease free polypropelene tubes, diluting with PBS, adding polymer in PBS, and incubating at room temperature for 30 minutes. si-NPs were formulated based on the charge ratio defined as the number of positively charged tertiary amines (assumed to be 50% at physiologic pH) on the DMAEMA block (N) to the number of negatively charged phosphate groups on the backbone of siRNA (P). Complexes were formed anywhere between 0.5 and 8 N/P. A 2% agarose gel was prepared with 0.5 µg/mL ethidium bromide and allowed to gel at room temperature. si-NPs and controls were run for 40 minutes at 100 V. This experiment was also conducted after pre-incubating the si-NPs in 50% serum to verify serum stability. Dynamic light scattering and ζ–potential were used for physicochemical characterization of the si-NPs, and TEM was used to further verify si-NP size and morphology.

Synthesis of si-NP-loaded PUR Scaffolds

Polyester triols were synthesized as previously described from a glycerol starter targeting 900 Da and a backbone comprising 60 wt% ε-caprolactone, 30 wt% glycolide, and 10 wt% D,L-lactide [24, 245, 246]. si-NPs were synthesized as described above using an N/P of 4 and 4 nmol of fluorescently labeled (6-FAM) siRNA against GAPDH or non-labeled siRNA with a scrambled sequence. si-NPs were frozen and lyophilized and the resulting powder was rigorously mixed into 134 μmol of the polyol component of PUR using a Hauschild DAC 150 FVZ-K SpeedMixer (FlackTek, Inc., Landrum, SC). A slight excess of lysine triisocyanate (387 μmol) was then added and scaffolds were allowed to cure at room temperature forming a porous PUR foam over approximately 10 minutes. 134 μmol of water was included in the polyol because it reacts with LTI to produce CO_2 which acts as a blowing agent and creates pores in the scaffold. The resulting 200 mg foams were sectioned into discs with a diameter of 13mm and a thickness of approximately 3mm.

PUR Characterization

Confocal microscopy (Zeiss LSM 510Meta) equipped with differential interference contrast (DIC) was used to analyze the distribution of si-NPs in the scaffold. The 13mm diameter by 3mm cylindrical foams were immersed in 1mL of PBS in a 24 well plate. Releasate was collected at regular intervals approximating an infinite sink condition, and release data were fit to the Weibull function [166, 247]. Releasate was analyzed by TEM and DLS for presence and size of released si-NPs.

Cell Culture and siRNA Knockdown

Mouse Embryonic Fibroblasts (NIH3T3) were cultured in Dulbecco's Modified Eagle's Medium (DMEM, Gibco Cell Culture, Carlsbad, CA) supplemented with 5% Bovine Calf Serum (BCS, Gibco), and 1% penicillin-streptomycin (Gibco). For gene silencing experiments, NIH3T3

mouse embryo fibroblasts were seeded at a density of 12,500 cells/cm^2 in a 12 well plate and allowed to adhere overnight. Fresh NPs or released NPs were added in fresh media with a final concentration of 6.25nM to 50nM siRNA and allowed to incubate for 24 hours. Each group was analyzed with n=3, and each replicate was run in triplicate during qRT-PCR. The cells were lysed and homogenized with QIAshredder (Qiagen), and RNA was purified using the RNeasy® Mini Kit (Qiagen). RNA quantity and quality was assessed with a nanodrop spectrophotometer ND-1000 (Thermo Scientific). cDNA was synthesized with iScript™ cDNA synthesis kit (BIO-RAD) on a C1000™ thermal cycler. Quantitative PCR was done using IQ™ Real Time SYBR Green PCR Supermix on a quantitative thermal cycler (Bio-Rad iCycler iQ). GAPDH expression was normalized to β-Actin expression using the ΔΔCT method. Primers used were: β-actin Forward 5'-CTACGAGGGCTATGCTCTCCC-3', β-actin backward 5'-CGTCCTCATGCTACTCAGGCC-3', GAPDH Forward 5'-CTCACTCAAGATTGTCAGCAATG-3', GAPDH Backward 5'-GAGGGAGATGCTCAGTGTTGG-3'.

Imaging of Cell Uptake of si-NPs Post-release from PUR Scaffolds

NIH3T3s were seeded at 12,500 cells/cm^2 in 8 well chamber slides and incubated for 4 hours with FAM labeled siRNA containing si-NPs released from PUR scaffolds. The media was removed, and the cells were washed 3x with PBS and fixed in 4% paraformaldehyde for 30 minutes. After 2 washes in PBS, cell nuclei were counterstained with Hoechst 33258 (5 µg/mL, Sigma) and then washed an additional 3x. Images were acquired on a fluorescent microscope.

Cytotoxicity

NIH3T3 cells were seeded at a density of 12,500 cells/cm^2 in a 96 well plate and allowed to adhere overnight. si-NPs were then added in fresh media and allowed to incubate for 24 hours. The cells were then lysed and analyzed for intracellular LDH with a Cytotoxicity Detection Kit

(Roche Applied Science) as previously described [248], and a plate reader (infinite F500, Tecan Group Ltd., Mannedorf, Switzerland) set for absorbance at 492nm with reference at 595nm.

Statistical analysis

All data are reported as means ± standard error of the mean (SEM). Analysis of Variance (ANOVA) was used to determine treatment effects and $p<0.05$ was considered significant.

3.3. Results

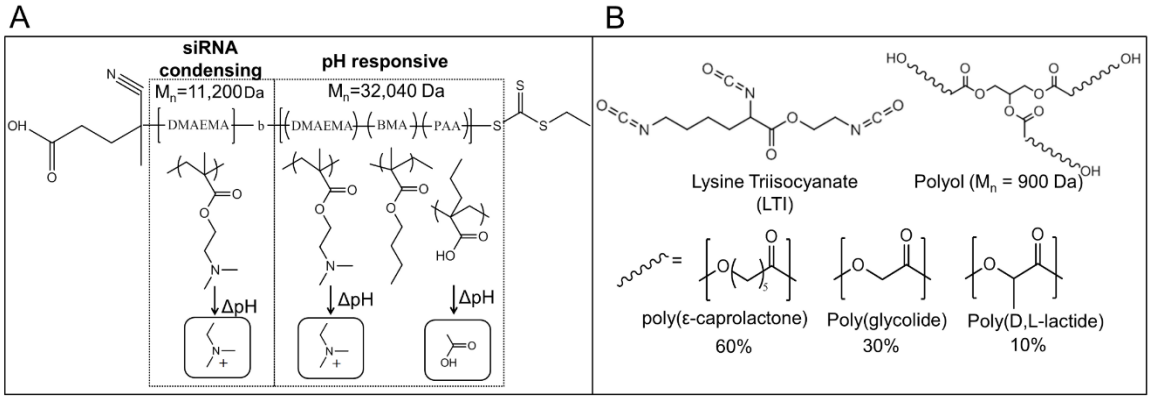

Fig 3.1Chemical composition of materials used for siRNA delivery. (A) Chemical structure of the micelle-forming, pH-responsive diblock copolymer used for siRNA packaging and intracellular delivery. The homo-DMAEMA first block was designed for siRNA condensation due to the positive charge on the tertiary amines. The second block is pH-responsive and tuned for endosomal escape due to micelle destabilization and endosomolytic activity triggered by protonation of PAA and DMAEMA. (B) Chemical structure of polyurethane precursors. LTI reacts with the –OH groups of the polyol to form urethane bonds and create the PUR network.

Polymer synthesis and characterization

4-cyano-4-(ethylsulfanylthiocarbonyl) sulfanylvpentanoic acid (ECT) was synthesized as previously described [23]. 2-propyl acrylic acid (PAA) was synthesized using established methods [244]. RAFT polymerization was used to synthesize a mCTA of DMAEMA (M_n = 11200g/mol, PDI = 1.40, (**Appendix Fig. A2**). The pDMAEMA mCTA was used to polymerize a second block with a resultant M_n of 32040 g/mol for a total M_n of 43240 g/mol (PDI = 1.41) as shown in **Appendix Fig. A2**. ^{1}H-NMR was used to confirm the percent composition of the second block which was determined to be 30%PAA, 25%DMAEMA, and 45%BMA (**Appendix Fig. 3A**).

When dissolved in D_2O, ^{1}H-NMR peaks from the core-forming terpolymer are suppressed, verifying the formation of micelles in an aqueous environment. (**Appendix Fig. 3B**). The polymer structure is depicted in **Fig. 3.1**.

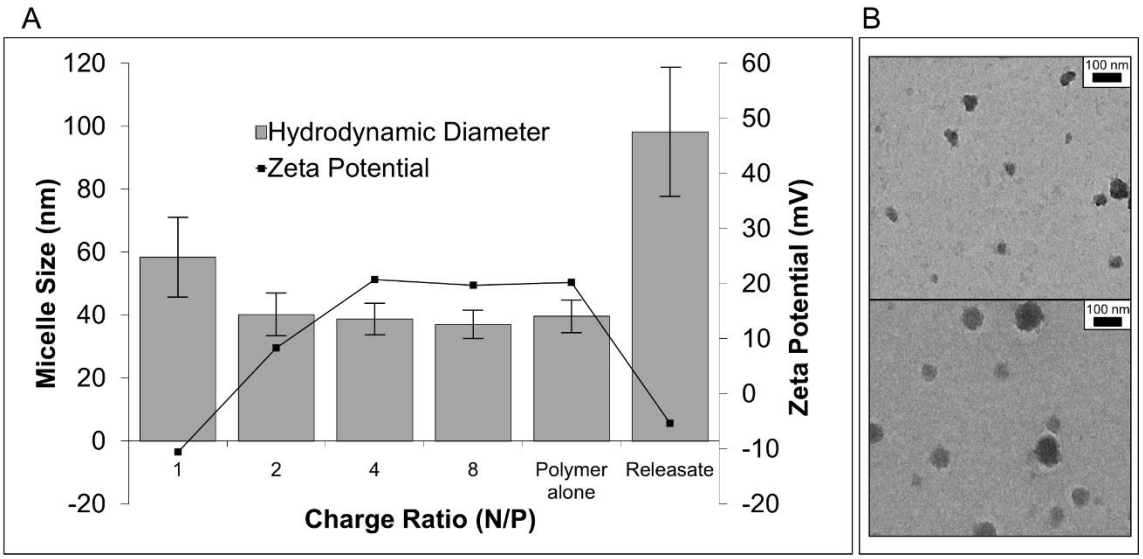

Fig 3.2 Physicochemical characterization of freshly prepared and PUR-released si-NPs. (A) Dynamic light scattering demonstrated that si-NP diameter was around 40-nm at N/P ratios of 2 or greater, and at N/*P* = 1, the charge neutrality caused the NPs to be less stable and larger. This is further represented by the ζ-potential, which was slightly negative at N/P of 1, 8.3 mV at N/P of 2, and approximately 20 mV at all N/P of 4 or greater. (B) The TEM image confirmed the micellar architecture and size of fresh si-NPs (top). Releasate si-NPs had a larger diameter of approximately 100 nm as shown both by DLS and TEM (B, bottom), and PUR-released si-NPs also had significantly reduced ζ-potential that was approximately charge neutral.

si-NP synthesis and characterization

Micellar nanoparticles were self-assembled in an aqueous environment and characterized for size and morphology by DLS and TEM respectively. TEM and DLS (**Fig. 3.2**) report similar diameters of 31 nm and 39.6 nm respectively, with the smaller diameter seen with TEM being due to micelle dehydration. DLS of serially diluted samples revealed a critical micelle concentration (CMC) below 2μg/mL, based on a DLS-detected loss of micelle stability (**Fig. 3.3A**). DLS was also used to demonstrate the dependency of the CMC on pH. The results confirm that micelle structure was destabilized at pH 5 at a concentration of 100 μg/mL, which is important for micelle endosomolytic behavior (**Fig. 3.3B**) [133]. Gel electrophoresis determined serum stable complexation of siRNA into si-NPs across a range of N:P ratios (**Appendix Fig. A4**).

si-NP-loaded PUR scaffolds

PUR foams were synthesized by reacting polyester triols (polyol) with lysine triisocyanate forming the porous polyurethane foam (**Fig. 3.1B**). Differential interference contrast microscopy (DIC) of PUR scaffolds revealed an intact, connected porous structure (**Fig. 3.4B,E**) with a mean pore diameter of 150μm ± 64μm. Confocal microscopy shows a relatively homogenous distribution of fluorescently labeled siRNA containing NPs throughout the PUR matrix (**Fig. 3.4A-C**) comparable to the distribution seen in the PUR containing naked siRNA (**Fig. 3.4D-F**).

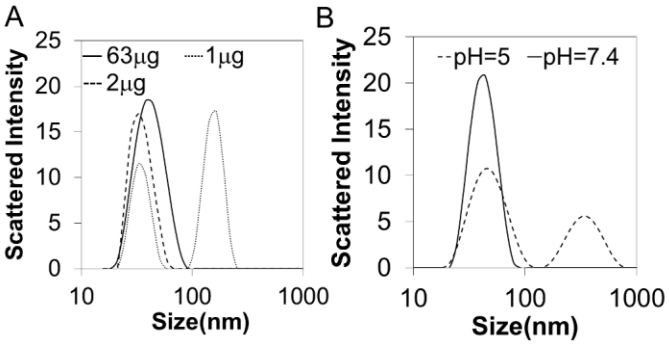

Fig 3.3 Micelle stability is dependent on concentration and pH. (A) critical micelle concentration (CMC) determination using DLS demonstrated disruption of micelles occurred at 2 μg/mL. (B) DLS also revealed pH-dependent destabilization of the micelles at pH = 5 at a concentration of 100 μg/mL.

siRNA-NP Release Kinetics and Modeling

Release from the scaffold was quantitatively assessed using si-NPs made with fluorescently labeled siRNA. Approximately 20% of the payload was released in the first 12 hours followed by a sustained release approaching 80% cumulative release by 21 days (**Fig 3.5**). Conversely, the much smaller naked siRNA diffuses from the scaffold much faster than si-NPs, reaching nearly 100% in 3 days. Importantly, TEM and DLS of releasate demonstrated that intact si-NPs, although of larger diameter than fresh si-NPs (approximately 100nm), were delivered from the PUR scaffolds (**Fig. 3.2**).

The Weibull function has been previously used to evaluate the drug release mechanisms of drug eluting matrices that efficiently release their payload (cumulative release exceeding 60%) [166, 247]. The release of si-NPs was fit to the Weibull empirical model in Equation 3.1:

$$Eqn\ 3.1: \qquad \frac{M_t}{M_\infty} = 1 - \exp\left(-a \cdot t^b\right)$$

where M_t is the mass of si-NPs released at time t, M_∞ is the total mass of si-NPs, *a* is a constant based on the system, and *b* is a constant based on the release kinetics.

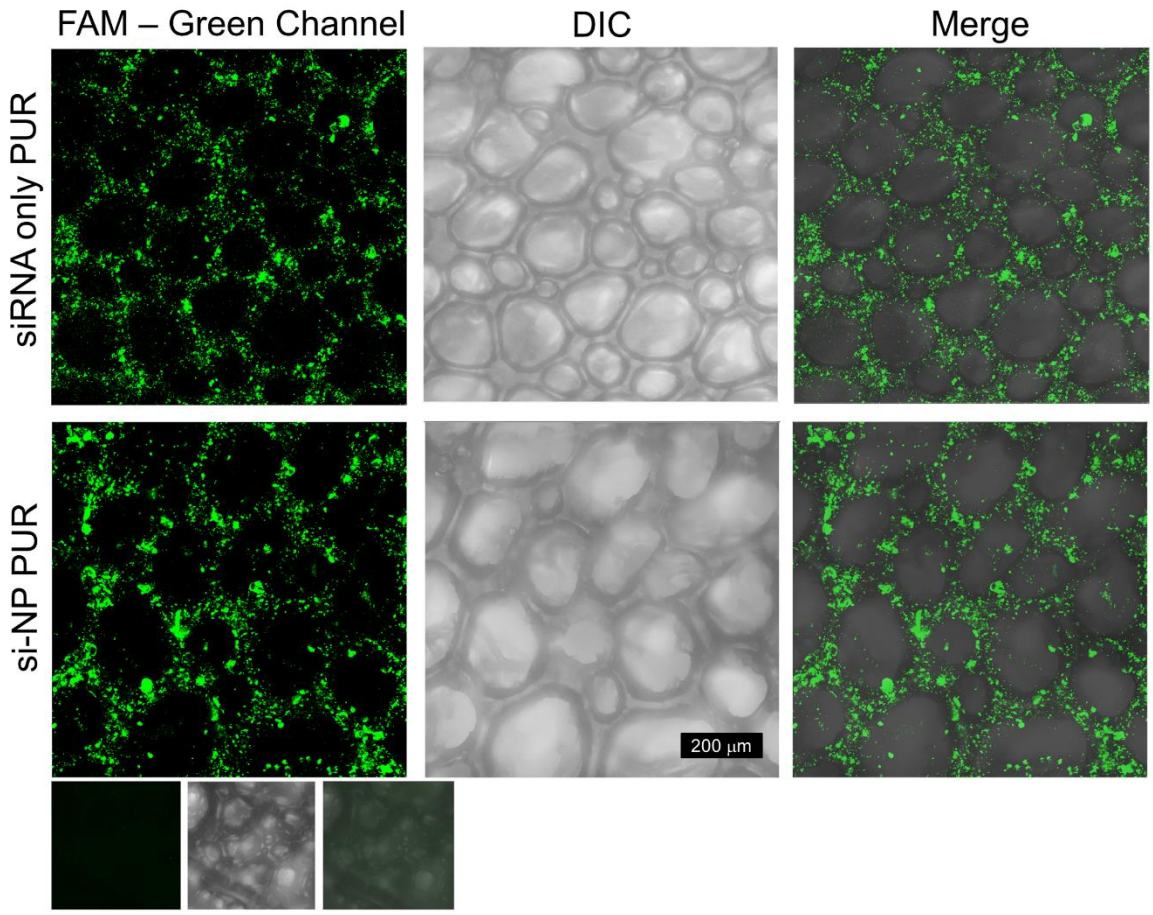

Fig 3.4 FAM-labeled siRNA and si-NPs distribution within the PUR scaffold. Comparison of fluorescent confocal images of PUR scaffolds loaded with FAM-labeled siRNA or si-NPs. Row 1 is a scaffold loaded with naked siRNA. Row 2 is a scaffold loaded with si-NPs. The 3rd row is an empty scaffold to verify that there is no green auto-fluorescence of the PUR scaffold. Note that scaffold pores contain no fluorescence, and the distribution between naked siRNA and si-NPs is similar.

Previous reports suggest that values of b < 0.75 indicate that Fickian diffusion is the dominant release mechanism [166, 247]. The values obtained from the best fit were found to be a=1.892, b=0.699, R^2=0.995 for siRNA only and a=0.317, b=0.560, with R^2 = .996 for si-NPs.

For additional evidence supporting diffusion-controlled release of siRNA, we performed a scaling analysis to compare the predicted and measured initial release rates. The Stokes-Einstein equation (Equation 3.2) and the Higuchi equation [249] (Equation 3.3) were utilized together to further validate the diffusion-controlled release mechanism. These equations, where D is the diffusivity, M_t is the rate of mass transfer, and r is the radius of the particle, provide relationships that allow the initial mass transfer rate to be related to the inverse of the square root of the radius of the solute:

$$Eqn\ 3.2: \qquad D \sim \frac{1}{r}$$

$$Eqn\ 3.3: \qquad M_t \sim \sqrt{D}$$

Assuming all conditions except hydrodynamic diameter are maintained constant between the two samples except yields the following scaling prediction:

$$Eqn\ 3.4: \qquad \frac{M_{siRNA}}{M_{si-NP}} = \frac{\sqrt{r_{si-NP}}}{\sqrt{r_{siRNA}}}$$

This analysis was completed assuming a hydrodynamic diameter of 2.56 nm for the siRNA, which was the value suggested by Barone et al for a 28 mer duplex RNA [250]. The hydrodynamic diameter of 38.69 nm that was experimentally determined using DLS for a charge ratio of 4/1 for si-NPs was used. Based on the measured initial release of 17% for si-NPs and 66% for naked siRNA, the left side of Eqn. 4 reduces to 3.88 and the right side 3.87. Thus the scaling analysis is consistent with the notion that the release of siRNA from the scaffolds is governed by Fickian diffusion.

Cytotoxicity experiments showed that the si-NPs were cytocompatible at the doses used (**Appendix Fig. A5**). Gene expression analyzed by qRT-PCR showed significant reduction ($p<0.05$) in mRNA levels for GAPDH mediated by releasate collected between 0-24h, 24-48h, and 48-96h, while controls containing scrambled siRNA showed no activity (**Fig. 3.6A**). Further experimentation showed that PUR-released si-NPs produced dose dependent silencing of

GAPDH expression with the highest dose of 50 nM producing approximately 50% gene knockdown (**Fig. 3.6B**) while freshly prepared si-NPs produced a dose dependent silencing with 83% reduction at 50nM. The finding that there was a strong correlation between dose and gene silencing, indicated a siRNA dependent effect, and importantly, scrambled siRNA controls had no observable activity. The microscopic observation of diffuse fluorescent siRNA in the cytoplasm of cultured cells confirmed the maintenance of endosomolytic behavior, cytoplasmic delivery, and bioactivity of the PUR-released si-NPs (**Fig 3.6C**).

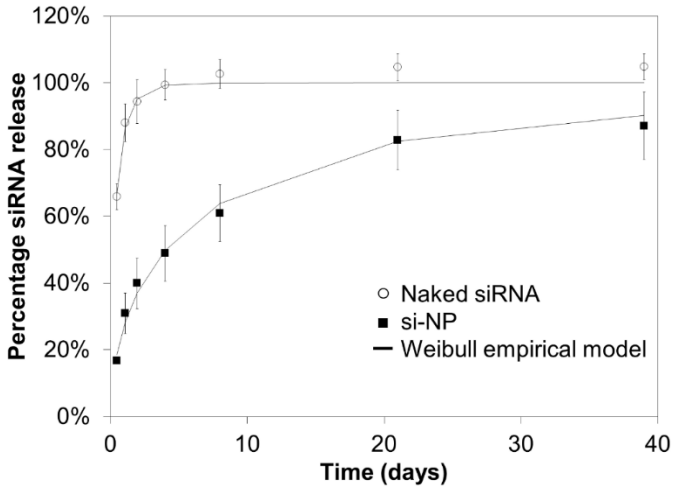

Fig 3.5 Release of siRNA and si-NPs from PUR scaffolds is diffusion controlled. The Weibull empirical model equation best-fit was determined and is overlaid here for each data set. Naked siRNA is rapidly released with an initial burst of over 60% at 12 h and is entirely released by 3 days. si-NPs have a slower rate of release with a burst release of less than 20% during the first 12 h, followed by sustained release that approaches 80% by 21 days.
PUR-released si-NP

3.4. Discussion

Technologies that enable the efficient and sustained delivery of siRNA are a high-impact but relatively unmet need. This is primarily due to the number and complexity of the delivery barriers that exist. Here, a new platform is presented that is capable of both sustained and effective delivery of siRNA from a PUR scaffold capable of providing a biocompatible and biodegradable tissue template that can be cured *in situ* using a clinically-translatable injectable formulation. Due to nuclease susceptibility and membrane impermeability of naked siRNA, little

success has been found with carrier-free siRNA delivery methodologies, and thus, the siRNA was first loaded into the pH-responsive micellar si-NPs prior to formulation with the biomaterial matrix.

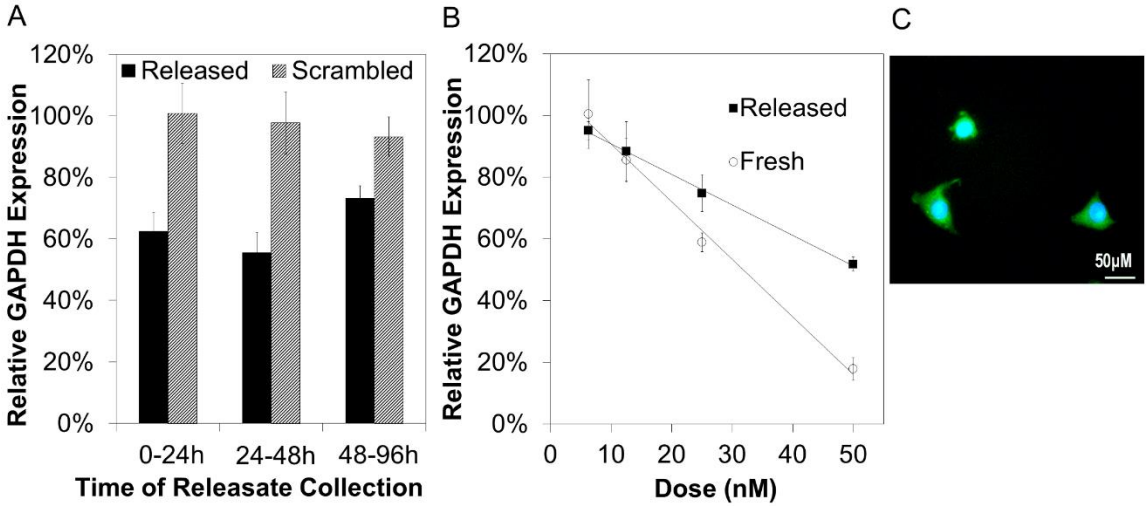

Fig 3.6 Fresh and released si-NPs are delivered intercellularly and mediate gene specific silencing. qRT-PCR was used to measure expression of the model gene GAPDH relative to β-actin and then normalized to no treatment controls. (A) Bioactivity of freshly prepared and PUR-released si-NPs collected during the defined time frames 0–24 h, 24–48 h, and 48–96 h indicates that bioactivity of si-NPs released from the PUR is not significantly altered over time. Statistical significance relative to scrambled control siRNA containing si-NPs was noted at all time points ($p < 0.05$). (B) Dose response of PUR-released si-NPs demonstrated a linear relationship ($R^2 = 0.999$) between siRNA dose and silencing activity, suggesting an siRNA-dependent gene silencing effect. Minor reduction in siRNA bioactivity was apparent in PUR-released si-NPs relative to fresh si-NPs. (C) Diffuse green fluorescence is noted in the cytoplasm of NIH3T3s after 4 h of incubation with PUR-released si-NPs. This presence of FAM-labeled siRNA in the cytoplasm confirmed effective siRNA cytoplasmic delivery.

The RAFT synthesized polymer shown in **Fig. 3.1A** is the basis for the si-NPs and was specifically designed for improved cytoplasmic uptake, siRNA protection, and endosome escape [23, 133]. Toxicity of typically-utilized polyplexes made with cationic polymers [251] and the limitations associated with inefficient bioactivity due to lysosomal degradation or extracellular clearance [252] motivated the development of the polymer. si-NPs are formulated at positive charge ratios (typically 4:1) providing a net positive charge which facilitates efficient cell uptake by most cell types [253, 254]. Once in the endosome, decreasing pH destabilizes the micelle structure due to protonation of PAA and DMAEMA monomers and exposes the membrane-disruptive core [255]. The configuration of the second block (**Fig. 3.1A**) is finely tuned to provide a sharp pH response at the desired pH by incorporating appropriate amounts of hydrophobic BMA

[256] and pH responsive DMAEMA and PAA. **Fig. 3.3B** confirmed the pH-dependent micelle destabilization using DLS and it is hypothesized that this destabilization allows the hydrophobic 2nd block to penetrate and disrupt endosomal membranes and facilitate siRNA delivery to the cytoplasm [107, 130, 257, 258]. Once internalized, siRNA may be competitively dissociated from the polymer through interactions within the cytoplasm by other ionic molecules [253] thus gaining access to the RNAi machinery in the cytoplasm.

Recently, biomaterials have been pursued for sustained siRNA delivery, with natural materials such as alginate, collagen and agarose being mostly used in these applications due to their biocompatibility [19-22]. However, these natural materials generally lack tunability and have been limited to rapid burst release of siRNA. The best sustained delivery to date has been achieved using PCLEEP nanofiber scaffolds, however, the manufacture of the scaffold requires complex equipment (electrospinning apparatus) and must be pre-made to a defined size and geometry [193]. Therefore, there still remains a significant need for a more clinically translatable biomaterial that can conform to tissue defects of varied sizes and shapes where it will cure *in situ* and deliver siRNA locally in a sustained manner.

PUR scaffolds provide multiple advantages as a biomaterial for controlled drug delivery to tissue defects for several reasons. PUR scaffolds can be easily adapted to be injectable making clinical use easier and requiring no additional fabrication equipment [168, 169]. After injection, PURs react *in situ* to form a biocompatible and biodegradable tissue scaffold with inter-connected pores that effectively serves as a template for cell influx and tissue formation and remodeling [24]. The mechanism of degradation includes hydrolytic degradation (on the order of months) and macrophage-mediated oxidative degradation by reactive oxygen species (ROS) secretion (on the order of weeks) that is ideal for the timescale of wound healing [25]. Finally, PUR has been shown to deliver biologics efficiently, typically delivering as much as 80% of the payload [24, 165, 166]. However, a previous study has reported that 50-μm PLGA microspheres with rhPDGF bound to the surface supported <10% release over 21 days, suggesting that primary amines in the protein

reacted with the polyisocyanate, resulting in loss of activity [24]. The present study has confirmed for the first time that nanoparticulate carriers incorporated in reactive PUR scaffolds support high-efficiency, diffusion-controlled release as seen in **Fig. 3.5**. The release data demonstrates cumulative release of si-NPs approaching 80% over 21 days compared to naked siRNA which was released rapidly, approaching 100% delivery of the payload in three days. The mechanism of release for both free siRNA and si-NPs was found to be diffusion-controlled based on the Weibull model. Further, scaling analysis with the Stokes-Einstein and Higuchi equations demonstrated that the initial release rates of siRNA and si-NPs scales appropriated to the hydrodynamic diameter of the solute. The diffusion-based release suggests that an additional level of control exists by altering si-NP diffusivity in the PUR matrix to tune the rate of release by varying the nanoparticle size.

It is hypothesized that, in many applications, sustained delivery of siRNA into tissue defects will be ideal for producing a therapeutic effect since siRNA produces relatively transient gene silencing activity [259]. It is hypothesized that when the formulation tested here is translated *in vivo*, the initial burst release will establish gene silencing while the continual, slower siRNA delivery over the next few weeks will sustain the initial effect over a few weeks. Importantly, several approaches exist for tuning PUR-based drug delivery to be more rapid or more sustained [165].

Fig. 3.6A demonstrates that the activity of released NPs is not significantly reduced over the time frames tested (0-24, 24-48, 48-96 hours). Sustained delivery of active complexes is critical to compensate for transiency of siRNA in a highly proliferative environment (i.e. tissue regeneration). **Fig. 3.6B** demonstrates that the siRNA-mediated reduction in GAPDH of PUR-released si-NPs is dose dependent. However, it is evident that there is partial loss of bioactivity post-release from the scaffold compared to fresh si-NPs. It is possible that this reduction in silencing is due to reorganization of the micelle structure or a partial si-NP aggregation during lyophilization and incorporation into the PUR. There was a detectable difference in size revealed

by TEM and DLS (**Fig. 3.2**) of fresh micelles versus PUR-released micelles, and the □□potential of PUR-relesate si-NPs was also found to be reduced. It could also be possible that unreacted components in the PUR specifically adsorb to the surface of the released si-NPs, thereby reducing the ζ-potential of the si-NPs resulting in aggregation. Our unpublished data have shown that 1-2% of the PUR mass leaches from the reactive material during the first 45 minutes of cure when incubated in serum medium. The primary components in the leachates include polyester triol, dipropylene glycol, and triethylene diamine. Hydrolytic degradation of the cured scaffolds releases α-hydroxy acids [25], which could bind electrostatically to the positive surface of the si-NPs. However, further studies will be necessary to better understand and overcome the alteration of the si-NPs during processing, and excipients such as agarose and sucrose may provide one route for improving their stability during lyophilization [260].

3.5. Conclusions

Injectable poly(ester urethane) foams were successfully utilized for sustained release of bioactive si-NPs for an extended period of 21 days. The si-NPs synthesized using RAFT were found to remain intact and bioactive following incorporation into and release from PUR scaffolds, although changes in si-NP size and bioactivity were evident relative to fresh si-NPs. As a platform technology, the combination of PUR scaffolds and pH-responsive micellar siRNA carriers provides a logical approach to basic scientific studies of long-term siRNA-mediated gene silencing at local, pathological or healing tissue sites. The described system also has the potential to be applied to control cell phenotype and fate in tissue constructs developed *in vitro*. Finally, as a therapeutic, the described approach may be applied to reduce expression of deleterious genes and improve regeneration in tissue defects.

Chapter 4

Aim 2 – In vivo development of siRNA platform

Aim 3 – Silencing of PHD2 Promotes Angiogenesis *in Vivo*

Text for Chapter 4 taken from:

> **Nelson CE**, Kim AJ, Adolph EJ, Gupta MK, Yu F, Hocking KM, Davidson JM, Guelcher SA, Duvall CL. Tunable Delivery of siRNA from a Biodegradable Scaffold to Promote Angiogenesis *in Vivo.* Advanced Materials. *Early View.* DOI: 10.1002/adma.201303520 .

4.1 Introduction

Clinical translation of siRNA-based therapies has been hampered by delivery barriers, including siRNA susceptibility to nuclease degradation, cell and endosomal membrane impermeability, and inability to achieve sufficient and sustained bioactivity at the target site [230, 261]. Numerous nanotechnological and medicinal chemistry strategies have been tested to enhance the pharmaceutical properties of siRNA [27], and most of the recent focus has been on delivery of siRNA for cancer and liver targets, with the latter motivated by the fact that many intravenously-administered nanoparticles nonspecifically biodistribute to the liver. Tremendous progress has been made toward systemic delivery applications, and promising clinical data has begun to appear [16, 262]. However, there is a significant, unmet need for clinically-translatable platform technologies that enable controlled and efficient *in vivo* delivery of small interfering RNA (siRNA) to therapeutically silence expression of disease-related genes [12]. The use of siRNA-based strategies in regenerative medicine and tissue engineering is a relatively understudied but promising application of RNA interference (RNAi). Topical delivery has been pursued clinically: for example, delivery to the eye for macular degeneration [226], to the lung for RSV [14], and to the skin for pachyonychia congenita [227]. A primary limitation to topical delivery for regenerative applications is that siRNA has a relatively short half-life, especially in rapidly dividing cells (i.e., representative of regenerating tissue), where the maximum silencing effect has been noted to be at two days post-transfection [17], with gene silencing bioactivity being exhausted by one week

[18]. In one successful approach, agarose hydrogels containing siRNA packaged with Lipofectamine 2000 was found to produce potent siRNA silencing *in vivo*. However, this commercial transfection reagent is optimized for *in vitro* use, and rapid diffusion out of the hydrogel or loss of activity of the lipoplexes necessitates multiple applications [21, 22, 171]. Other natural biomaterials such as alginate, collagen, and agarose have also been applied as depots for local delivery of siRNA [19, 20]. Other hydrogel and microparticle depots have been developed to achieve sustained, local delivery of siRNA intratumorally and at sites of inflammation [170, 173, 175, 191], though none of these applications provided controlled siRNA delivery from a biomaterial scaffold that promoted host cell infiltration and tissue regeneration.

More recently, biodegradable, synthetic scaffolds developed toward applications in regenerative medicine have demonstrated controlled and sustained siRNA delivery *in vitro* (i.e., ranging 20-50 days of release *in vitro*), including prefabricated ε-caprolactone and ethyl ethylene phosphate copolymer (PCLEEP) nanofibers [193], poly(lactic-co-glycolic acid) (PLGA) nanofibers [194], and our porous polyester urethane (PEUR) scaffold design [181]. These classes of porous tissue scaffolds have the advantages of being easily tunable and of being adaptable for filling critically-sized defects with biodegradable templates that promote new tissue in-growth. PEUR scaffolds have been shown to promote regeneration in both excisional cutaneous wounds and bone defects and have desirable properties, including the potential for injectable delivery of components that form a porous scaffold in situ, degradability into biocompatible products at rates dictated by the composition of the polyester triol and the isocyanate, and controlled release of growth factors and other therapeutic agents [24, 25, 165, 177, 178, 263]. We recently adopted PEUR scaffolds for delivery of siRNA-loaded polymeric nanoparticles [181], and the current report showcases the ability of this platform to achieve a high level of gene silencing efficiency and tunability *in vivo*, along with a proof of concept application of this delivery platform for enhancement of angiogenesis within tissue defects.

4.2 Results and Discussion

Polymeric nanoparticles with pH-dependent endosomal escape behavior have been shown to enhance siRNA intracellular bioavailability [23, 124, 264]. To leverage this efficient delivery approach, siRNA loaded nanoparticles were made from the diblock copolymer poly[$DMAEMA_{71}$-b-(BMA_{103}-co-PAA_{68}-co-$DMAEMA_{57}$)] (**Fig. 4.1A**, Mn=43kDA, PDI = 1.41), which was synthesized using reversible addition-fragmentation chain transfer (RAFT). RAFT is a controlled radical polymerization technique amenable to biomedical applications because it enables synthesis of monodisperse and well-defined polymers with block or other architectures and telechelic end chemistries that provide opportunities for site-specific bioconjugation [241, 242, 248, 265]. Poly[$DMAEMA_{71}$-b-(BMA_{103}-co-PAA_{68}-co-$DMAEMA_{57}$)] was self-assembled into siRNA loaded micellar NPs (si-NPs, D_h = 39.6±12.6 nm, ζ-potential = +20.2 mV) that had been optimized for pH-dependent membrane disruption tuned for endo-lysosomal escape [23, 133] (**Appendix Fig. A6**). Trehalose (0, 1.25, 2.5, 5 wt% of PEUR denoted as 0T, 1.25T, 2.5T, and 5T respectively) was added to samples of si-NPs to optimize the stability through lyophilization [266] and to act as a porogen in the cured PEUR scaffolds. Lyophilized si-NPs samples with varied quantities of trehalose were resuspended into polyester triol prepolymers (**Fig. 4.1B**) and fabricated into scaffolds through a reactive foaming process with lysine triisocyanate (LTI) or hexamethylene diisocyanate trimer (HDIt) (**Fig. 4.1C**).

The scaffolds were then incubated in PBS to trigger diffusion of si-NPs from the PEURs in order to assess the physicochemical properties and bioactivity of the released si-NPs. Analysis of the supernatants revealed that si-NPs released from the PEUR scaffolds were similar to freshly-made si-NP samples in terms of size and ζ-potential, suggesting that no aggregation or destabilization occurred during scaffold formation (**Fig. 4.1D**). Confocal microscopy of mouse embryo fibroblasts (NIH3T3s) treated with scaffold-released si-NPs with cy5.5-labeled siRNA demonstrated that there was a similar level of uptake and intracellular staining pattern relative to NIH3T3s treated with an equivalent concentration of freshly prepared si-NPs (**Fig. 4.1E**).

Likewise, the gene silencing dose response from scaffold-released si-NPs loaded with siRNA against the model gene peptidylpropyl isomerase B (PPIB) was statistically equivalent to that achieved with freshly made si-NPs (**Fig. 4.1F**). Addition of the excipient trehalose and preparation/lyophilization of si-NPs in dH_2O rather than salt-containing PBS prior to incorporation into PEUR scaffolds improved stability of the si-NPs during scaffold fabrication. Stabilization of si-NP physicochemical properties was also functionally significant in terms of bioactivity and resulted in improved bioactivity relative to our previous *in vitro* studies where the released si-NPs (lyophilized in salt-containing PBS) were larger in size, had lower ζ-potential, and suffered from a 33% reduction in gene silencing relative to freshly made si-NPs (**Fig. 4.1D**) [181].

PEUR scaffolds were next cured as cylinders containing si-NPs loaded with FAM-labeled 23-mer double stranded DNAs (a model for siRNA) and 0, 1.25, 2.5, and 5 wt% trehalose relative to the mass of the polyurethane precursors. SEM imaging of the scaffolds demonstrated interconnected pores necessary for si-NP release and cell infiltration (**Fig. 4.1 G-J**), and confocal microscopy revealed homogenous loading of the si-NPs throughout the scaffolds (**Fig. 4.1K-N**). The kinetics of si-NP release from the scaffolds were monitored using fluorescence. The rate of si-NP release was dependent on the quantity of trehalose in the scaffold (**Fig. 4.1O**). Trehalose can act as a stabilizer and a porogen [267], and with this system, the release rate of the si-NPs correlated to the quantity of trehalose present. Trehalose is hydrophilic and microdomains of trehalose rapidly dissolve upon exposure to water creating microchannels that accelerate NP diffusion through the scaffold. The effects of the isocyanate chemistry were also assessed, and the si-NP release rate was measured with PEUR scaffolds made from both LTI and HDIt, the latter being more hydrophobic and is known to degrade more slowly [25, 169]. For *in vitro* tests, the diffusivity of the si-NPs was lower in the PEUR scaffolds made with HDIt than LTI scaffolds. This property increased the versatility and provided an additional level of control for this system for *in vitro* siRNA delivery (**Fig 4.1P**). Modeling with the Weibull function [247] showed that the release mechanism could be characterized as diffusion-controlled in all cases (**Appendix Table A2 and A3**).

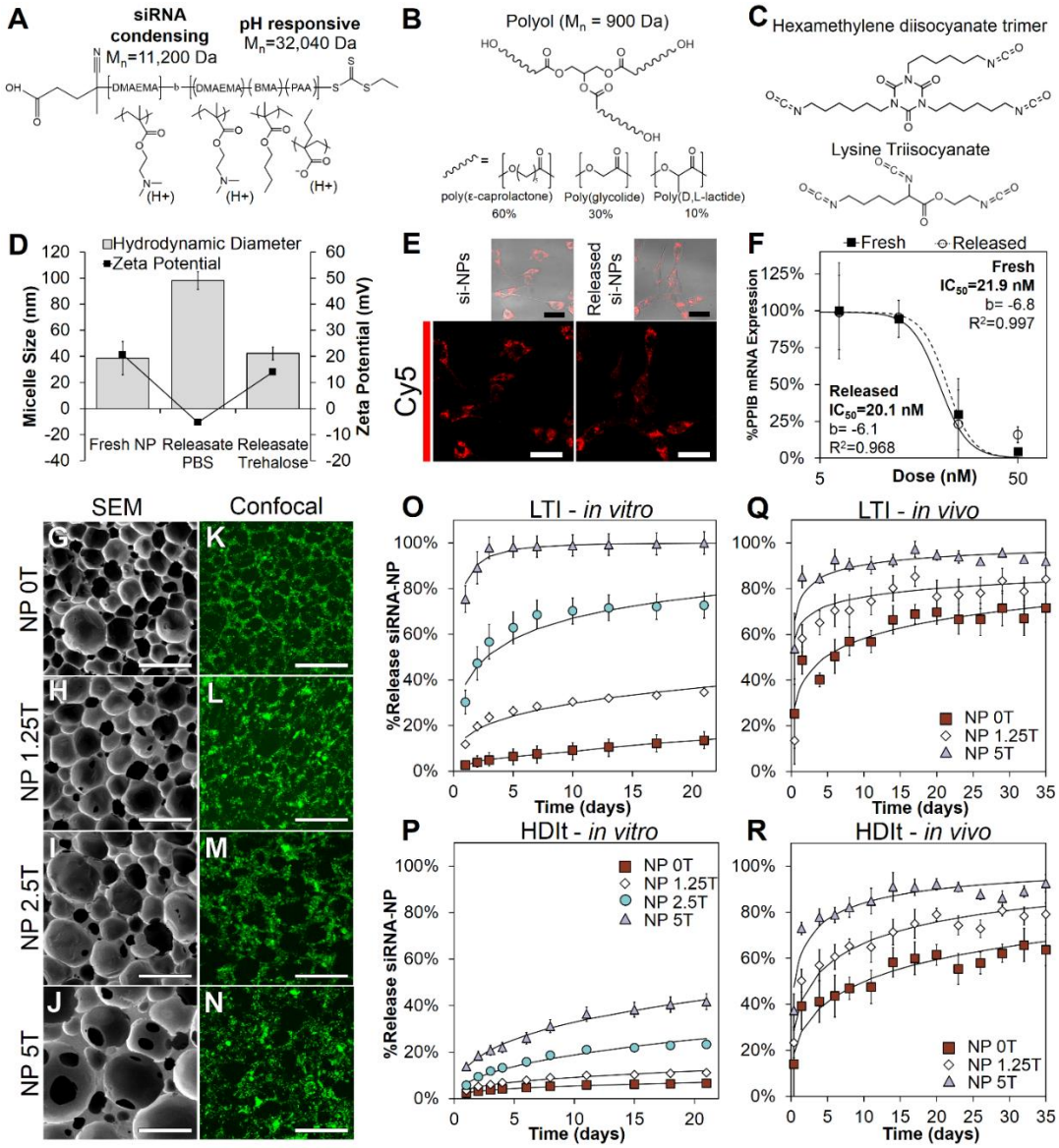

Fig 4.1 Material synthesis and characterization of the PEUR scaffold si-NP delivery platform. A) The structure of the diblock copolymer developed previously[30] contains an siRNA condensing block composed of DMAEMA and a pH-responsive block composed of a copolymer of DMAEMA, BMA, and PAA. B) The polyester alcohol (polyol or triol) that was used in the synthesis of polyurethanes were composed of copolymers of poly(ε-caprolactone), poly(glycolide), and poly(D,L-lactide). C) Isocyanate-containing crosslinking components used for PEUR formation included hexamethylene diisocyanate trimer (HDIt) and lysine triisocyanate (LTI). D) The excipient trehalose stabilized the size and ζ-potential of released si-NPs compared to si-NPs prepared in PBS. E) PEUR scaffold-released si-NPs deliver siRNA into the cytoplasm of cells *in vitro* similar to freshly prepared si-NPs (scale = 30μm). F) Gene silencing activity was similar in PEUR scaffold-released si-NPs compared to freshly-made si-NPs as revealed by RT-PCR IC_{50} analysis of target gene expression (p=NS). G-J) SEM images of PEUR scaffolds (LTI-based materials shown) containing varying weight% of trehalose (5% by weight is 5T) demonstrate the porous scaffold architecture (Scale = 300μm). K-N) Maximum intensity projections from confocal microscopy showed homogenous loading of si-NPs into the scaffold (note dark areas correspond to pores, scale = 300μm). O-P) Temporal release profile of si-NPs from PEUR scaffolds *in vitro* demonstrated diffusion controlled release (characterized by Weibull model) that could be modulated through varying the concentration of trehalose or alteration of the isocyanate chemistry. Q-R) The rate of release of si-NPs *in vivo* was increased relative to the release *in vitro* but was also tunable based on varying the concentration of the excipient trehalose.

To measure release kinetics *in vivo*, PEUR scaffolds were synthesized containing si-NPs made with cy5-labeled siRNA (description in Appendix B). The scaffolds were implanted subcutaneously in balb/c mice, and the temporal release profile was characterized *in vivo* through fluorescence imaging with an IVIS200®. Release of si-NPs from the PEUR scaffolds was faster *in vivo* relative to *in vitro* (**Fig. 4.1Q-R, images in Appendix Fig. A7**), which may be attributable to both increased mechanical forces and cell-mediated effects on the scaffold (i.e. oxidative degradation) [25]. Similar to the *in vitro* studies, the *in vivo* release kinetics were tunable based on the quantity of trehalose added, and the release mechanism was found to be diffusion-controlled based on the Weibull model (**Fig. 4.1O-R, black line**). **Table 4.1** reports the time that it took for each formulation tested to release 50, 60, or 75% of the total payload in vivo. ANOVA analysis showed that isocyanate chemistry was a significant predictor of release kinetics when this variable was tested across all of the scaffold formulations ($p<0.05$). This analysis suggests that the through the right combination of isocyanate and trehalose concentration, a variety of release profiles are available, which provides a significant advantage for *in vivo* applications. Relatively long-term release has been achieved *in vivo* using biodegradable hydrogel depots [174] but no previous platform has demonstrated locally-sustained siRNA release for several weeks and an ability to finely tune the release kinetics *in vivo* from a tissue scaffold that promotes cell infiltration and regeneration. Reports on regenerative scaffolds including PCLEEP nanofibers, PLGA nanofibers, and porous PEUR have been applied to achieve sustained release *in vitro* [181, 193, 194], but tunability and *in vivo* validation were not achieved. The current platform provides the unique capability to match siRNA delivery to the time course of expression of a target gene and to tune the system so that siRNA release, scaffold degradation, and cell/tissue infiltration can be temporally aligned in order to optimize tissue regeneration.

Table 4.1 Days of release required for 50%, 60%, and 75% release to be reached

Group	Formulation	50% (days ± SE)	60% (days ± SE)	75% (days ± SE)
1	LTI – 0T	4.67 (±1.46)[4,6]	10.57 (±2.94) [4,6]	45.27[a]
2	LTI – 1.25T	2.89 (±0.37)[4,6]	5.41 (±4.97)[4]	7.73(±6.86)[3]
3	LTI – 5T	0.07[a]	0.21[a]	1.16(±0.31)[2,5,6]
4	HDIT – 0T	10.09(±5.17)[1,2,5,6]	20.86(±2.81) [1,2,5,6]	61.27[a]
5	HDIT – 1.25T	2.90(±1.32)[4]	6.16(±2.31) [4]	18.83(±7.49)[3]
6	HDIT - 5T	0.52(±0.17)[1,2,4]	1.21(±0.13) [1,4]	4.30(±1.83)[5]

[a] Extrapolated from Weibull model [b] Superscripts denote significance ($p<.05$) to the designated group

Dicer substrate siRNA (DsiRNA, see description with **Appendix Table A1**) designed against the model gene PPIB was used to form si-NPs that were incorporated into PEUR scaffolds made with the "slow" release LTI formulation (0T in **Fig 4.1O**). The PPIB si-NPs efficiently reduced target gene expression within the subcutaneously implanted scaffolds, with 82%, 95%, 83% gene silencing achieved at days 5, 12, and 21, respectively (**Fig 4.2A**). Importantly, PEUR scaffolds loaded with si-NPs containing a scrambled sequence of DsiRNA showed no significant gene silencing at any time point relative to control scaffolds containing no si-NPs. This remarkable gene silencing was achieved with a relatively low dose of 200 μg DsiRNA/kg of mouse (300 pmol total dose). Next, the dose response behavior using this 0T LTI PEUR scaffold was thoroughly characterized at day 12. This study revealed a low IC_{50} of 41.8 μg/kg (mass siRNA / mass mouse; total dose of 62.7 pmol, **Fig 4.2B**) calculated from a 4-parameter model (**Appendix Equation A2**). The potency and sustained action of siRNA with this system compares favorably with other recent regenerative applications of siRNA *in vivo*, for example, agarose depots loaded with 20 pmol siRNA achieved 76% knockdown of the target gene p53 at day 10, but this required 2 repeated applications and use of the commercial transfection reagent Lipofectamine 2000 to improve cell uptake [21]. Tissue regenerative siRNA delivery applications *in vivo* using synthetic biomaterials are limited, but a recent report using poly-D,L-lactic acid-*p*-dioxanone-polyethylene

glycol block co-polymer (PLA-DX-PEG) pellets implanted into mouse dorsal muscle pouches served as a depot for the delivery of relatively high doses of 10 - 30 nmol siRNA per site and achieved ~75% gene silencing at day 1 that was sustained for 7 days, with ~50% silencing at day 7 [192]. The current scaffold based approach provided longer-term gene silencing with a 100-fold lower siRNA dose, while also providing a porous template that promotes tissue regeneration.

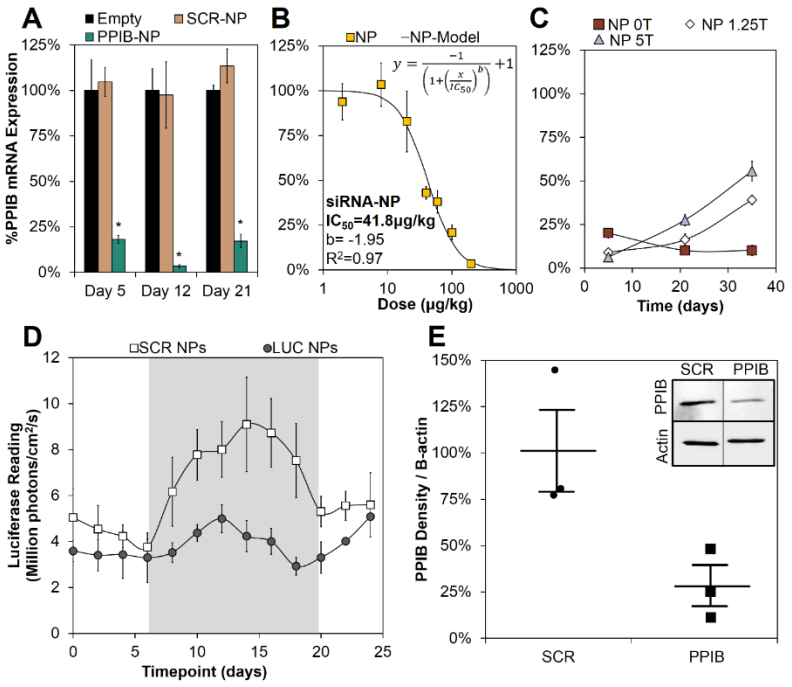

Fig 4.2 The si-NP-loaded PEUR scaffolds provide a potent and temporally-tunable gene silencing platform. A) PPIB mRNA was significantly silenced by siRNA-NP-PEUR at day 5, 12, and 21 ($p<0.002$ for all groups, n=4) in subcutaneous implants in mice at a siRNA dose of 200µg/kg. B) A dose response at day 12 demonstrated a low IC50 for siRNA-NP-PEUR of 41.8 µg/kg C) The temporal gene silencing profile was tuned through the use of trehalose to control release kinetics (day 5 $p<.0005$ 0T vs 5T, day 35 $p<.0005$ 0T vs 5T). D) Western blotting for PPIB at day 12 showed significant protein reduction in PPIB siRNA loaded scaffolds (n=3, $p<.05$). E) A longitudinal study demonstrated significant luciferase reduction over the time course of wound healing, highlighted in gray, in a COL1A2 luciferase reporter mouse model ($p<.01$, n=5).

Next, the correlation between si-NP release kinetics and the resulting time course of gene silencing was tested. For the LTI-based PEUR scaffolds, the fast releasing 5T formulation resulted in 94% PPIB silencing at day 5, compared to 80% for the slower release 0T scaffolds ($p<0.005$). However, the faster releasing 5T scaffolds had a more transient gene silencing effect and produced 45% PPIB silencing at day 35 compared to the slower releasing 0T scaffolds which produced 90% silencing at 35 days ($p<0.0005$). A similar analysis was performed for HDIT as reported in **Appendix Fig. A8**, and the results showed a similar correlation between si-NP release kinetics and the temporal gene silencing profile. To further validate our measurements,

knockdown of PPIB protein from scaffold explants at day 12 was evaluated (200 μg DsiRNA/kg mouse, 0T/LTI). As shown in the western blot in the inset (**Fig. 4.2E**) approximately 75% less PPIB protein was detected ($p<0.05$). The combination of low dose, sustained silencing effect, and tunability achieved here is unprecedented for *in vivo* delivery of siRNA from a regenerative tissue scaffold. The potency of our system may have been enhanced by direct, substrate-mediated transfection of si-NPs into cells migrating into the cell-inductive PEUR scaffold. For example, high local concentration of plasmid DNA, achieved through immobilization onto the surface of materials, has been shown to increase transfection efficiency 10-100 fold relative to plasmid polyplexes freely diffusing within the cell's surroundings [182-184]. This uptake mechanism mimics the pathway hijacked by viruses that attach to extracellular matrix proteins to enhance their rate of cellular internalization [185, 186].

Transgenic mice with a collagen α-2(I) chain (COL1A2) luciferase reporter were next utilized to assess the ability of the si-NP-PEUR platform to effectively silence a wound-related gene throughout the entire time course of healing. The COL1A2 reporter is upregulated between approximately days 7-14 in mouse incisional and laser irradiated wounds [268, 269]. A COL1A2 luciferase reporter mouse model was used to allow a longitudinal, quantitative, and protein-level readout of luciferase silencing using intravital bioluminescence imaging. The mice received subcutaneously-implanted PEUR scaffolds (OT, LTI) containing si-NPs loaded with DsiRNA against luciferase or a scrambled control sequence. In the control animals, the activity of the COL1A2 reporter was elevated between approximately days 8-20 post-wounding (highlighted in gray) (**Fig. 4.2D**). However, incorporation of luciferase DsiRNA maintained the local luciferase activity at approximately baseline levels, and there was a significant reduction in luciferase activity in these scaffolds relative to scaffolds containing si-NPs loaded with scrambled siRNA ($p<0.01$, $n=4$). The efficient and sustained gene silencing achieved throughout the full time course of wound healing suggests that this platform can be utilized to abrogate the function of a therapeutic target gene throughout the healing process.

To exclude a nonspecific biological response to the si-NPs, histology of tissue explants and PCR against signal transducer and activator of transcription factor 1 (STAT-1, a readout for TLR activation [270]) and tumor necrosis factor α (TNFα) was performed. Histology revealed that there was no inflammation or toxicity associated with incorporation of the si-NPs into the PEUR scaffolds (**Appendix Fig. A9**), and PCR for STAT-1 and TNFα showed that the si-NPs did not increase these inflammatory markers relative to empty scaffolds (**Appendix Fig. A10**).

Prolyl hydroxylase 2 (PHD2) activity triggers degradation of the pro-angiogenic transcription factor hypoxia inducible factor 1α (HIF1α) during normoxia. When PHD2 is naturally inactivated (i.e., under hypoxic conditions) or silenced through RNAi, HIF1α mediates transcription of pro-angiogenic genes such as vascular endothelial growth factor (VEGF), fibroblast growth factor 2 (FGF-2), and others [271]. To demonstrate the therapeutic potential of our platform for promoting tissue regeneration, si-NPs were formulated with PHD2 DsiRNA (PHD2-NPs or scrambled siRNA (SCR-NP) and incorporated into PEURs scaffolds that were implanted subcutaneously. At 14d, PCR revealed an ~80% reduction in PHD2 levels (**Fig. 4.3A**) which resulted in a ~200% increase in VEGF and ~300% increase in FGF-2 mRNA levels. For an evaluation of neovessel formation with the scaffolds, immunohistochemistry (IHC) for CD31 was done at 14d and 33d, and development of stable, functional vascular structures was imaged and quantified using micro-CT following systemic vascular perfusion with a contrast agent at 33d. CD31 IHC showed visually increased vessel density in PHD2-NP-containing scaffolds (**Fig. 3B)** and a significant, 280% increase in vessel area at day 33 (**Fig. 4.3C-D**). Scaffolds characterization with micro-CT provided quantitative histograms that demonstrated that PHD2-NPs increased both number and size of vessels within the scaffolds (**Fig. 4.3E,** representative images in **Fig. 4.3F**). Quantitative 3D image analysis [272] showed that PHD2-NPs increased the vascular volume by 300% and increased the mean vascular thickness by 137% (**Fig. 4.3G**). These data convincingly demonstrate the regenerative potential of this platform, as formation of robust, mature vessels is one of the primary challenges in tissue regeneration. We anticipate that sustained RNAi-induced

modulation of transcription factors, such as HIF1α, that control groups of related genes has the potential to produce better-orchestrated and more robust effects on tissue regeneration compared to delivery of a single growth factor (e.g., VEGF of FGF), which is the current standard. For example, VEGF has had limited therapeutic success because it produces immature vessels that suffer from instability and poor long-term function [273].

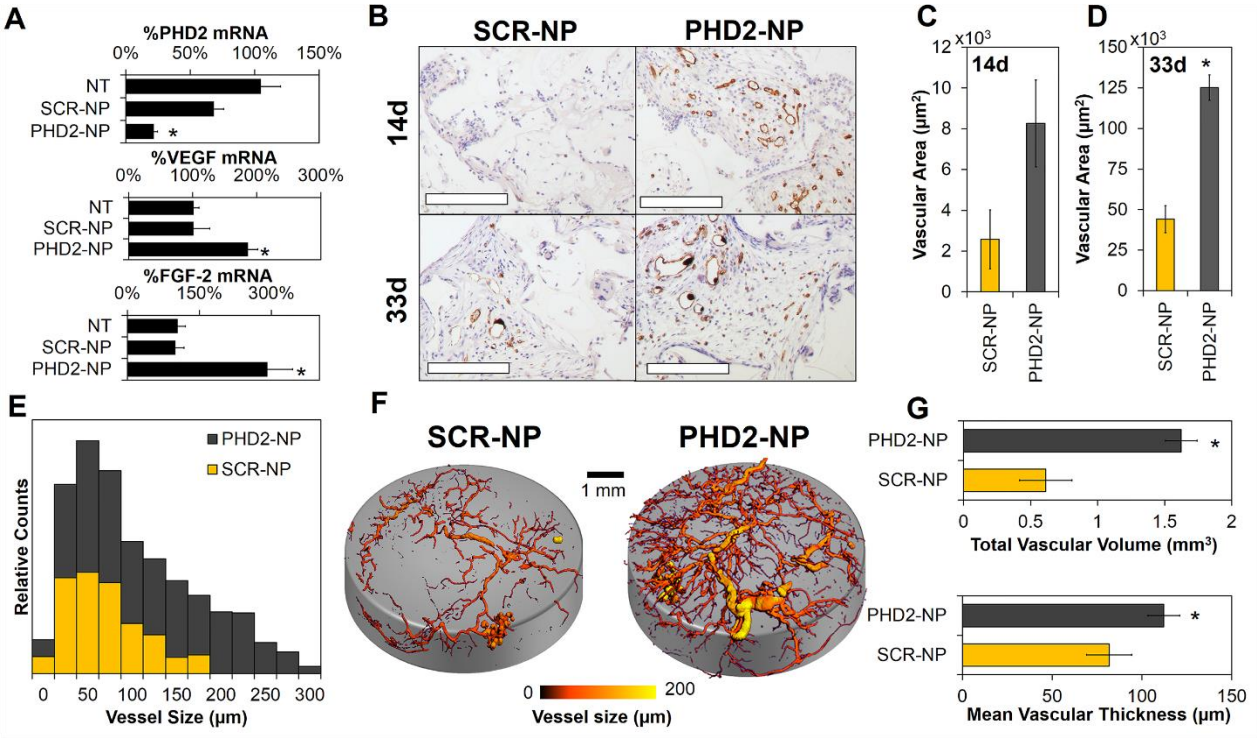

Fig 4.3. **Sustained silencing of PHD2 increases angiogenesis within PEUR tissue scaffolds**. A) 80% silencing of PHD2 increased VEGF and FGF-2 expression by 200% and 290% respectively (*p<0.01). B) CD31 staining was significantly increased within PHD2 scaffolds at day 14 and day 33 (Scale = 200 µm, vessels appear read, nuclei are counterstained purple with hematoxylin, and white space represents residual PEUR scaffold). C-D) CD31 sections were quantified showing a significant increase in vessel area at day 33 (*p<0.01). E) Micro-CT of explanted PHD2-NP scaffolds showed a significant increase in both vessel number and vessel size for PHD2-NP scaffolds as shown in the histogram. F) Micro-CT images visually demonstrate the increased vasculature within the scaffolds. G) Quantitative analysis of 3D micro-CT vessel images revealed a significant increase in vascular volume and mean vascular thickness within PHD2-NP-loaded scaffolds.

4.3 Conclusions

This study validates that si-NP delivery from tissue inductive PEUR scaffolds provides a new, tunable platform technology for efficient, local gene silencing. The *in vitro* and *in vivo* data suggest that this platform is highly versatile for siRNA delivery *in vitro* or *in vivo* through tuning the quantity of trehalose added during PEUR scaffold fabrication and by alteration of the chemistry of the isocyanate. This provides the opportunity to tune this delivery system based on the desired expression profile of the therapeutically targeted gene or to optimally match rates of scaffold degradation, tissue growth, and siRNA delivery. PHD2 silencing studies demonstrated that this platform can promote angiogenesis *in vivo*. These proof-of-concept data validate that this platform provides a powerful research tool and also represents a technology with the potential to be utilized therapeutically for manipulation of genes whose silencing promotes tissue regeneration.

4.4 Experimental Section

si-NP synthesis and characterization

Dicer substrate siRNAs (DsiRNAs) were obtained from IDT and screened *in vitro* for activity before use *in vivo*. A diblock copolymer composed of 2-(dimethylamino)ethyl methacylate (DMAEMA), 2-propylacrylic acid (PAA), and butyl methacrylate (BMA) was synthesized using reversible addition-fragmentation chain transfer (RAFT) polymerization as described previously [23, 181]. NPs were fabricated by dissolving in ethanol, followed by slow addition of dH_2O, which spontaneously triggered formation of micelles. Subsequently, siRNA was electrostatically loaded onto the surface of NPs. Dynamic light scattering (DLS, Zetasizer nano-ZS Malvern Instruments Ltd, Worcestershire, U.K.) was used to analyze size and zeta potential of the si-NPs.

si-NP-PEUR synthesis and characterization

The polymeric NPs (1mg) were mixed with siRNA (5 nmol, 0.08mg) in an RNAse free polypropylene tube and allowed to electrostatically condense for 30min. Trehalose was added to the si-NPs at varying concentrations from 0 to 5 wt% of PEUR and allowed to stabilize for 30 min. The solutions were frozen and then lyophilized. Lyophilized si-NP samples were suspended into a 900 Da polyester triol with a backbone comprised of 60 wt% ε-caprolactone, 30 wt% glycolide, and 10 wt% D,L-lactide. PEUR scaffolds were synthesized by reacting 67 µmol of the polyol component of PEUR with a slight excess of lysine triisocyanate (LTI, 193 µmol, 35mg) in the presence of 67 µmol water. The water reacts with the isocyanate to produce CO_2 and serves as a blowing agent that creates the pores within the scaffold. The polyol and LTI were mixed using a Hauschild DAC 150 FVZ-K SpeedMixer (FlackTek, Inc., Landrum, SC). Alternatively, 42 µmol of polyol was reacted with a slight excess of hexamethylene diisocyanate trimer (HDIt, 111 µmol) in the presence of 63 µmol of water.

The resulting 100mg PEUR foams were sectioned into 6mm diameter x 1 mm thick discs and imaged with a fluorescent confocal microscope (Zeiss LSM 710 Meta Oberkochen, Germany) to analyze the distribution of fluorescently labeled si-NPs in the scaffold. Scaffold morphology was assessed with a scanning electron microscope (SEM Hitachi S4200, Tokyo, Japan) for structure and porosity. PEUR scaffolds were immersed in PBS, and releasate was collected and quantified using fluorescence for percent release. Released si-NPs were incubated on NIH3T3 mouse embryo fibroblasts at varying concentrations that were imaged with a fluorescent confocal microscope (Zeiss LSM 710 Meta) and measured for gene silencing by RT-PCR.

Subcutaneous Implant of si-NP-PEUR

The animal studies were conducted with adherence to the guidelines for the care and use of laboratory animals of the National Institutes of Health (NIH). All experiments with animals were approved by Vanderbilt University's Institutional Animal Care and Use Committee (IACUC). Cy5-

labled DsiRNA was complexed into NPs and loaded into PEUR scaffolds in the same quantities outlined above. Scaffolds were sectioned into approximately 6 mm x 1mm discs and sterilized by ethylene oxide treatment. 8-10 week balb/c mice were purchased from Charles River Laboratories. The animals were fed a standard chow diet *ad libitium* and had free access to water. The mice were anesthetized with 1.5-2% isoflurane and maintained at 37°C. The mice abdomen was shaved and sterilized. A 1 cm incision was made in the ventral side of the skin in the abdomen of the mice. A pocket was made with sterilized haemostatic forceps on each side of the midline and 6 mm scaffolds were implanted subcutaneously. The incision was sutured, and the mice were allowed to recover at 37°C. Analgesic agent (ketoprofen, 5 mg/kg) was injected as needed.

In vivo release kinetics

Release of si-NPs from the scaffold was quantified by measuring the loss of Cy5 fluorescence over time in regions of interest (ROIs) defined by the PEUR implant using an IVIS 200® imaging system (Caliper Life Sciences, Hopkinton, Massachusetts). Mice were anesthetized with 1.5-2% isoflurane and maintained at 37°C and measured with constant image settings every 2-3 days.

In vivo gene silencing

siRNA against cyclophilin B (PPIB) was formulated into si-NPs, incorporated into PEUR scaffolds, and implanted subcutaneously for 5, 12, 21, or 35 days using the procedure described above. At defined endpoints, the mice were anesthetized heavily with isoflurane and sacrificed by cervical dislocation. The scaffolds were collected postmortem and bisected in half for preparation for both histology and PCR. RNA was extracted with TRIZOL (Invitrogen, Carlsbad, CA) and purified with RNEasy spin column (Qiagen, Venlo, Netherlands). The expression of PPIB was evaluated by RT-PCR using the ΔΔCt method normalizing to GAPDH. Histological sections were used to evaluate the host response to the implants through H&E staining. RT-PCR for

inflammatory markers was also performed to evaluate immune response and activation of toll like receptor signaling. A western blot was used to confirm protein level silencing using primary antibodies anti-PPIB (Sigma) and anti-B-actin (Santa Cruz Biotechnology). The full method is described in Appendix B.

In vivo gene silencing during the time course of wound healing

For a longitudinal, protein level readout, firefly luciferase siRNA was formulated into si-NPs, incorporated into PEUR scaffolds, and implanted into transgenic balb/c mice with a COL1A2 luciferase reporter using the same procedure described above. The bioluminescence at the scaffold site was evaluated every 2 days for 24 days using an IVIS® 100 bioluminescence imaging system.

In vivo silencing of PHD2

PHD2 or scrambled siRNA was formulated into si-NPs that were incorporated into PEUR scaffolds and implanted subcutaneously into balb/c mice. Mice were sacrificed at day 14 and scaffolds were evaluated for gene expression by real-time RT-PCR. At day 33, scaffold vascularization was assessed with microCT using established methods [272, 274-276] (full method can be found in Appendix B). H&E staining and CD31 immunohistochemistry were done on scaffolds explanted at days 14 and 33.

Chapter 5

Aim 4 – Development of a systemic carrier for siRNA

Text for Chapter 5 taken from:

> **Nelson CE**‡, Kintzing JR‡, Hanna A, Shannon JM, Gupta MK, Duvall CL. Balancing Cationic and Hydrophobic Content of PEGylated siRNA Polyplexes Enhances Endosome Escape, Stability, Blood Circulation Time and Bioactivity *in Vivo.* ACS Nano. 2013, 7(10): 8870-8880.
>
> ‡ Equally Contributing Authors

5.1 Introduction

Small interfering RNA (siRNA) is emerging as a therapeutic approach for potent, gene-specific silencing [12], but clinical use of siRNA hinges on the development of safe and effective delivery technologies [230]. A variety of cationic biomaterials have been developed for siRNA packaging and delivery including polymers, lipids, polysacaccharides, cell penetrating and fusogenic peptides, and dendrimers [27, 67]. Cationic vehicles are effective for *in vitro* delivery because they condense siRNA into nano-sized complexes with positive surface charge that promotes endocytosis by electrostatically adsorbing onto anionic cell membranes [277]. However, intravenous administration of cationic lipoplexes or polyplexes, which is desirable for many therapeutic applications, often results in particle instability and nonspecific interactions with blood components that induce opsonization, aggregation of red blood cells, platelet activation, excessive biodistribution to the lungs, and, in extreme cases, rapid mortality [136-139].

Polyethylene glycol (PEG) has been used extensively to improve the biocompatibility of drug delivery nanoparticles and tissue engineered hydrogels. Functionalization of the exterior of drug delivery nanocarriers with PEG blocks adsorption of proteins, inhibits hemolysis or aggregation of erythrocytes, avoids immune stimulation, improves circulation time, protects the cargo from enzymatic degradation, and generally provides colloidal stability and ‘stealth’ [278-283]. PEGylation of cationic carriers has been successfully utilized to endow these properties

onto common polycations such as polyethylenimine (PEI), poly-L-lysine, polyamidoamine (PAMAM) and poly(propylene imine) (PPI) dendrimers, and poly(N,N-Dimethylaminoethyl methacrylate) (PDMAEMA) [146-150].

Poly(EG-*b*-DMAEMA) (PEG-DMAEMA) demonstrates efficient siRNA packaging and relatively low cytotoxicity [150], and studies on the effects of PEG architecture have shown that performance of a PEG-DMAEMA diblock structure is superior to brush or copolymer architectures [280]. PDMAEMA, like PEI, is believed to operate through the proton sponge effect for endosomal escape.[284, 285] However, it has been found that active, pH-dependent membrane disruptive mechanisms improve intracellular bioactivity relative to pure proton sponge [286]. Recently, it has been shown that copolymerization of the hydrophobic monomer butyl methacrylate (BMA) with DMAEMA, DEAMA, or DMAEMA and propyl acrylic acid (PAA) in a core-forming block [132, 248] could be used to tune the pH-dependent membrane disruptive behavior of micelleplexes; these micelleplexes were designed to be pre-assembled and nucleic acids were subsequently condensed onto coronas consisting of homopolymer blocks of DMAEMA [133, 287, 288].

Hydrophobic modification has also been found to have other beneficial effects on cationic delivery systems including serum stability, membrane binding, improved dissociation in the cytoplasm, and decreased cytotoxicity [289]. Recently, a self-assembled micelleplex made from a triblock polymer poly(EG-*b*-nBA-*b*-DMAEMA) that packaged siRNA in the corona was found to have improved gene silencing *in vitro* and had increased tumor uptake relative to poly(EG-b-DMAEMA)-based polyplexes [290]. While polymer blocks of DMEAMA with nBA are beneficial for stability, they do not generate polymers with active, pH-dependent membrane disruption behavior, possibly reducing the gene silencing activity due to endosomal entrapment. The polymers are also-pre-assembled and condense siRNA onto the positively charged micelle corona that contains a mixture of PDMAEMA and PEG. Though it wasn't reported, this also presumably resulted in micelleplexes with a positive zeta potential, which would hinder *in vivo* circulation time and performance [291, 292].

In this work, a novel series of copolymers of DMAEMA and BMA, ranging from 0-75 mol% BMA, were synthesized using a simple, one pot RAFT polymerization reaction from a PEGylated macro-chain transfer agent (macro-CTA). This polymer series was designed for core-complexation of siRNA into PEG-corona polyplex nanoparticles (NPs) whose assembly is electrostatically-triggered upon simple mixing with siRNA in buffer of appropriate pH. This strategy enables formulation of surface charge neutral siRNA-loaded NPs core-stabilized by a combination of electrostatic and hydrophobic interactions. The balance of cationic and hydrophobic content in the poly(DMAEMA-*co*-BMA) NP core-forming block was carefully titrated in order to identify improved PEGylated polycation variants that are optimized for *in vivo* performance based on a combination of improved stability and inertness in the blood circulation and pH-dependent membrane disruptive behavior finely-tuned for efficient endosomal escape and cytoplasmic delivery. The performance of polyplexes made from PEG-(DMAEMA-*co*-BMA) polymers with varied quantities of BMA were benchmarked against the standardized and previously-optimized PEG-DMAEMA diblock architecture [150].

5.2 Results and Discussion

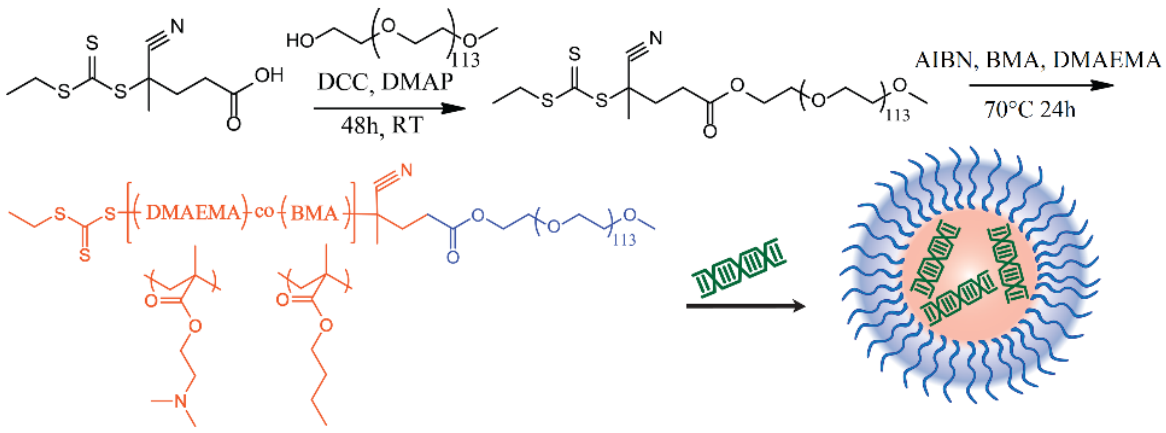

Fig. 5.1 Polymer synthesis scheme for PEG-(DMAEMA-*co*-BMA).

Polymer Synthesis and Characterization

A series of pH-responsive diblock copolymers were synthesized from a PEG_{5K} macro-CTA using RAFT polymerization (**Fig. 5.1**). Six polymers were synthesized with varied copolymer ratios of DMAEMA and BMA in the second block ranging from 0-75% BMA by adjusting the composition in the feed (**Table 5.1**). The synthesis was completed by the RAFT polymerization technique, which has numerous advantages including formation of monodisperse polymers [241, 242] as obtained here (all $M_w/M_n \leq 1.1$). Additionally, the single step polymerization was a facile and scalable synthesis that yielded easily-purified polymers with composition and molecular weight that closely matched the targeted values. This polymer series was designed to overcome the challenges related to systemic intravenous administration of polyplex nanoparticles with highly cationic surfaces [137-139]. It was posited that polyplex NPs comprising a PEG shell and a poly(DMAEMA-*co*-BMA) core will produce optimal properties for navigating both systemic circulation and intracellular (i.e., endosomal) delivery barriers following intravenous delivery.

Table 5.1 Molecular weight and percent composition of the polymer library

Polymer Name (%BMA in feed)	Mn(g/mol)	PDI	%BMA	%DMAEMA
0B	17035	1.092	0.0	100.0
25B	18747	1.075	23.8	76.2
40B	20765	1.117	39.6	60.4
50B	18040	1.040	48.3	51.7
60B	19938	1.081	58.6	41.4
75B	17349	1.053	74.5	25.5

Characterization of pH-dependent Polymer Micelle Assembly and Disassembly in Absence of siRNA

In order to identify optimal formulation conditions for efficient siRNA packaging, DLS was used to assess the pH-dependent micelle assembly/disassembly behavior of the polymers across a range of pHs, from 7.4 to 4.0. As expected, the relative acidity required to trigger polymer micelle disassembly was directly related to the %BMA content in the poly(DMAEMA-*co*-BMA) block. The 0B and 25B polymers did not spontaneously form micelles at any pH tested, while

polymers with 50% or more BMA content formed micelles (~25nm diameter, **Fig. 5.2**) at pH 7.4, with the 40B polymer appearing to be in a transition state at this pH. The 40B, 50B, and 60B polymeric micelles dissociated as the pH was lowered, and the pH where this transition occurred was inversely proportional to the %BMA in the polymer (**Fig. 5.2C-E, Fig. 5.2D inset** TEM images visually confirmed NP assembly for 50B at pH 7.4). The 75B polymer remained in stable micellar state at all pHs tested, suggesting that it did not accumulate sufficient cationic charge, even at pH 4.0, to destabilize the increased hydrophobic interactions between BMA (**Fig. 5.2F**).

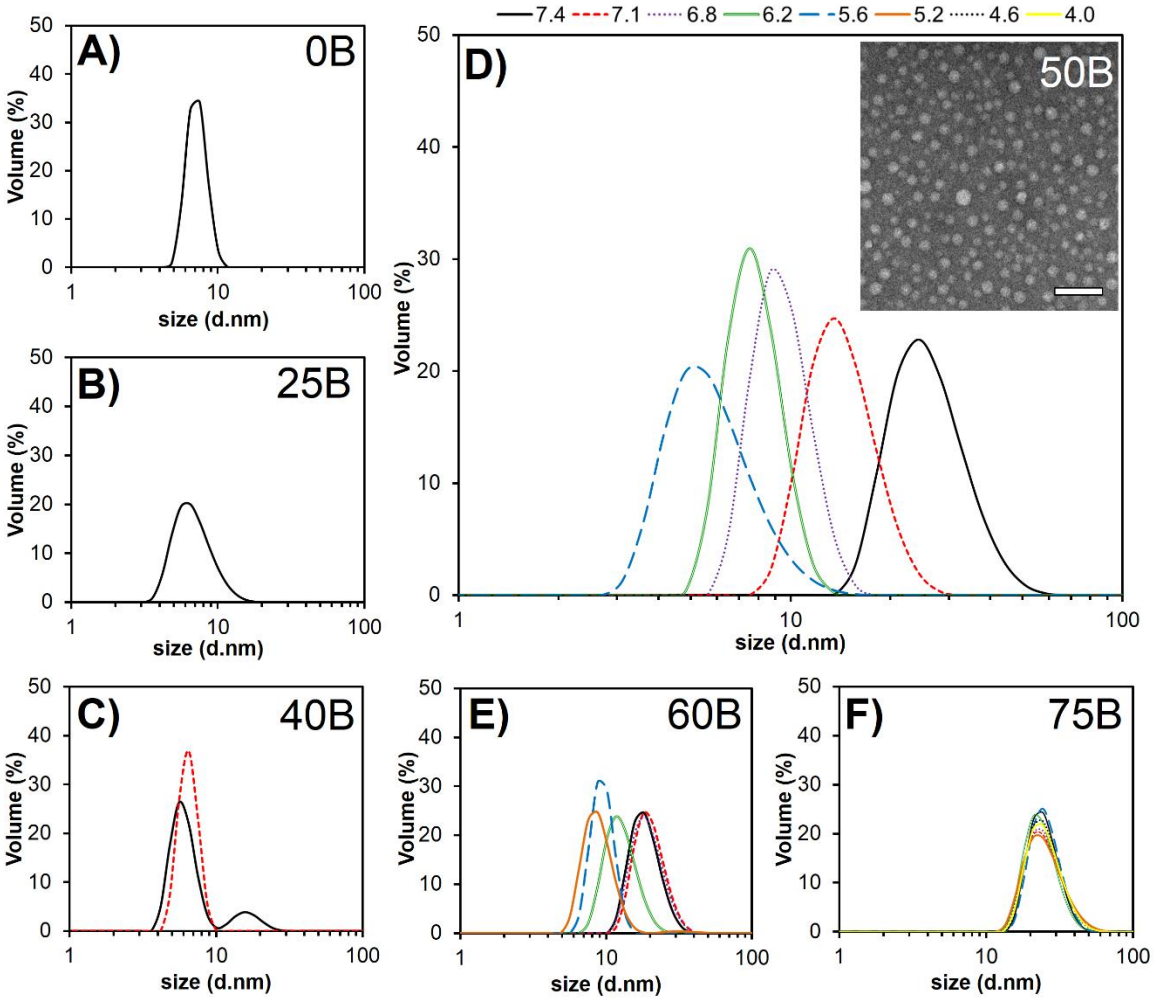

Fig. 5.2 DLS measurements characterizing pH-dependent assembly/disassembly behavior of PEG-(DMAEMA-*co*-BMA)] polymers. DLS at varying pH values for polymers with A) 0% BMA, B) 25%BMA, C) 40%BMA, D) 50%BMA, E) 60% BMA, F) 75% BMA. DLS data are shown for decreasing pH values down to pH 4.0 or until full NP disassembly occurred. Polymer 50B demonstrated the most dynamic pH-dependent behavior over the physiologically-relevant range tested. The inset TEM of 50B polymer at pH 7.4 shows spherical nanoparticles (scale bar = 100nm)

When the polymers are “pre-assembled” into micelles, the cationic poly(DMAEMA-*co*-BMA) polymer block is located in the particle core and is not readily accessible to electrostatically bind to siRNA. As a result, the polymers with a higher mole % of BMA in the poly(DMAEMA-*co*-BMA) block must be dissolved in a more acidic buffer to ensure that the DMAEMA tertiary amines are highly protonated, causing the polymers to exist as solubilized unimers due to electrostatic repulsion between poly(DMAEMA-*co*-BMA) blocks. In this unimeric state, the cationic polymer segments are fully exposed, and mixing with siRNA triggers electrostatic interactions that drive formation of polyplex NPs core-stabilized by electrostatic (PEG-DMAEMA) or a combination of electrostatic and hydrophobic interactions PEG-(DMAEAM-co-BMA). The data in Figure 2 suggest that polymers with 60 mole % BMA or less in the poly(DMAEMA-*co*-BMA) block exist in a unimeric state at pH 5.2, and as a result, this pH was used for formulation of siRNA-loaded polyplex NPs in subsequent studies.

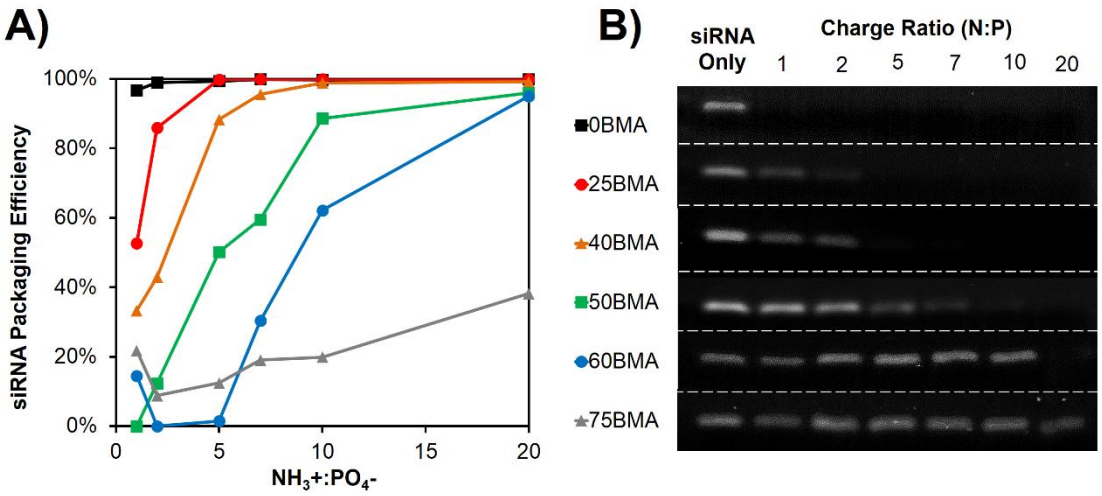

Fig. 5.3 Formulation of siRNA polyplex NPs at pH 5.2. A) siRNA packaging efficiency was dependent on both polymer composition and N:P ratio. B) Gel images used to quantify siRNA packaging efficiency (concatenated image containing 6 gels, each of which was internally controlled for quantification purposes).

Assembly and Characterization of siRNA-loaded Polyplex NPs

The polymers were mixed with siRNA at pH 5.2 to trigger polyplex NP formation, and it was found that the N:P ratio required to fully complex siRNA was proportional to the % BMA in

the polymer. Agarose gel electrophoretic mobility shifts were used to calculate the % siRNA packaging efficiency achieved using different formulation conditions (**Fig. 5.3**). However, even polymers 40B and 50B were able to efficiently package siRNA at an N:P of 10 or greater. In contrast, the 75B polymers were found to encapsulate only 38% of the siRNA even at an N:P of 20. The polyplex NPs formed from all polymers at N:P of 10:1 had hydrodynamic diameter of ~100 nm and approximately neutral zeta potential (**Appendix Fig. A14**). It was also found that reduction of the pH to 4.0 enabled efficient siRNA complexation of 50B at a lower charge ratio of 5:1, further supporting the importance of pH in siRNA packaging efficiency of these formulations (**Appendix Fig. A15**).

Cellular Uptake, Gene Silencing, and Cytotoxicity

Flow cytometry revealed that 0B polyplexes had the highest uptake and transfected nearly 100% of cells. 50B polyplex NPs were internalized significantly more than 40B or 60B (**Fig. 5.4A**). Despite the higher relative uptake of 0B ($p<0.05$), 50B polyplexes produced significantly greater luciferase silencing (94% reduction in the protein level at 48h when compared to scrambled control siRNA) relative to all other polymers in MDA-MB-231 breast cancer cells transduced to constitutively express luciferase (**Fig. 5.4B**, $p<0.05$). Though the benchmark formulation (0B) produced the greatest uptake, it produced only 20% luciferase silencing. The increased gene silencing activity of 50B NPs suggests that they are more efficient in navigating intracellular delivery barriers (*i.e.*, increased cytoplasmic release) relative to 0B polyplexes. Treatment with the polyplex NPs was also shown to be non-toxic to MDA-MB-231 cells (not shown) and NIH3T3 fibroblasts at the concentrations used in gene silencing experiments (**Fig. 5.4C**). The complete data set is listed in **Appendix Fig. A18-S20**.

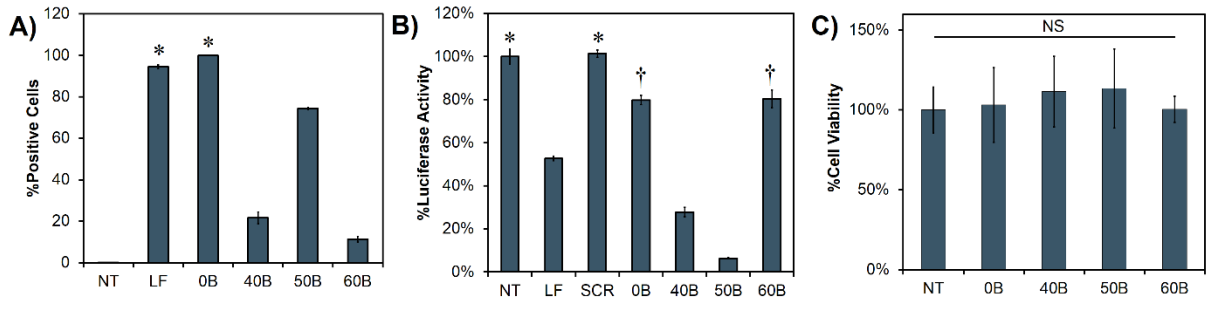

Fig. 5.4 50B-based polyplex NPs have the optimal combination of siRNA uptake, gene silencing bioactivity, and cytocompatibility *in vitro*. A) Flow cytometry measurement of transfection efficiency and B) bioluminescence measurement of luciferase knockdown *in vitro*; NT=no treatment, LF=Lipofectamine 2000, SCR=50B polyplexes loaded with scrambled siRNA. C) There was no cytotoxicity of any of the formulations at the concentrations tested. Statistical significance was evaluated by ANOVA at a confidence level of $p<0.05$ and all groups were found to be significantly different except for the paired groups marked with *,†, or NS.

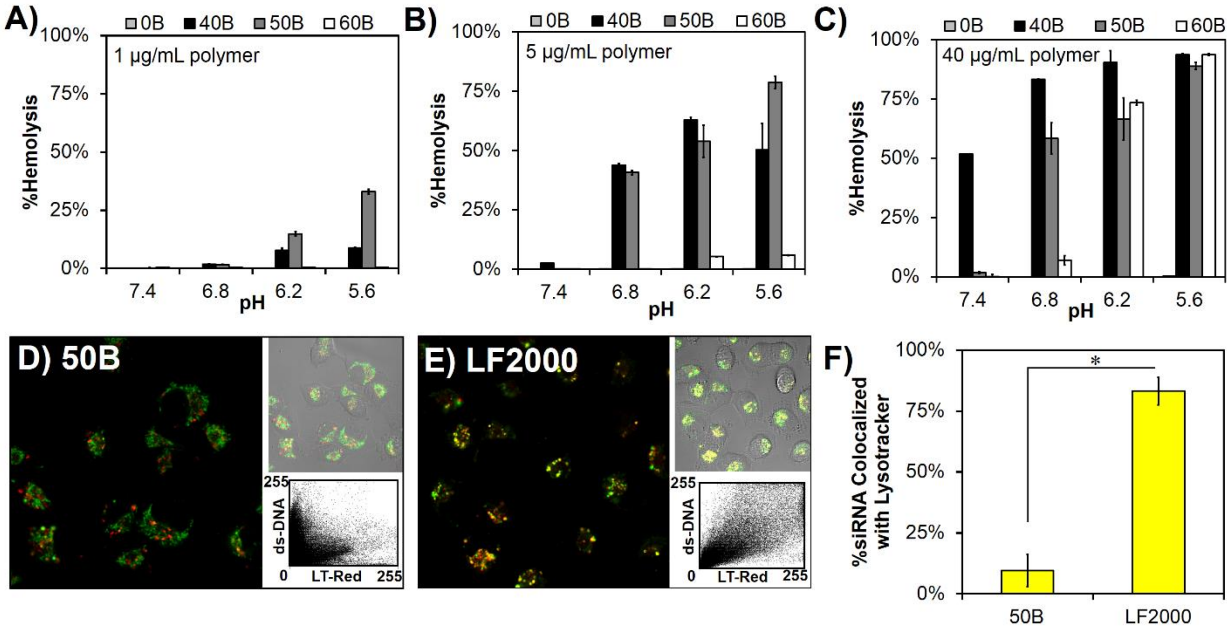

Fig. 5.5 Polyplexes formulated with 50B show active endosome disruption and escape. A-C) Hemolysis was both pH and composition dependent, with 50B siRNA polyplexes showing the most desirable pH-dependent membrane disruption behavior; 50B polyplexes did not disrupt erythrocyte membranes at pH 7.4, but produced robust hemolysis at pH 6.8, which is representative of early endosomes. All polyplexes were made at N:P of 10:1, and hemolysis was measured at A) 1 µg/mL, B) 5 µg/mL and C) 40 µg/mL polymer. D-E) Confocal images showing colocalization of the endosome/lysosome dye Lysotracker® with the cy5-labeled dsDNA cargo. Colocalization graphs are shown as insets. F) 50B polyplexes showed decreased % colocalization of dsDNA cargo with lysosomes relative to Lipofectamine2000 (* signifies $p<0.01$).

Endo-lysosomal Escape

A major intracellular delivery barrier of siRNA nanocarriers is endosomal entrapment and trafficking for lysosomal degradation or exocytosis [252]. The current polymer family was designed to form polyplex NPs that destabilize at endo-lysosomal pHs, exposing the membrane disruptive poly(DMAEMA-*co*-BMA) polymer block. As a screen for active endosomal escape behavior, the pH-dependent membrane disruptive activity of siRNA-loaded polyplex NPs was measured using a red blood cell hemolysis assay [293]. At all N:P ratios tested, polyplexes made with 40B, 50B, and 60B generated switch-like, pH-dependent membrane disruption. Percent hemolysis of each polymer increased as the polymer concentration was increased and as the buffer pH was decreased. The pH where the hemolytic transition occurred mirrored the trend seen for destabilization of polymer NPs (**Fig. 5.2**) and was inversely dependent on the %BMA content in the poly(DMAEMA-*co*-BMA) block (**Fig. 5.5A-C)**. Polyplex NPs made with the 50B polymer had optimal pH-responsive behavior based on producing membrane disruption in a pH environment representative of early and late endosomes but not at physiologic pH. Furthermore, the pH-dependent membrane disruptive behavior of 50B was similar between the polymer-only micelle and polyplex NP forms (**Appendix Fig. A16**). This suggests that presence of the anionic siRNA did not inhibit pH-dependent particle destabilization and exposure of the membrane disruptive poly(BMA-*co*-DMAEMA) block of polyplex NPs exposed to acidic pH. Although they did not fully disassemble like the polymer-only micelles (**Fig. 5.2**), the polyplex NP hydrodynamic diameter increased upon exposure to buffers of decreasing pH, suggesting that swelling and/or reorganization of the polyplex structure leads to exposure of the core-forming block under these conditions (**Appendix Fig. A17**).

To assess intracellular trafficking and endo-lysosomal escape, confocal microscopy was used to measure colocalization with the fluorescent dye Lysotracker®. Diffuse staining of the cy5-labeled dsDNA cargo was visualized in cells incubated with 50B polyplexes for 24h (**Fig. 5.5D**), and 50B polyplex delivery resulted in significantly lower Lysotracker® colocalization relative to

Lipofectamine (colocalization appears yellow, **Fig. 5.5E**). The colocalization was further visualized by plotting color values of non-background image pixels in a dot plot where colocalized signal falls on the y=x line, free siRNA falls on the y-axis, and lysosomes not containing siRNA fall on the x-axis (inset graphs). These combined data quantitatively and qualitatively suggest that polyplexes are able to efficiently overcome intracellular endo-lysosomal delivery barriers. This outcome is in agreement with the results from the pH-dependent hemolysis experiment, which suggests that 50B polyplexes are finely tuned to disrupt membranes in pH values representative of the endo-lysosomal pathway. These combined results suggest that 50B polyplexes improve the intracellular bioavailability of internalized siRNA, and this may mechanistically account for 50B having the highest gene silencing bioactivity of the polymers screened *in vitro* (**Fig. 5.4B**).

Polyplex Stability and Hemocompatibility

For intravenous siRNA delivery systems, avoidance of destabilization and/or nonspecific interactions with cells and other blood components is key to general hemocompatibility and for maximizing blood circulation time in order to allow for passive tumor accumulation or active tissue targeting of intact, bioactive NPs. Nanoparticle PEGylation improves these properties,[294] and we hypothesized that optimization of the polyplex core could be an avenue to further enhance stability. Polyplex NPs made with 40B, 50B, and 60B were stable and did not aggregate or dissociate over a period of 24 h in PBS as assessed with DLS (**Appendix Fig. A21**). Förster Energy Resonance Transfer (FRET) was used as another measure of stability where 50B-NPs were co-loaded with FAM- and cy5- labeled dsDNA. FRET emission of the acceptor dye is only observed when the two fluorophores are co-encapsulated in the core of the NPs.[295] FRET-NPs made with 50B also retained an equivalent %FRET after 48 hours of storage at room temperature, further indicating that siRNA remains stably encapsulated in the core of the polyplexes (**Appendix Fig. A21**).

Ex vivo experiments in human whole blood were done to measure nonspecific red blood cell interactions and stability of polyplexes. After a 1 hour incubation in whole blood, polyplex NPs made with 50B were 74% retained in the serum fraction, whereas commercial standards PEI (5%) and Lipofectamine 2000 (48%) were more significantly associated with the cellular fraction following centrifugation (**Fig. 5.6A**). As a measure of whole blood stability, FRET-NPs were incubated for 1 hour in whole blood, and measurement of the FRET signal in the serum fraction showed that the 50B polyplex NPs retained a high %FRET signal of 77% while Lipofectamine 2000 showed a significant ($p<0.05$) decrease in relative %FRET to 35% of the baseline signal (**Fig. 5.6B**).

Rapid urine excretion of many intravenously-delivered cationic siRNA polyplexes occurs due to dissociation in the kidney glomerular basement membrane (GBM), which has high composition of the anionic macromolecule heparan sulfate [123, 296]. To model this phenomenon *in vitro*, we incubated FRET-NPs with heparinized saline (2 U/mL) and measured stability over time. This experiment showed that destabilization was dependent on the composition of the core-forming polymer block, indicating that 40-60% BMA resulted in significantly greater stability ($p<0.05$) compared to 0B and 25B polyplex NPs (**Fig. 5.6C**). Higher concentrations of heparin (>10 U/mL) were capable of dissociating the higher %BMA polyplexes 40B-60B (**Appendix Fig. A22**). These data suggest that incorporation of hydrophobic content will slow the rate of kidney filtration of siRNA-loaded polyplex NPs.

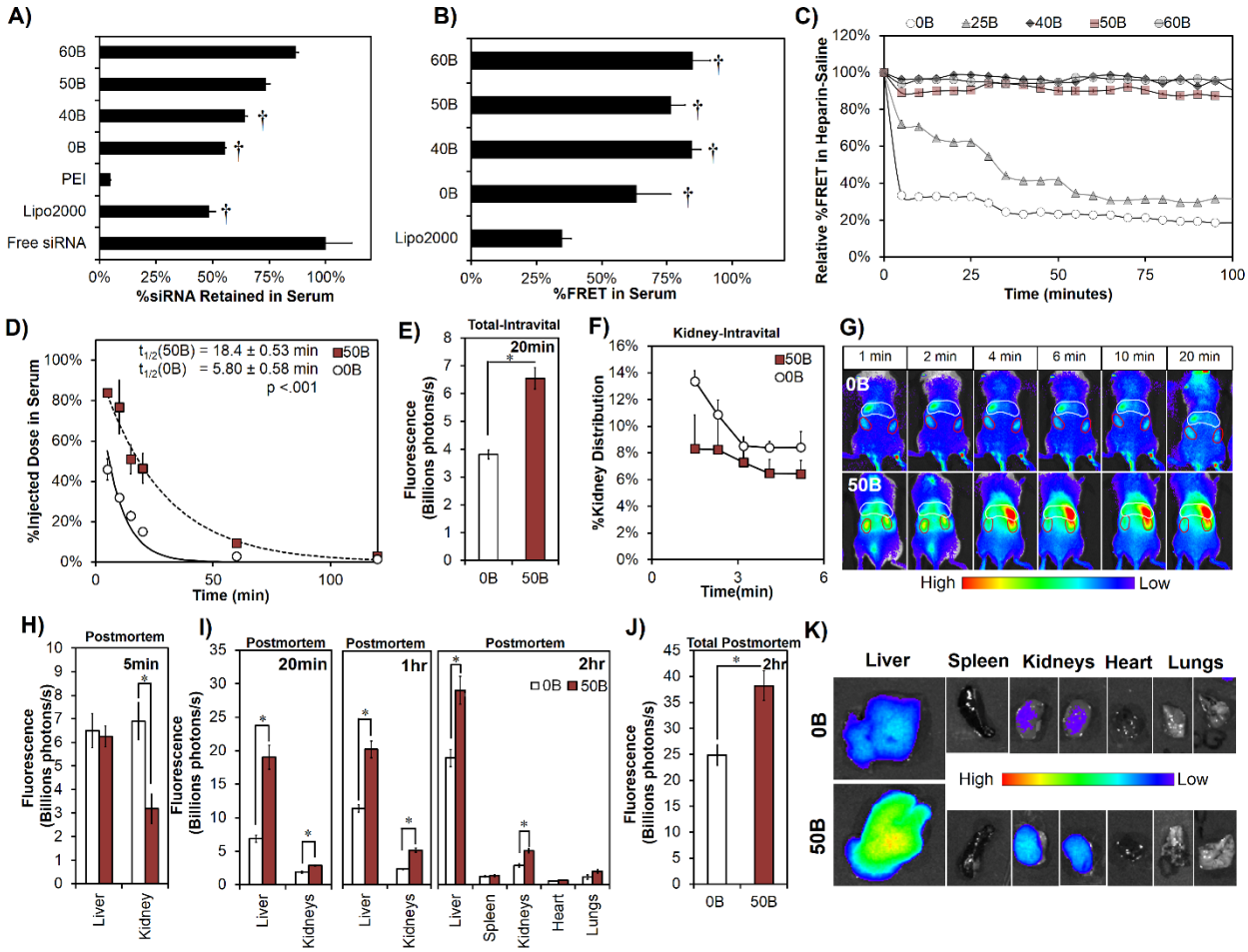

Fig. 5.6 50B polyplex NPs demonstrate enhanced stability upon exposure to heparin and human whole blood and have a longer circulation half-life and improved tissue biodistribution *in vivo*. A) When incubated in blood at 37°C, a significant fraction of the PEGylated polyplexes remained in the serum, indicating that they nonspecifically interact with erythrocytes to a significantly lesser degree than PEI ($p<0.05$). B) FRET-NP incubation in diluted human whole blood suggested that all PEGylated polyplex NPs were significantly more serum stable than the commercial standard Lipofectamine 2000 ($p<0.05$). Statistical significance for A-B was evaluated by ANOVA at a confidence level of $p<0.05$ where all groups were found to be significant except for those designated with †. C) Stability of FRET-NPs incubated in 2 U/mL of heparin was enhanced for polyplexes with 40-60% BMA content in the core-forming polymer block. D) The circulation half-life was 18.4 min for 50B and 5.8 min for 0B ($p<0.05$, $n=3$). E) When measured intravitally, systemic biodistribution was significantly higher ($p<0.05$) for the 50B injected mice. F) Intravital imaging of intravenously injected 50B and 0B polyplex NPs reveals rapid kidney distribution and systemic clearance of 0B. G) Representative time course images are shown noting significantly more overall systemic biodistribution of fluorescent siRNA delivered via 50B polyplexes relative to the more rapidly cleared 0B polyplexes. H) Imaging of siRNA fluorescence in kidneys excised at 5 minutes post injection confirmed increased, rapid renal filtration of siRNA delivered via 0B polyplex NPs relative to the 50B group. I) Postmortem tissue biodistribution showed preferential accumulation in liver and kidneys, with significantly decreased systemic clearance of 50B vs 0B at 20 min, 1 hr, and 2 hrs post-injection ($p<0.05$, $n=3$). J) Measurement of cumulative fluorescence in all of the organs at 2hr post injection showed significantly increased biodistribution and retention in the organs for 50B relative to 0B polyplex NPs ($p<0.05$). K) Representative tissue biodistribution images are shown from 2h. Statistical significance for in vivo experiments was evaluated with ANOVA at a confidence level of $p<0.05$, and * designates significance.

Circulation half-life and biodistribution

Increased resistance to heparin-mediated destabilization of 50B-based polyplex NPs was found to be functionally significant *in vivo* and yielded a 3.2-fold increase in the blood circulation half-life (18.4 ± 0.53 vs. 5.80 ± 0.58 minutes) and 3.4-fold increase in area under the curve (AUC) (14.0mg*h/L vs. 4.1 mg*h/L) relative to the benchmark polymer 0B ($p<0.05$ for both half-life and AUC, **Fig. 5.6D**). The blood circulation half-life of 0B was consistent with previous studies on PEGylated polycationic siRNA carriers, which have typically shown values <5 min and is associated with rapid decomplexation and systemic removal in the kidney [123, 296]. Our combined data suggest that increased hydrophobicity in the core of polyplexes made with 50B polymers increased NP stability in the presence of heparin, slows renal clearance *in vivo*, and increases blood circulation time. These data suggest 50B will biodistribute more efficiently to other tissues and will be potentially targeted more efficiently to tumors or other pathological sites.

To this end, tissue biodistribution of 0B and 50B siRNA polplex NPs were examined intravitally immediately following injection and at postmortem endpoints of 5 min, 20 min, 1 hr, and 2 hr post-injection. In agreement with the 50B polyplexes having less rapid renal decomplexation and siRNA removal through the urine acutely following injection, there was an immediate spike in concentration of siRNA in the kidneys of 0B polyplex-treated mice, and overall systemic clearance of siRNA was faster than following delivery with 50B polyplexes (**Fig. 5.6E-F**). This trend is shown visually in representative mice (**Fig. 5.6G**), and the full panel of intravital images is shown in **Appendix Fig. A23**. Imaging of kidneys excised from mice that were euthanized 5 minutes post-injection confirmed the intravital imaging data and showed a 2.2-fold increase in siRNA distribution in the kidney for 0B relative to 50B (**Fig. 5.6H**). Liver biodistribution was noted at 5 min, 20 min, 1 hr and 2 hr endpoints for 0B and 50B NPs and suggested that uptake in the liver is the primary route for removal of intact NPs (**Fig. 5.6I-K**). There was significantly greater quantity of siRNA in the liver and kidneys for 50B than 0B ($p<0.05$) at 20 min, 1 hr, and 2 hrs. Because 50B is partially susceptible to heparin decomplexation, the kidneys also

have higher fluorescence at the later time points based on continued clearance of the longer-circulating 50B formulations. The integrated fluorescence across all organs was 1.5 fold higher in 50B polyplexes than 0B after 2h ($p<0.05$, **Fig. 5.6J**), which is also consistent with slower removal through the urine and better overall biodistribution of 50B relative to 0B polyplexes. Importantly, we saw little uptake in the lungs and heart that would be associated with acute pulmonary toxicity that occurs with ineffectively-shielded cationic polyplexes [139].

The combined data from **Fig. 5.6** suggest that both polyplex surface PEGylation and incorporation of hydrophobic content in the core are beneficial for enhancing circulation half-life. PEG shielding improves circulation by decreasing aggregation with or adsorption to blood components, but does not fully shield the polyplex core from interaction with competing anions prevalent in the kidneys. The optimal combination of core hydrophobicity and PEG shielding achieved with 50B polyplexes increased the circulation half-life and is anticipated to improve passive tumor accumulation or, through functionalization with targeting ligands, retention in other target tissues. Poorer stability of 0B resulted in decreased systemic biodistribution due to rapid decomplexation and removal through renal filtration. This agrees with previous literature suggesting that siRNA delivered via simple polycations are substantially excreted through the urine within 1 min post-delivery [123, 296].

PPIB gene silencing in vivo

The last objective was to confirm that 50B polyplex NPs remained bioactive *in vivo*. The liver, kidneys, and spleen were selected as target tissues based on their known reticuloendothelial system (RES) function and the results of the biodistribution analysis. An siRNA targeting the model/housekeeping gene PPIB was delivered because of the consistent expression level of PPIB, and knockdown was analyzed in tissues extracted 48 hours after intravenous injection. As shown in **Fig. 5.7**, 50B polyplex NPs robustly silenced PPIB in the liver by ~74% following an intravenous dose of 2 mg/kg siRNA. Furthermore, 50B generated significantly greater gene

silencing than 0B polyplexes injected at the same dose of 2mg/kg ($p<0.05$). Similarly, 50B polyplexes significantly silenced PPIB in the kidneys and spleen relative to scrambled controls ($p<0.05$), and 50B silencing was significantly greater in the spleen relative to 0B ($p<0.05$, for 0B versus 50B in the kidney). Improved *in vivo* gene silencing by 50B polyplexes relative to 0B is consistent with their active, pH-dependent membrane disruptive function and increased *in vitro* bioactivity, stability, circulation time, and overall tissue biodistribution. The similar level of gene silencing measured in the different organs also implies widespread tissue distribution of intact, bioactive 50B polyplex NPs and that these NPs may be used to preferentially accumulate in a variety of target tissues if implemented with the appropriate targeting ligand. Importantly, all polyplex injections were well-tolerated by the mice, and no elevation in serum markers of liver toxicity ALT or AST were detected in mice treated with 50B or 0B at days 2 or 8 post-injection (**Appendix Fig. A25**).

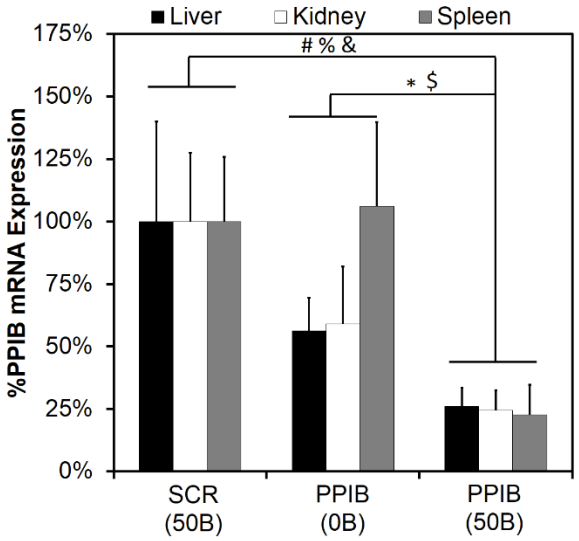

Fig 5.7 *In vivo* gene silencing following intravenous delivery of 50B polyplex NPs. Gene silencing of the model gene PPIB was evaluated by PCR 48h after intravenous injection of 2 mg/kg siRNA doses. Significant differences were noted in the liver, kidney, and spleen between 50B and SCR groups ($p<0.05$) and in the liver and spleen between 50B and 0B ($p<0.05$). Markers of statistical differences: #,* - Liver; % - Kidney; &,$ - Spleen.

5.3 Conclusions

We have synthesized and screened a small library of PEG-(DMAEMA-*co*-BMA) polymers for formulation of *in vivo*-ready siRNA nanocarriers designed to overcome key delivery barriers in the systemic circulation and inside target cells. PEG was used in the corona to impart hemo-compatibilty and stability, and the combination of surface PEGylation and titration of hydrophobic content into the polyplex core resulted in better stabilized polyplexes with longer blood circulation

times. The 50B polymer had optimally-balanced cationic and hydrophobic content in the core-forming block and formed polyplex NPs with improved resistance against destabilization in the kidneys *in vivo* and pH-dependent membrane disruptive activity ideally tuned for endosomal escape. This resulted in slower renal clearance, increased circulation time, improved tissue biodistribution, and more potent gene silencing bioactivity *in vivo*. The 50B siRNA polyplex nanoparticles provide a promising platform for future applications involving EPR-driven delivery to tumors *in vivo* or active receptor-ligand targeting to increase accumulation and uptake in specific cells or tissues.

5.4 Materials and Methods

Materials

All materials were obtained from Sigma-Aldrich and used as received unless otherwise noted. An alumna column was utilized to remove inhibitors from DMAEMA and BMA monomers, and final purification of polymers was done with PD10 desalting columns (GE Healthcare, Waukesha WI).

Synthesis of 4-cyano-4-(ethylsulfanylthiocarbonyl) sulfanylpentanoic acid (ECT) and PEG-ECT

The RAFT chain transfer agent (CTA) ECT was synthesized as previously described [132], and the R-group of the CTA was subsequently conjugated to PEG [297]. Briefly, dicyclohexylcarbodimide (DCC, 4mmol, 0.82g) was added to the stirring solution of mono methoxy-poly(ethylene glycol) (Mn = 5000, 2 mmol, 10g), ECT (4mmol, 1.045g), and DMAP (10mg) in 50 mL of dichloromethane. The reaction mixture was stirred for 48h. The precipitated cyclohexyl urea was removed by filtration and dichloromethanane layer was concentrated and precipitated into diethyl ether twice. The precipitated PEG-ECT was washed three times with diethyl ether and dried under vacuum (Yield ~10g). ^{1}H NMR (400 MHz $CDCL_3$) revealed 91% substitution of the PEG (**Appendix Fig. A11**).

Polymer Synthesis and Characterization

Reversible addition fragmentation chain transfer (RAFT) polymerization was used to synthesize a library of copolymers using the PEG-ECT macro-CTA. In all cases, the degree of polymerization (DP) was 150, and the monomer plus CTA was 40% wt/vol in dioxane. The polymerization reaction was carried out at 70°C for 24 h using AIBN as the initiator with a 5:1 [CTA]:[Initiator] molar ratio. A series of polymerizations were carried out with monomer feed ratios of 0:100, 25:75, 40:60, 50:50, 60:40, and 75:25 mol% [BMA]:[DMAEMA]. The reaction was stopped by exposing the polymerization solution to air, and the resulting diblock polymers were precipitated into an excess of pentane. The isolated polymers were vacuum dried, re-dissolved in water, further purified using PD10 columns, and lyophilized. Polymers were characterized for composition and molecular weight by ^{1}H nuclear magnetic resonance spectroscopy (NMR, Bruker 400Mhz Spectrometer equipped with 9.4 Tesla Oxford magnet). Absolute molecular weight of the polymers was determined using DMF mobile phase gel permeation chromatography (GPC, Agilent Technologies, Santa Clara, CA, USA) with inline Agilent refractive index and Wyatt miniDAWN TREOS light scattering detectors (Wyatt Technology Corp., Santa Barabara, CA). All results are shown in **Appendix Fig. A12 and A13**.

Characterization of pH-dependent Polymer Micelle Assembly and Disassembly in the Absence of siRNA

Each lyophilized polymer was dissolved in 100% ethanol, and aliquots of this solution were mixed with an 8-fold excess of phosphate buffer at pHs 7.4, 7.1, 6.8, 6.2, 5.6, and 5.2 or citrate buffers of 4.6, and 4.0 to make a 1 mg/mL stock solution. Each stock solution was diluted an additional 10-fold into phosphate or citrate buffer of the same pH to form 100 µg/mL polymer stocks, and the pH-dependence of self-assembly of each polymer into NPs was assessed using dynamic light scattering (DLS, Malvern Zetasizer Nano ZS, Malvern UK). For imaging by

transmission electron microscopy (TEM), carbon film-backed copper grids (Electron Microscopy Sciences, Hatfield, PA) were inverted onto droplets containing aqueous NP suspensions (1 mg/mL) and blotted dry. Next, samples were inverted onto a droplet of 3% uranyl acetate, allowed to counterstain for 2 min, and again blotted dry. Finally, samples were desiccated *in vacuo* for 2 h prior to imaging on a Philips CM20 system operating at 200 kV (Philips, EO, Netherlands).

Assembly and Characterization of siRNA-loaded Polyplex NPs

Polyplex NPs loaded with siRNA were made by mixing pH 4.0 stock solutions of polymer and siRNA at N:P ratios of 5, 7, 10, or 20. The final charge ratio was calculated as the molar ratio of cationic amines on the DMAEMA (50% are assumed to be protonated at physiologic pH) to the anionic phosphates on the siRNA. After mixing, these solutions were diluted 5-fold to 100 µL with phosphate buffer to adjust the final pH to 7.4. After mixing, samples were incubated for 30 minutes, and 15 ng siRNA for each sample was loaded onto a 4% agarose gel containing ethidium bromide to assess siRNA packaging efficiency. The gels were run at 100 volts for 35 minutes and imaged with a UV transilluminator. Quantification was conducted using ImageJ version 1.45s (Freeware, NIH, Bethesda, MD). Hydrodynamic diameter and zeta potential of the resulting polyplex NPs were measured using a Malvern Zetasizer Nano ZS.

Cell Culture

Human epithelial breast cancer cells (MDA-MB-231) were cultured in Dulbecco's Modified Eagle's Medium (DMEM, Gibco Cell Culture, Carlsbad, CA) supplemented with 10% Fetal Bovine Serum (FBS, Gibco), and 0.1% gentamicin (Gibco). Mouse Embryonic Fibroblasts (NIH3T3) were cultured in Dulbecco's Modified Eagle's Medium (DMEM, Gibco Cell Culture, Carlsbad, CA) supplemented with 10% Bovine Calf Serum (BCS, Gibco), and 1% penicillin-streptomycin (Gibco).

Flow Cytometry Assessment of siRNA Intracellular Delivery

MDA-MB-231 breast cancer cells were seeded in 24-well plates at a density of 40,000 cells/cm^2 and allowed to adhere overnight. The cells were treated with polyplexes loaded with Alexa488-labeled DNA (21mer duplexes mimicking siRNA molecules) at a final concentration in each well of 100 nM in media supplemented with 10% FBS. After the designated treatment time, cells were washed with PBS and trypsinized. Cells were centrifuged and resuspended in PBS containing trypan blue to quench extracellular fluorescence. Relative cell fluorescence was quantified via flow cytometry to measure NP intracellular delivery (FACSCalibur, BD Biosciences, Franklin Lakes, NJ).

Cytotoxicity

Cytotoxicity of siRNA-loaded polyplex NPs was determined by measuring relative cell number based on luciferase activity. NIH3T3s were transduced with a lentivirus to constitutively express luciferase (LR-3T3s), and it was confirmed that cell number was directly proportional to luciferase signal (**Appendix C**) [298]. LR-3T3s were seeded in black-walled 96-well plates at a density of 12,500 cells/cm^2 and allowed to adhere overnight. Next, cells were treated with fresh polyplexes at concentrations of 50, 100, and 200 nM siRNA/well (100 µL volume, n=5 for each treatment). After incubation for 24 h, the cells were given fresh luciferin-containing media (150 µg/mL). Bioluminescence was quantified using an IVIS Imaging System 200 series (Xenogen).

In Vitro Gene Silencing

MDA-MB-231 breast cancer cells were transduced with a lentivirus to constitutively express luciferase (L231, **Appendix C**). L231 cells were seeded in black, clear bottom 96 well plates at a density of 12,500 cells/cm^2 and allowed to adhere overnight. Next, cells were treated for 24 h with polyplex NPs containing anti-luciferase siRNA (Ambion) in 10% FBS media. Media was then replaced with luciferin-containing media (150 µg/mL), and bioluminescence was

measured using an IVIS 200 Series imaging system (Xenogen). Next, cells were incubated for an additional 24 h in slow growth media (DMEM supplemented with 1% FBS, and 0.1% gentamicin), and bioluminescence was subsequently re-measured. Bioluminescence data was normalized to total protein content in cell lysates which was measured via the Bradford assay (Bio-Rad).

Hemolysis Assay

Whole blood was extracted from anonymous, consenting human donors and red blood cells (RBCs) were isolated according to well established protocols.[293] RBCs were then incubated with the free polymers or with siRNA-loaded polyplex NPs (concentrations ranging 1 - 40 μg/mL) in buffers of 7.4, 6.8, 6.2, and 5.6, which model the environments in the extracellular space and in the more acidic vesicles of the endo-lysosomal pathway. After 1 h of incubation, the RBCs were centrifuged and the supernatant was spectrophotometrically analyzed at 451 nm in order to determine percent hemolysis relative to Triton X-100 detergent.

Confocal Microscopy Imaging of Endo-lysosomal Escape

MDA-MB-231 cells were seeded at a density of 12,500 cells/cm^2 in 8-well chamber slides (Nunc – Thermo Fisher Scientific Inc., Waltham, MA). The cells were treated with cy5-labeled dsDNA loaded polyplex NPs at 100 nM or Lipofectamine 2000 according to manufacturer's specifications. After treatment, media was replaced with Lysotracker® (Invitrogen Life Technologies, Grand Island, NY) containing media (75 nM), and cells were incubated for 1 h before imaging with confocal microscopy (Zeiss LSM 710Meta, Oberkochen, Germany) equipped with differential interference contrast (DIC). Images were analyzed using ImageJ with a colocalization extension JaCOP previously described [299].

Analysis of Polyplex Stability and Hemocompatibility

NPs were loaded with Förster Resonance Energy Transfer (FRET, using FAM and Cy5) pair-labeled 23mer dsDNAs (a model for siRNA) (FRET-NPs). Fluorescent intensity was measured using a spectrophotofluorometer with an excitation wavelength of 488nm (Jobin Yvon/Horiba Fluorolog-3 FL3-111, Horiba Scientific, Kyoto Japan). FAM emission was collected at 520nm ± 3nm, and Cy5 emission was obtained at 670nm ± 3nm. %FRET was calculated as a ratio of the fluorescent intensity as follows:

Eqn. 5.1 $$\%FRET = \frac{I_{670}}{I_{520}+I_{670}}$$

For serum stability measurements, FRET-NPs were added into human whole blood diluted 1:3 in PBS at 100 nM (50 nM for each DNA). Treated blood samples were loaded into a black, round bottom 96 well plate and placed on a shaker for 5 minutes before incubating at 37^{o}C for 1 h. Plates were then centrifuged at 500 x g for 5 minutes, and then 50 µL of supernatant (diluted blood serum) from each well was transferred into a black, clear bottom 96 well plate. Fluorescence was measured using a Microplate Reader and %FRET was calculated using Eqn 1. In parallel experiments to assess hemocompatibility *ex vivo*, polyplex NPs loaded with FAM-labeled dsDNA were used to quantify the percent of NPs in the supernatant, as a measure of inertness, or ability to reduce nonspecific adsorption to or aggregation with RBCs.

Because siRNA decomplexation by heparan sulfate-containing glomerular basement membrane (GBM) in the kidney is a primary cause for rapid systemic clearance of polycation-siRNA nanoparticles [123, 296], the stability of FRET-NPs was measured in the presence of 2 U/mL of heparin sodium salt in DPBS. The fluorescence emission was measured over time using a microplate reader with an excitation wavelength of 488 nm and an emission wavelength of 670 nm (Tecan Infinite F500, Männedorf, Switzerland).

Biodistribution

Balb/c mice (6-8 weeks of age) were injected intravenously into the tail vein with polyplex NPs containing a dsDNA (model for siRNA) labeled with 5' IRDye® 800CW (Integrated DNA Technologies, IDT). Blood samples were collected at 2, 5, 10, 15, and 20 minutes (maximum 2 blood collections per mouse). Separate cohorts of mice were euthanized for additional blood sample collection and organ harvesting for biodistribution analysis at 5min, 20 min, 1 hour, and 2 hours post-injection. Blood was centrifuged at 500xg for 5 minutes and the supernatant was measured for fluorescence using a plate reader (Tecan) with 790 nm excitation and 810 nm emission. In addition, mice were monitored intravitally using an IVIS 200 for the first 20 minutes post-injection in order to measure the kinetics of biodistrubition to the liver and kidneys. The backs of mice were shaved the day before injection and imaged with the dorsal side facing the camera to visualize and measure kidney and liver biodistribution. Regions of interest (ROIs) were drawn around the liver, kidneys, and the entire mouse to measure organ-specific and total fluorescence, respectively. An IVIS 200 was used to quantify the biodistribution in the explanted lungs, heart, liver, kidney, and spleen using Living Image™ 4.3 quantification software.

In Vivo PPIB Silencing

Balb/c mice (6-8 weeks of age) were injected intravenously into the tail vein with polyplex NPs containing a dicer-substrate siRNA designed against cyclophilin B (PPIB, IDT) at a dose of 2 mg/kg. Mice were sacrificed at 48h, and the RNA was extracted from organs with TRIZOL (Invitrogen, Carlsbad, CA) and purified with RNEasy spin column (Qiagen, Venlo, Netherlands). The expression of PPIB was evaluated by RT-PCR using the ΔΔCt method normalizing to GAPDH.

Statistical Methods

All measurements are presented as mean ± standard error of the mean. ANOVA was used to determine statistical significance, and $p<0.05$ was considered significant.

Ethics Statement

The animal studies were conducted with adherence to the guidelines for the care and use of laboratory animals of the National Institutes of Health (NIH). All experiments with animals were approved by Vanderbilt University's Institutional Animal Care and Use Committee (IACUC). Human whole blood was collected from anonymous donors in accordance with an approved Institutional Review Board (IRB) protocol.

Chapter 6

Synopsis and Future Directions

6.1 Summary

As biologists continue to elucidate the molecular mechanisms for disease, there is a growing need for engineered platforms to solve the drug delivery challenges associated with correcting and treating the diseased state. Biomacromolecular drug delivery stands to improve a host of diseases by reaching molecular targets previously considered ‘undruggable’. Of these biomacromolecules, small interfering RNA (siRNA) is of particular interest due to siRNA’s specific and potent post-transcriptional gene silencing. These studies set out to develop a platform for local siRNA delivery that solves the delivery challenges of siRNA in a safe and biocompatible manner and applied this platform for sustained silencing of the angiogenesis regulator prolyl hydroxylase domain protein 2 (PHD2) to improve tissue regeneration.

In Aim 1, the platform was developed from the ground up and tested *in vitro.* pH-responsive endosomolytic nanoparticles (NPs) were synthesized through the controlled radical polymerization technique and used to condense siRNA into nanoparticles (si-NPs). These si-NPs were lyophilized and incorporated into a polyurethane (PUR) scaffold which permitted sustained release to the local environment. Importantly, this study showed that the si-NP-PUR platform released bioactive nanoparticles that were non-toxic. However, there was a loss in activity of the si-NPs when released from the scaffold.

In Aim 2, the bioactivity of the si-NPs was improved through the use of a non-reactive excipient trehalose. In addition, trehalose also provided a mechanism for tuning the release rate of si-NPs from the scaffold. These new formulations were tested *in vivo* for tunable and sustained release, biocompatibility, and gene silencing. Importantly, this study showed potent gene silencing in mouse subcutaneous implants that was controllable based on the concentration of trehalose and sustained for 35 days.

Aim 3 sought to apply this platform for the sustained silencing of a therapeutically relevant gene as a proof of principle and to demonstrate clinical translatability. In order to improve angiogenesis in the tissue engineered scaffold, prolyl hydroxylase domain protein 2 (PHD2) was sought as a negative regulator of the transcription factor hypoxia inducible factor 1α (HIF-1α). Previous studies had shown that stabilization of HIF-1α triggered a 'growth-program' resulting in the up-regulation of pro-angiogenic genes (e.g. VEGF and FGF-2) along with pro-healing genes (e.g. SDF-1) [217, 218, 300]. This study showed that through the sustained silencing of PHD2, pro-angiogenic genes were increased two-three fold resulting in a three-fold increase in vascular cross sectional area by IHC and a three-fold increase in vascular volume by microCT.

Finally, Aim 4 applied this platform to the sustained silencing of PHD2 in full thickness excisional wounds in streptozotocin (STZ) induced diabetic rats. This study is described in more detail in Appendix D. Though gene silencing was not witnessed at the later time points (day 7 and day 14), PHD2 treated rat wounds showed a significant increase in vascular area by histology (**Appendix Fig. A28**). Both the PHD2 treated and SCR treated groups re-epithelialized in 2 weeks showing no apparent difference in wound healing capcity. Future work will address the limitations of this study and apply new materials to improve the gene silencing (section 6.4).

An important aspect of siRNA delivery exists in intravenous delivery and it was considered an important problem to pursue in addition to the aims above. Chapter 5 detailed the development of a modified nanoparticle optimized for IV delivery that improves pharmacokinetics of siRNA. Importantly, PEG-shielded, hydrophobically stabilized nanoparticles improved circulation time 3.2 fold compared to previously published PEG-DMAEMA resulting in significant gene silencing in the liver, kidneys, and spleen.

Together, these studies show that synthetic biomaterials may be used to address the delivery barriers of siRNA resulting in delivery platforms that can be modified and adapted for a wide range of pathologies.

6.2 Concerns and Limitations

Though the platforms developed in these studies were tested for toxicity and biocompatibility, it is important to note the following concerns related to nucleic acid delivery. The innate immune recognition of siRNA and the pathological response to cationic nanomaterials are two major hurdles that materials scientist and biologists are addressing and overcoming to allow clinical translation of gene silencing. Both of the following hurdles can be addressed with thorough screening of target and control siRNAs and careful consideration of the side-effects of the chosen delivery system.

Innate Immunity

Technologies for intracellular delivery of siRNA have advanced rapidly and are potentially approaching widespread adoption for clinical use. However, it should be cautioned that intracellular delivery of siRNA can lead to recognition by toll-like receptors (TLRs). TLRs recognize molecular patterns that are associated with pathogens including double stranded RNA, which can be representative of the viral genome. TLR response could result in pathological symptoms clinically, and it has also led to the false interpretation of pre-clinical results in studies related to viral repression, oncology, angiogenesis, and inflammation [55]. As a result of this phenomenon, it is recommended that siRNA studies carefully look for potential TLR-mediated effects. It is also advisable to replicate studies with multiple siRNA sequences against the gene of interest in order to ensure that any phenotypic changes are solely attributable to silencing of the target gene. Importantly, there is also ongoing work to create siRNAs that avoid immune activation entirely, and we are optimistic that these nonspecific effects will become more completely understood and entirely avoidable. For example, it is thought that immune recognition is sequence dependent [56] and that carefully selected siRNA sequences may avoid activation of the immune system. Also, chemical modifications of siRNA with 2-OMe nucleotides can help to eliminate TLR activation while producing negligible effects on gene silencing efficacy [55]. In our

work, we examined potential TLR responses by measuring TNFα and STAT-1 mRNA levels and found no large increase indicative of TLR recognition (**Appendix Fig. A10**) [301].

Inflammatory Response to Cationic Materials

The nanoparticles developed in these studies were designed to improve cytocompatibility over off-the-shelf lipid transfection reagents or polycationic materials such as PEI (**Appendix Fig. A5**). Many of the recently developed materials for delivering siRNA into the cytoplasm of cells employ cationic surface charge to electrostatically condense and entrap siRNA. A large body of research has shown that these cationic materials may alter gene expression independent of the siRNA that is being targeted [302] which may result in incorrect interpretation of data including falsely interpreting negative results or clouding positive results.

Applying cationic delivery materials for siRNA-mediated wound healing may create a deleterious side-effect on tissue regeneration by increasing inflammatory signaling that is desired to be repressed. This was witnessed when comparing scrambled siRNA loaded into cationic nanoparticles inside polyurethanes with a decrease noted in blood vessel formation (**Appendix Fig. A26A-B**). Also, bone marrow derived macrophages treated with nanoparticles with a scrambled siRNA showed a significant increase in TNFα levels indicating polarization of the macrophages toward and M1 phenotype (**Appendix Fig. A26C**). In this work, we have still shown a significant increase in blood vessel formation when PHD2 siRNA was used relative to NT and no apparent increase in toxicity. We noted a slight non-significant increases in TNFα levels in mouse subcutaneous implants when treated with a non-targeted, scrambled siRNA sequence (**Appendix Fig A10**) indicating the inflammation from the delivery platform we have selected is manageable and can be overcome with selected siRNA. In section 6.4, a brief discussion on possible future work to more effectively delivery siRNA without the cationic materials is provided.

6.3 Broader Impacts

Ongoing work discussed in section 6.4 will apply this material to larger animal models for ischemic and chronic wound healing. Successful tests may generate industrial interest in applying the platform for clinical translation. While it is expected that this platform will be a strong candidate for clinical development, it is possible that clinical translation of this specific platform may not occur. However, the impact of this technology is not limited to the clinic as this material is a powerful research tool for investigating loss of function for tissue engineering research.

Therapeutic for Chronic Wound Healing

The platform developed in this work may generate interest in the medical device and pharmaceutical industry as a novel method for local gene silencing. Gene silencing is beginning to generate industry interest with an increasing number of clinical trials showing promise [28]. However, there are still no clinically approved siRNA therapies, with only one clinically approved gene therapy [303] as the RNAi industry slowly recovers from an initial reluctance by the pharmaceutical industry. The cost associated with bringing a combination drug/device is astronomical approaching $700 million to $1.3 billion, according to the Tufts Center for the Study of Drug Development. To justify clinical development, the potential market must be large enough to support the product. Currently, the market for chronic wound healing is large ($25B) and is rapidly increasing due to the increasing prevalence in comorbidities. In fact, bioactive wound healing has an estimated market size of ~$1B and is considered one of the fastest growing segments of advanced wound care. The morbidity and mortality associated with non-healing wounds is also high including amputations and sepsis so products that reduce the clinical burden will be highly desired. Based on the cost analysis provided in Appendix D, the potential product would be competitive with other bioactive wound healing technologies. Acquisition by companies looking to expand their role in bioactive wound healing is a likely exit strategy (See Smith & Nephew's recent acquisition of Healthpoint Biotherapeutics).

Tissue Engineering Research Tool

An additional impact that this platform may have is by creating a large body of knowledge by silencing genes locally and observing the effects on tissue regeneration, wound healing, or other biologic fates. This will decrease the cost and time loss accompanying creating mouse knockout models for tissue regeneration studies and allow only local silencing for more diverse genes. This platform may also be used for cell studies as a 3D tissue engineered construct as the polyurethane promotes cell ingrowth and division *in vitro.*

6.4 Future Work

Based on the challenges laid out in 6.2 there is a wealth of future research that may be investigated including (1) improved siRNA chemistry to eliminate the need for an additional transfection material and (2) improving scaffold material such that the degradation rate matches the cell infiltration rate [163]. As described in Appendix D.2, the diabetic rat excisional wound healed rapidly in control groups, so a more chronic wound model may be pursued. As this platform is refined and improved, it will become important to test the materials in animal models for ischemic/chronic wound healing more representative of human skin. The porcine ischemic model may be a good model of human skin wounds that are pre-disposed to ulceration [304]. Another ongoing work will be the characterization of other silenced genes that may benefit regenerative medicine. An added benefit of this platform is that if PHD2 is deemed ineffective at promoting wound healing in diabetes, other siRNAs may be replaced with only minor screening requirements.

6.5 Conclusion

With the increasing knowledge of the molecular mechanisms of disease and rapid advancements in materials science, RNAi is poised to become a high impact therapeutic much in the way mono-clonal antibodies have developed in the last two decades. Coupled with an

increasing prevalence of chronic wounds, technologies that harness bioactive molecules to target the molecular basis of disease stand to greatly benefit quality of life.

Bibliography

[1] Meyer-Ingold W. Wound therapy: growth factors as agents to promote healing. Trends in biotechnology. 1993;11:387-92.
[2] Hu FB. Globalization of diabetes: the role of diet, lifestyle, and genes. Diabetes care. 2011;34:1249-57.
[3] Sahnoun M, Charreyre M-T, Veron L, Delair T, D'Agosto F. Synthetic and characterization aspects of dimethylaminoethyl methacrylate reversible addition fragmentation chain transfer (RAFT) polymerization. Journal of Polymer Science Part A: Polymer Chemistry. 2005;43:3551-65.
[4] Sen CK, Gordillo GM, Roy S, Kirsner R, Lambert L, Hunt TK, et al. Human skin wounds: a major and snowballing threat to public health and the economy. Wound Repair Regen. 2009;17:763-71.
[5] Dillingham TR, Pezzin LE, Shore AD. Reamputation, mortality, and health care costs among persons with dysvascular lower-limb amputations. Arch Phys Med Rehab. 2005;86:480-6.
[6] Thangarajah H, Vial IN, Grogan RH, Yao D, Shi Y, Januszyk M, et al. HIF-1alpha dysfunction in diabetes. Cell Cycle. 2010;9:75-9.
[7] Steed DL. Clinical evaluation of recombinant human platelet-derived growth factor for the treatment of lower extremity diabetic ulcers. Diabetic Ulcer Study Group. J Vasc Surg. 1995;21:71-8; discussion 9-81.
[8] Berra E, Benizri E, Ginouves A, Volmat V, Roux D, Pouyssegur J. HIF prolyl-hydroxylase 2 is the key oxygen sensor setting low steady-state levels of HIF-1 alpha in normoxia. Embo J. 2003;22:4082-90.
[9] Wu SR, Nishiyama N, Kano MR, Morishita Y, Miyazono K, Itaka K, et al. Enhancement of angiogenesis through stabilization of hypoxia-inducible factor-1 by silencing prolyl hydroxylase domain-2 gene. Molecular Therapy. 2008;16:1227-34.
[10] Fraisl P, Aragones J, Carmeliet P. Inhibition of oxygen sensors as a therapeutic strategy for ischaemic and inflammatory disease. Nature Reviews Drug Discovery. 2009;8:139-52.
[11] Bertrand JR, Pottier M, Vekris A, Opolon P, Maksimenko A, Malvy C. Comparison of antisense oligonucleotides and siRNAs in cell culture and in vivo. Biochem Bioph Res Co. 2002;296:1000-4.
[12] Fire A, Xu SQ, Montgomery MK, Kostas SA, Driver SE, Mello CC. Potent and specific genetic interference by double-stranded RNA in Caenorhabditis elegans. Nature. 1998;391:806-11.
[13] Hammond SM, Bernstein E, Beach D, Hannon GJ. An RNA-directed nuclease mediates post-transcriptional gene silencing in Drosophila cells. Nature. 2000;404:293-6.
[14] Zamora MR, Budev M, Rolfe M, Gottlieb J, Humar A, Devincenzo J, et al. RNA interference therapy in lung transplant patients infected with respiratory syncytial virus. Am J Respir Crit Care Med. 2011;183:531-8.
[15] Whitehead KA, Langer R, Anderson DG. Knocking down barriers: advances in siRNA delivery. Nat Rev Drug Discov. 2009;8:129-38.
[16] Davis ME, Zuckerman JE, Choi CHJ, Seligson D, Tolcher A, Alabi CA, et al. Evidence of RNAi in humans from systemically administered siRNA via targeted nanoparticles. Nature. 2010;464:1067-70.
[17] Layzer JM, McCaffrey AP, Tanner AK, Huang Z, Kay MA, Sullenger BA. In vivo activity of nuclease-resistant siRNAs. RNA. 2004;10:766-71.
[18] Dykxhoorn DM, Palliser D, Lieberman J. The silent treatment: siRNAs as small molecule drugs. Gene Ther. 2006;13:541-52.
[19] Krebs MD, Jeon O, Alsberg E. Localized and Sustained Delivery of Silencing RNA from Macroscopic Biopolymer Hydrogels. Journal of the American Chemical Society. 2009;131:9204-+.
[20] Vinas-Castells R, Holladay C, di Luca A, Diaz VM, Pandit A. Snail1 down-regulation using small interfering RNA complexes delivered through collagen scaffolds. Bioconjug Chem. 2009;20:2262-9.
[21] Nguyen PD, Tutela JP, Thanik VD, Knobel D, Allen RJ, Chang CC, et al. Improved diabetic wound healing through topical silencing of p53 is associated with augmented vasculogenic mediators. Wound Repair and Regeneration. 2010;18:553-9.

[22] Lee JW, Tutela JP, Zoumalan RA, Thanik VD, Nguyen PD, Varjabedian L, et al. Inhibition of Smad3 expression in radiation-induced fibrosis using a novel method for topical transcutaneous gene therapy. Arch Otolaryngol Head Neck Surg. 2010;136:714-9.
[23] Convertine A, Benoit D, Duvall C, Hoffman A, Stayton P. Development of a novel endosomolytic diblock copolymer for siRNA delivery. Journal of Controlled Release. 2009;133:221-9.
[24] Li B, Davidson JM, Guelcher SA. The effect of the local delivery of platelet-derived growth factor from reactive two-component polyurethane scaffolds on the healing in rat skin excisional wounds. Biomaterials. 2009;30:3486-94.
[25] Hafeman AE, Zienkiewicz KJ, Zachman AL, Sung HJ, Nanney LB, Davidson JM, et al. Characterization of the degradation mechanisms of lysine-derived aliphatic poly(ester urethane) scaffolds. Biomaterials. 2011;32:419-29.
[26] Yao Y, Wang C, Varshney RR, Wang DA. Antisense makes sense in engineered regenerative medicine. Pharm Res. 2009;26:263-75.
[27] Rettig GR, Behlke MA. Progress Toward In Vivo Use of siRNAs-II. Mol Ther. 2012;20:483-512.
[28] Kanasty R, Dorkin JR, Vegas A, Anderson D. Delivery materials for siRNA therapeutics. Nat Mater. 2013;12:967-77.
[29] Peer D, Lieberman J. Special delivery: targeted therapy with small RNAs. Gene Ther. 2011;18:1127-33.
[30] Jeong JH, Mok H, Oh YK, Park TG. siRNA conjugate delivery systems. Bioconjug Chem. 2009;20:5-14.
[31] Vicentini FT, Borgheti-Cardoso LN, Depieri LV, de Macedo Mano D, Abelha TF, Petrilli R, et al. Delivery systems and local administration routes for therapeutic siRNA. Pharm Res. 2013;30:915-31.
[32] Napoli C, Lemieux C, Jorgensen R. Introduction of a Chimeric Chalcone Synthase Gene into Petunia Results in Reversible Co-Suppression of Homologous Genes in trans. Plant Cell. 1990;2:279-89.
[33] Guo S, Kemphues KJ. Par-1, a Gene Required for Establishing Polarity in C-Elegans Embryos, Encodes a Putative Ser/Thr Kinase That Is Asymmetrically Distributed. Cell. 1995;81:611-20.
[34] Elbashir SM, Harborth J, Lendeckel W, Yalcin A, Weber K, Tuschl T. Duplexes of 21-nucleotide RNAs mediate RNA interference in cultured mammalian cells. Nature. 2001;411:494-8.
[35] Vogl DT, Gewirtz AM. Nucleic Acid Therapies for Cancer Treatment. Totowa, N.J: Humana; 2008.
[36] Paddison PJ, Caudy AA, Bernstein E, Hannon GJ, Conklin DS. Short hairpin RNAs (shRNAs) induce sequence-specific silencing in mammalian cells. Genes Dev. 2002;16:948-58.
[37] Bernstein E, Caudy AA, Hammond SM, Hannon GJ. Role for a bidentate ribonuclease in the initiation step of RNA interference. Nature. 2001;409:363-6.
[38] Kim DH, Behlke MA, Rose SD, Chang MS, Choi S, Rossi JJ. Synthetic dsRNA Dicer substrates enhance RNAi potency and efficacy. Nat Biotechnol. 2005;23:222-6.
[39] Tokatlian T, Segura T. siRNA applications in nanomedicine. Wiley Interdiscip Rev Nanomed Nanobiotechnol. 2010;2:305-15.
[40] Opanasopit P, Nishikawa M, Hashida M. Factors affecting drug and gene delivery: effects of interaction with blood components. Crit Rev Ther Drug Carrier Syst. 2002;19:191-233.
[41] Owens Iii DE, Peppas NA. Opsonization, biodistribution, and pharmacokinetics of polymeric nanoparticles. International Journal of Pharmaceutics. 2006;307:93-102.
[42] Duvall CL, Convertine AJ, Benoit DSW, Hoffman AS, Stayton PS. Intracellular Delivery of a Proapoptotic Peptide via Conjugation to a RAFT Synthesized Endosomolytic Polymer. Mol Pharmaceut. 2010;7:468-76.
[43] Al-Taei S, Penning NA, Simpson JC, Futaki S, Takeuchi T, Nakase I, et al. Intracellular traffic and fate of protein transduction domains HIV-1 TAT peptide and octaarginine. Implications for their utilization as drug delivery vectors. Bioconjug Chem. 2006;17:90-100.
[44] Belting M, Sandgren S, Wittrup A. Nuclear delivery of macromolecules: barriers and carriers. Adv Drug Deliv Rev. 2005;57:505-27.

[45] Flynn CR, Cheung-Flynn J, Smoke CC, Lowry D, Roberson R, Sheller MR, et al. Internalization and intracellular trafficking of a PTD-conjugated anti-fibrotic peptide, AZX100, in human dermal keloid fibroblasts. J Pharm Sci. 2010;99:3100-21.
[46] Ma PX. Biomimetic materials for tissue engineering. Adv Drug Deliv Rev. 2008;60:184-98.
[47] Elbashir SM, Lendeckel W, Tuschl T. RNA interference is mediated by 21-and 22-nucleotide RNAs. Gene Dev. 2001;15:188-200.
[48] Elbashir SM, Harborth J, Weber K, Tuschl T. Analysis of gene function in somatic mammalian cells using small interfering RNAs. Methods. 2002;26:199-213.
[49] Reynolds A, Leake D, Boese Q, Scaringe S, Marshall WS, Khvorova A. Rational siRNA design for RNA interference. Nat Biotech. 2004;22:326-30.
[50] Aigner A. Delivery systems for the direct application of siRNAs to induce RNA interference (RNAi) in vivo. J Biomed Biotechnol. 2006;2006:71659.
[51] Aigner A. Gene silencing through RNA interference (RNAi) in vivo: strategies based on the direct application of siRNAs. J Biotechnol. 2006;124:12-25.
[52] Kleinman ME, Yamada K, Takeda A, Chandrasekaran V, Nozaki M, Baffi JZ, et al. Sequence- and target-independent angiogenesis suppression by siRNA via TLR3. Nature. 2008;452:591-7.
[53] Jackson AL, Linsley PS. Recognizing and avoiding siRNA off-target effects for target identification and therapeutic application. Nat Rev Drug Discov.9:57-67.
[54] Behlke MA. Chemical modification of siRNAs for in vivo use. Oligonucleotides. 2008;18:305-19.
[55] Judge A, MacLachlan I. Overcoming the innate immune response to small interfering RNA. Hum Gene Ther. 2008;19:111-24.
[56] Judge AD, Sood V, Shaw JR, Fang D, McClintock K, MacLachlan I. Sequence-dependent stimulation of the mammalian innate immune response by synthetic siRNA. Nat Biotechnol. 2005;23:457-62.
[57] Judge AD, Bola G, Lee AC, MacLachlan I. Design of noninflammatory synthetic siRNA mediating potent gene silencing in vivo. Mol Ther. 2006;13:494-505.
[58] Lee H, Lytton-Jean AK, Chen Y, Love KT, Park AI, Karagiannis ED, et al. Molecularly self-assembled nucleic acid nanoparticles for targeted in vivo siRNA delivery. Nature nanotechnology. 2012;7:389-93.
[59] Lee JB, Hong J, Bonner DK, Poon Z, Hammond PT. Self-assembled RNA interference microsponges for efficient siRNA delivery. Nat Mater. 2012;11:316-22.
[60] Neff CP, Zhou J, Remling L, Kuruvilla J, Zhang J, Li H, et al. An aptamer-siRNA chimera suppresses HIV-1 viral loads and protects from helper CD4(+) T cell decline in humanized mice. Science translational medicine. 2011;3:66ra6.
[61] Lorenz C, Hadwiger P, John M, Vornlocher HP, Unverzagt C. Steroid and lipid conjugates of siRNAs to enhance cellular uptake and gene silencing in liver cells. Bioorganic & medicinal chemistry letters. 2004;14:4975-7.
[62] Soutschek J, Akinc A, Bramlage B, Charisse K, Constien R, Donoghue M, et al. Therapeutic silencing of an endogenous gene by systemic administration of modified siRNAs. Nature. 2004;432:173-8.
[63] Wolfrum C, Shi S, Jayaprakash KN, Jayaraman M, Wang G, Pandey RK, et al. Mechanisms and optimization of in vivo delivery of lipophilic siRNAs. Nat Biotechnol. 2007;25:1149-57.
[64] Nishina K, Unno T, Uno Y, Kubodera T, Kanouchi T, Mizusawa H, et al. Efficient in vivo delivery of siRNA to the liver by conjugation of alpha-tocopherol. Mol Ther. 2008;16:734-40.
[65] Alam MR, Ming X, Fisher M, Lackey JG, Rajeev KG, Manoharan M, et al. Multivalent cyclic RGD conjugates for targeted delivery of small interfering RNA. Bioconjug Chem. 2011;22:1673-81.
[66] Kubo T, Yanagihara K, Takei Y, Mihara K, Sato Y, Seyama T. Lipid-Conjugated 27-Nucleotide Double-Stranded RNAs with Dicer-Substrate Potency Enhance RNAi-Mediated Gene Silencing. Mol Pharmaceut. 2012;9:1374-83.
[67] Li HM, Nelson CE, Evans BC, Duvall CL. Delivery of Intracellular-Acting Biologics in Pro-Apoptotic Therapies. Curr Pharm Design. 2011;17:293-319.

[68] Gusbeth UFPaCA. Perturbation of human skin due to application of high voltage. Bioelectrochem. 2000;51:41-51.
[69] Rols MP, Delteil C, Golzio M, Dumond P, Cros S, Teissie J. In vivo electrically mediated protein and gene transfer in murine melanoma. Nat Biotechnol. 1998;16:168-71.
[70] Cahill K. Cell-penetrating peptides, electroporation and drug delivery. Iet Syst Biol. 2010;4:367-78.
[71] Banga AK, Prausnitz MR. Assessing the potential of skin electroporation for the delivery of protein- and gene-based drugs. Trends Biotechnol. 1998;16:408-12.
[72] Kigasawa K, Kajimoto K, Hama S, Saito A, Kanamura K, Kogure K. Noninvasive delivery of siRNA into the epidermis by iontophoresis using an atopic dermatitis-like model rat. Int J Pharm. 2010;383:157-60.
[73] Langkjaer L, Brange J, Grodsky GM, Guy RH. Iontophoresis of monomeric insulin analogues in vitro: effects of insulin charge and skin pretreatment. J Control Release. 1998;51:47-56.
[74] Hao JS, Li SK, Liu CY, Kao WWY. Electrically assisted delivery of macromolecules into the corneal epithelium. Exp Eye Res. 2009;89:934-41.
[75] Mitragotri S, Kost J. Low frequency sonophoresis: A noninvasive method of drug delivery and diagnostics. Biotechnol Progr. 2000;16:488-92.
[76] Potter H. Electroporation in Biology - Methods, Applications, and Instrumentation. Anal Biochem. 1988;174:361-73.
[77] Chakrabarti R, Wylie DE, Schuster SM. Transfer of Monoclonal-Antibodies into Mammalian-Cells by Electroporation. J Biol Chem. 1989;264:15494-500.
[78] Fretz MM, Hogset A, Koning GA, Jiskoot W, Storm G. Cytosolic delivery of liposomally targeted proteins induced by photochemical internalization. Pharm Res. 2007;24:2040-7.
[79] Raemdonck K, Naeye B, Hogset A, Demeester J, De Smedt SC. Prolonged gene silencing by combining siRNA nanogels and photochemical internalization. J Control Release. 2010;145:281-8.
[80] Lee WR, Pan TL, Wang PW, Zhuo RZ, Huang CM, Fang JY. Erbium:YAG laser enhances transdermal peptide delivery and skin vaccination. J Control Release. 2008;128:200-8.
[81] Lee WR, Shen SC, Zhuo RZ, Wang KC, Fang JY. Enhancement of Topical Small Interfering RNA Delivery and Expression by Low-Fluence Erbium: YAG Laser Pretreatment of Skin. Human Gene Therapy. 2009;20:580-8.
[82] El-Sayed A, Futaki S, Harashima H. Delivery of Macromolecules Using Arginine-Rich Cell-Penetrating Peptides: Ways to Overcome Endosomal Entrapment. Aaps J. 2009;11:13-22.
[83] Lopes LB, Flynn C, Komalavilas P, Panitch A, Brophy CM, Seal BL. Inhibition of HSP27 phosphorylation by a cell-permeant MAPKAP Kinase 2 inhibitor. Biochem Bioph Res Co. 2009;382:535-9.
[84] Nishikawa M, Otsuki T, Ota A, Guan X, Takemoto S, Takahashi Y, et al. Induction of Tumor-specific Immune Response by Gene Transfer of Hsp70-cell-penetrating Peptide Fusion Protein to Tumors in Mice. Mol Ther. 2010;18:421-8.
[85] De Coupade C, Fittipaldi A, Chagnas V, Michel M, Carlier S, Tasciott E, et al. Novel human-derived cell-penetrating peptides for specific subcellular delivery of therapeutic biomolecules. Biochem J. 2005;390:407-18.
[86] Saalik P, Elmquist A, Hansen M, Padari K, Saar K, Viht K, et al. Protein cargo delivery properties of cell-penetrating peptides. A comparative study. Bioconjugate Chem. 2004;15:1246-53.
[87] Banoczi Z, Gorka-Kereskenyi A, Remenyi J, Orban E, Hazai L, Tokesi N, et al. Synthesis and in Vitro Antitumor Effect of Vinblastine Derivative-Oligoarginine Conjugates. Bioconjugate Chem. 2010;21:1948-55.
[88] Yu HH, Nakase I, Pujals S, Hirose H, Tanaka G, Katayama S, et al. Expressed protein ligation for the preparation of fusion proteins with cell penetrating peptides for endotoxin removal and intracellular delivery. Bba-Biomembranes. 2010;1798:2249-57.
[89] Heitz F, Morris MC, Divita G. Twenty years of cell-penetrating peptides: from molecular mechanisms to therapeutics. Brit J Pharmacol. 2009;157:195-206.

[90] Patel LN, Zaro JL, Shen WC. Cell penetrating peptides: Intracellular pathways and pharmaceutical perspectives. Pharm Res. 2007;24:1977-92.
[91] Fuchs SM, Raines RT. Pathway for polyarginine entry into mammalian cell. Biochemistry. 2004;43:2438-44.
[92] Raagel H, Saalik P, Pooga M. Peptide-mediated protein delivery-Which pathways are penetrable? Bba-Biomembranes. 2010;1798:2240-8.
[93] Van Rossenberg SM, Sliedregt-Bol KM, Meeuwenoord NJ, Van Berkel TJ, Van Boom JH, Van Der Marel GA, et al. Targeted lysosome disruptive elements for improvement of parenchymal liver cell-specific gene delivery. J Biol Chem. 2002;277:45803-10.
[94] Efremov RG, Nolde DE, Volynsky PE, Chernyavsky AA, Dubovskii PV, Arseniev AS. Factors important for fusogenic activity of peptides: molecular modeling study of analogs of fusion peptide of influenza virus hemagglutinin. Febs Letters. 1999;462:205-10.
[95] Monsigny M, Roche AC, Midoux P, Mayer R. Glycoconjugates as Carriers for Specific Delivery of Therapeutic Drugs and Genes. Adv Drug Deliver Rev. 1994;14:1-24.
[96] Plank C, Oberhauser B, Mechtler K, Koch C, Wagner E. The Influence of Endosome-Disruptive Peptides on Gene-Transfer Using Synthetic Virus-Like Gene-Transfer Systems. J Biol Chem. 1994;269:12918-24.
[97] Holm T, Raagel H, Andaloussi SE, Hein M, Mae M, Pooga M, et al. Retro-inversion of certain cell-penetrating peptides causes severe cellular toxicity. Biochim Biophys Acta. 2010.
[98] Thomas CE, Ehrhardt A, Kay MA. Progress and problems with the use of viral vectors for gene therapy. Nature Reviews Genetics. 2003;4:346-58.
[99] Waehler R, Russell SJ, Curiel DT. Engineering targeted viral vectors for gene therapy. Nature Reviews Genetics. 2007;8:573-87.
[100] Huang Z, King MR. An immobilized nanoparticle-based platform for efficient gene knockdown of targeted cells in the circulation. Gene Ther. 2009;16:1271-82.
[101] Peer D, Park EJ, Morishita Y, Carman CV, Shimaoka M. Systemic leukocyte-directed siRNA delivery revealing cyclin D1 as an anti-inflammatory target. Science. 2008;319:627-30.
[102] Immordino ML, Dosio F, Cattel L. Stealth liposomes: review of the basic science, rationale, and clinical applications, existing and potential. Int J Nanomedicine. 2006;1:297-315.
[103] Samad A, Sultana Y, Aqil M. Liposomal drug delivery systems: an update review. Curr Drug Deliv. 2007;4:297-305.
[104] Morrissey DV, Lockridge JA, Shaw L, Blanchard K, Jensen K, Breen W, et al. Potent and persistent in vivo anti-HBV activity of chemically modified siRNAs. Nat Biotechnol. 2005;23:1002-7.
[105] Thomas JL, Barton SW, Tirrell DA. Membrane Solubilization by a Hydrophobic Polyelectrolyte - Surface-Activity and Membrane-Binding. Biophys J. 1994;67:1101-6.
[106] Akinc A, Thomas M, Klibanov AM, Langer R. Exploring polyethylenimine-mediated DNA transfection and the proton sponge hypothesis. J Gene Med. 2005;7:657-63.
[107] Thomas JL, Tirrell DA. Polyelectrolyte-Sensitized Phospholipid-Vesicles. Accounts Chem Res. 1992;25:336-42.
[108] Behr JP. The proton sponge: a means to enter cells viruses never though of. Med Sci. 1996;12:56-8.
[109] Kyriakides TR, Cheung CY, Murthy N, Bornstein P, Stayton PS, Hoffman AS. pH-sensitive polymers that enhance intracellular drug delivery in vivo. J Control Release. 2002;78:295-303.
[110] Wagner E, Ogris M, Zauner W. Polylysine-based transfection systems utilizing receptor-mediated delivery. Adv Drug Deliv Rev. 1998;30:97-113.
[111] Boussif O, Zanta MA, Behr JP. Optimized galenics improve in vitro gene transfer with cationic molecules up to 1000-fold. Gene Ther. 1996;3:1074-80.
[112] Harada Y, Iwai M, Tanaka S, Okanoue T, Kashima K, Maruyama-Tabata H, et al. Highly efficient suicide gene expression in hepatocellular carcinoma cells by epstein-barr virus-based plasmid vectors combined with polyamidoamine dendrimer. Cancer Gene Ther. 2000;7:27-36.

[113] Anderson DG, Akinc A, Hossain N, Langer R. Structure/property studies of polymeric gene delivery using a library of poly(beta-amino esters). Mol Ther. 2005;11:426-34.
[114] Wang CY, Huang L. Polyhistidine Mediates an Acid-Dependent Fusion of Negatively Charged Liposomes. Biochemistry. 1984;23:4409-16.
[115] Pichon C, Goncalves C, Midoux P. Histidine-rich peptides and polymers for nucleic acids delivery. Adv Drug Deliver Rev. 2001;53:75-94.
[116] Midoux P, Kichler A, Boutin V, Maurizot JC, Monsigny M. Membrane permeabilization and efficient gene transfer by a peptide containing several histidines. Bioconjugate Chem. 1998;9:260-7.
[117] Takeshita F, Minakuchi Y, Nagahara S, Honma K, Sasaki H, Hirai K, et al. Efficient delivery of small interfering RNA to bone-metastatic tumors by using atelocollagen in vivo. Proc Natl Acad Sci U S A. 2005;102:12177-82.
[118] Takeshita F, Ochiya T. Therapeutic potential of RNA interference against cancer. Cancer Sci. 2006;97:689-96.
[119] Noh SM, Han SE, Shim G, Lee KE, Kim CW, Han SS, et al. Tocopheryl oligochitosan-based self assembling oligomersomes for siRNA delivery. Biomaterials. 2011;32:849-57.
[120] Song WJ, Du JZ, Sun TM, Zhang PZ, Wang J. Gold nanoparticles capped with polyethyleneimine for enhanced siRNA delivery. Small. 2010;6:239-46.
[121] Derfus AM, Chen AA, Min D-H, Ruoslahti E, Bhatia SN. Targeted Quantum Dot Conjugates for siRNA Delivery. Bioconjugate Chem. 2007;18:1391-6.
[122] Yezhelyev MV, Qi L, Oâ€™Regan RM, Nie S, Gao X. Proton-Sponge Coated Quantum Dots for siRNA Delivery and Intracellular Imaging. J Am Chem Soc. 2008;130:9006-12.
[123] Zuckerman JE, Choi CHJ, Han H, Davis ME. Polycation-siRNA nanoparticles can disassemble at the kidney glomerular basement membrane. P Natl Acad Sci USA. 2012;109:3137-42.
[124] Nelson CE, Kintzing JR, Hanna A, Shannon JM, Gupta MK, Duvall CL. Balancing Cationic and Hydrophobic Content of PEGylated siRNA Polyplexes Enhances Endosome Escape, Stability, Blood Circulation Time, and Bioactivity in Vivo. ACS Nano. 2013.
[125] Nam HY, McGinn A, Kim PH, Kim SW, Bull DA. Primary cardiomyocyte-targeted bioreducible polymer for efficient gene delivery to the myocardium. Biomaterials. 2010;31:8081-7.
[126] Christensen LV, Chang CW, Kim WJ, Kim SW, Zhong Z, Lin C, et al. Reducible poly(amido ethylenimine)s designed for triggered intracellular gene delivery. Bioconjug Chem. 2006;17:1233-40.
[127] Truong NP, Jia Z, Burgess M, Payne L, McMillan NA, Monteiro MJ. Self-catalyzed degradable cationic polymer for release of DNA. Biomacromolecules. 2011;12:3540-8.
[128] Lynn DM, Langer R. Degradable poly(beta-amino esters): Synthesis, characterization, and self-assembly with plasmid DNA. J Am Chem Soc. 2000;122:10761-8.
[129] Vandenbroucke RE, De Geest BG, Bonne S, Vinken M, Van Haecke T, Heimberg H, et al. Prolonged gene silencing in hepatoma cells and primary hepatocytes after small interfering RNA delivery with biodegradable poly(beta-amino esters). J Gene Med. 2008;10:783-94.
[130] Borden KA, Eum KM, Langley KH, Tirrell DA. Interactions of Synthetic-Polymers with Cell-Membranes + Model Membrane Systems .13. On the Mechanism of Polyelectrolyte-Induced Structural Reorganization in Thin Molecular Films. Macromolecules. 1987;20:454-6.
[131] Lackey CA, Press OW, Hoffman AS, Stayton PS. A biomimetic pH-responsive polymer directs endosomal release and intracellular delivery of an endocytosed antibody complex. Bioconjugate Chem. 2002;13:996-1001.
[132] Convertine AJ, Benoit DSW, Duvall CL, Hoffman AS, Stayton PS. Development of a novel endosomolytic diblock copolymer for siRNA delivery. Journal of Controlled Release. 2009;133:221-9.
[133] Convertine AJ, Diab C, Prieve M, Paschal A, Hoffman AS, Johnson PH, et al. pH-Responsive Polymeric Micelle Carriers for siRNA Drugs. Biomacromolecules. 2010.

[134] Murthy N, Campbell J, Fausto N, Hoffman AS, Stayton PS. Bioinspired pH-responsive polymers for the intracellular delivery of biomolecular drugs. Bioconjug Chem. 2003;14:412-9.
[135] Murthy N, Campbell J, Fausto N, Hoffman AS, Stayton PS. Design and synthesis of pH-responsive polymeric carriers that target uptake and enhance the intracellular delivery of oligonucleotides. J Control Release. 2003;89:365-74.
[136] Alexis F, Pridgen E, Molnar LK, Farokhzad OC. Factors affecting the clearance and biodistribution of polymeric nanoparticles. Mol Pharm. 2008;5:505-15.
[137] Lv H, Zhang S, Wang B, Cui S, Yan J. Toxicity of cationic lipids and cationic polymers in gene delivery. J Control Release. 2006;114:100-9.
[138] Dash PR, Read ML, Barrett LB, Wolfert MA, Seymour LW. Factors affecting blood clearance and in vivo distribution of polyelectrolyte complexes for gene delivery. Gene Ther. 1999;6:643-50.
[139] Verbaan FJ, Oussoren C, van Dam IM, Takakura Y, Hashida M, Crommelin DJ, et al. The fate of poly(2-dimethyl amino ethyl)methacrylate-based polyplexes after intravenous administration. Int J Pharm. 2001;214:99-101.
[140] Xu L, Anchordoquy T. Drug delivery trends in clinical trials and translational medicine: Challenges and opportunities in the delivery of nucleic acid-based therapeutics. J Pharm Sci. 2011;100:38-52.
[141] Yan X, Scherphof GL, Kamps JA. Liposome opsonization. J Liposome Res. 2005;15:109-39.
[142] Li SD, Huang L. Nanoparticles evading the reticuloendothelial system: role of the supported bilayer. Biochimica et biophysica acta. 2009;1788:2259-66.
[143] Zhang Y, Li H, Sun J, Gao J, Liu W, Li B, et al. DC-Chol/DOPE cationic liposomes: a comparative study of the influence factors on plasmid pDNA and siRNA gene delivery. Int J Pharm. 2010;390:198-207.
[144] Naeye B, Raemdonck K, Remaut K, Sproat B, Demeester J, De Smedt SC. PEGylation of biodegradable dextran nanogels for siRNA delivery. Eur J Pharm Sci. 2010;40:342-51.
[145] Wang XL, Xu R, Lu ZR. A peptide-targeted delivery system with pH-sensitive amphiphilic cell membrane disruption for efficient receptor-mediated siRNA delivery. Journal of Controlled Release. 2009;134:207-13.
[146] Glodde M, Sirsi SR, Lutz GJ. Physiochemical properties of low and high molecular weight poly(ethylene glycol)-grafted poly(ethylene imine) copolymers and their complexes with oligonucleotides. Biomacromolecules. 2006;7:347-56.
[147] Itaka K, Yamauchi K, Harada A, Nakamura K, Kawaguchi H, Kataoka K. Polyion complex micelles from plasmid DNA and poly(ethylene glycol)-poly(L-lysine) block copolymer as serum-tolerable polyplex system: physicochemical properties of micelles relevant to gene transfection efficiency. Biomaterials. 2003;24:4495-506.
[148] Luo D, Haverstick K, Belcheva N, Han E, Saltzman WM. Poly(ethylene glycol)-conjugated PAMAM dendrimer for biocompatible, high-efficiency DNA delivery. Macromolecules. 2002;35:3456-62.
[149] Taratula O, Garbuzenko OB, Kirkpatrick P, Pandya I, Savla R, Pozharov VP, et al. Surface-engineered targeted PPI dendrimer for efficient intracellular and intratumoral siRNA delivery. Journal of Controlled Release. 2009;140:284-93.
[150] Deshpande MC, Garnett MC, Vamvakaki M, Bailey L, Armes SP, Stolnik S. Influence of polymer architecture on the structure of complexes formed by PEG-tertiary amine methacrylate copolymers and phosphorothioate oligonucleotide. J Control Release. 2002;81:185-99.
[151] Hatakeyama H, Ito E, Akita H, Oishi M, Nagasaki Y, Futaki S, et al. A pH-sensitive fusogenic peptide facilitates endosomal escape and greatly enhances the gene silencing of siRNA-containing nanoparticles in vitro and in vivo. Journal of Controlled Release. 2009;139:127-32.
[152] Li HM, Yu SS, Miteva M, Nelson CE, Werfel T, Giorgio TD, et al. Matrix Metalloproteinase Responsive, Proximity-Activated Polymeric Nanoparticles for siRNA Delivery. Adv Funct Mater. 2013;23:3040-52.
[153] Chen Y, Bathula SR, Li J, Huang L. Multifunctional nanoparticles delivering small interfering RNA and doxorubicin overcome drug resistance in cancer. J Biol Chem. 2010;285:22639-50.

[154] Cao N, Cheng D, Zou S, Ai H, Gao J, Shuai X. The synergistic effect of hierarchical assemblies of siRNA and chemotherapeutic drugs co-delivered into hepatic cancer cells. Biomaterials. 2010.
[155] Lu W, Zhang G, Zhang R, Flores LG, 2nd, Huang Q, Gelovani JG, et al. Tumor site-specific silencing of NF-kappaB p65 by targeted hollow gold nanosphere-mediated photothermal transfection. Cancer Research. 2010;70:3177-88.
[156] Antony AC, Kincade RS, Verma RS, Krishnan SR. Identification of high affinity folate binding proteins in human erythrocyte membranes. J Clin Invest. 1987;80:711-23.
[157] Daniels TR, Delgado T, Rodriguez JA, Helguera G, Penichet ML. The transferrin receptor part I: Biology and targeting with cytotoxic antibodies for the treatment of cancer. Clin Immunol. 2006;121:144-58.
[158] Nelson CE, Kim AJ, Adolph EJ, Gupta MK, Yu F, Hocking KM, et al. Tunable Delivery of siRNA from a Biodegradable Scaffold to Promote Angiogenesis In Vivo. Advanced materials. 2014;26:607-14.
[159] Lee K, Silva EA, Mooney DJ. Growth factor delivery-based tissue engineering: general approaches and a review of recent developments. Journal of the Royal Society Interface. 2011;8:153-70.
[160] De Laporte L, Shea LD. Matrices and scaffolds for DNA delivery in tissue engineering. Advanced Drug Delivery Reviews. 2007;59:292-307.
[161] Place ES, Evans ND, Stevens MM. Complexity in biomaterials for tissue engineering. Nat Mater. 2009;8:457-70.
[162] De Laporte L, Shea LD. Matrices and scaffolds for DNA delivery in tissue engineering. Adv Drug Deliv Rev. 2007;59:292-307.
[163] Martin JR, Gupta MK, Page JM, Yu F, Davidson JM, Guelcher SA, et al. A porous tissue engineering scaffold selectively degraded by cell-generated reactive oxygen species. Biomaterials. 2014.
[164] Galperin A, Long TJ, Garty S, Ratner BD. Synthesis and fabrication of a degradable poly(N-isopropyl acrylamide) scaffold for tissue engineering applications. J Biomed Mater Res A. 2013;101:775-86.
[165] Li B, Yoshii T, Hafeman AE, Nyman JS, Wenke JC, Guelcher SA. The effects of rhBMP-2 released from biodegradable polyurethane/microsphere composite scaffolds on new bone formation in rat femora. Biomaterials. 2009;30:6768-79.
[166] Li B, Brown KV, Wenke JC, Guelcher SA. Sustained release of vancomycin from polyurethane scaffolds inhibits infection of bone wounds in a rat femoral segmental defect model. Journal of Controlled Release. 2010;145:221-30.
[167] Guelcher SA. Biodegradable Polyurethanes: Synthesis and Applications in Regenerative Medicine. Tissue Engineering Part B: Reviews. 2008;14:3-17.
[168] Adolph EJ, Hafeman A, Davidson J, Nanney L, Guelcher S. Injectable Polyurethane Composite Scaffolds Delay Wound Contraction and Support Cellular Infiltration and Remodeling in Rat Excisional Wounds. Journal of Biomedical Materials Research: Part A. (accepted).
[169] Hafeman AE, Li B, Yoshii T, Zienkiewicz K, Davidson JM, Guelcher SA. Injectable biodegradable polyurethane scaffolds with release of platelet-derived growth factor for tissue repair and regeneration. Pharm Res. 2008;25:2387-99.
[170] Nguyen K, Dang PN, Alsberg E. Functionalized, biodegradable hydrogels for control over sustained and localized siRNA delivery to incorporated and surrounding cells. Acta Biomater. 2013;9:4487-95.
[171] Wetterau M, George F, Weinstein A, Nguyen PD, Tutela JP, Knobel D, et al. Topical prolyl hydroxylase domain-2 silencing improves diabetic murine wound closure. Wound Repair and Regeneration. 2011;19:481-6.
[172] Mountziaris PM, Sing DC, Chew SA, Tzouanas SN, Lehman ED, Kasper FK, et al. Controlled release of anti-inflammatory siRNA from biodegradable polymeric microparticles intended for intra-articular delivery to the temporomandibular joint. Pharm Res. 2011;28:1370-84.

[173] Mountziaris PM, Tzouanas SN, Sing DC, Kramer PR, Kasper FK, Mikos AG. Intra-articular controlled release of anti-inflammatory siRNA with biodegradable polymer microparticles ameliorates temporomandibular joint inflammation. Acta Biomater. 2012;8:3552-60.
[174] Kim YM, Park MR, Song SC. Injectable polyplex hydrogel for localized and long-term delivery of siRNA. ACS Nano. 2012;6:5757-66.
[175] Kim YM, Park MR, Song SC. An injectable cell penetrable nano-polyplex hydrogel for localized siRNA delivery. Biomaterials. 2013;34:4493-500.
[176] Castleberry S, Wang M, Hammond PT. Nanolayered siRNA Dressing for Sustained Localized Knockdown. Acs Nano. 2013;7:5251-61.
[177] Guan J, Stankus JJ, Wagner WR. Biodegradable elastomeric scaffolds with basic fibroblast growth factor release. J Control Release. 2007;120:70-8.
[178] Nelson DM, Baraniak PR, Ma Z, Guan J, Mason NS, Wagner WR. Controlled release of IGF-1 and HGF from a biodegradable polyurethane scaffold. Pharm Res. 2011;28:1282-93.
[179] Lei YG, Huang SX, Sharif-Kashani P, Chen Y, Kavehpour P, Segura T. Incorporation of active DNA/cationic polymer polyplexes into hydrogel scaffolds. Biomaterials. 2010;31:9106-16.
[180] Lei YG, Rahim M, Ng Q, Segura T. Hyaluronic acid and fibrin hydrogels with concentrated DNA/PEI polyplexes for local gene delivery. Journal of Controlled Release. 2011;153:255-61.
[181] Nelson CE, Gupta MK, Adolph EJ, Shannon JM, Guelcher SA, Duvall CL. Sustained local delivery of siRNA from an injectable scaffold. Biomaterials. 2012;33:1154-61.
[182] Shea LD, Smiley E, Bonadio J, Mooney DJ. DNA delivery from polymer matrices for tissue engineering. Nat Biotechnol. 1999;17:551-4.
[183] Luo D, Saltzman WM. Enhancement of transfection by physical concentration of DNA at the cell surface. Nature Biotechnology. 2000;18:893-5.
[184] Segura T, Shea LD. Surface-tethered DNA complexes for enhanced gene delivery. Bioconjugate Chem. 2002;13:621-9.
[185] Hanenberg H, Xiao XL, Dilloo D, Hashino K, Kato I, Williams DA. Colocalization of retrovirus and target cells on specific fibronectin fragments increases genetic transduction of mammalian cells. Nature Medicine. 1996;2:876-82.
[186] Lei P, Bajaj B, Andreadis ST. Retrovirus-associated heparan sulfate mediates immobilization and gene transfer on recombinant fibronectin. J Virol. 2002;76:8722-8.
[187] Bengali Z, Rea JC, Shea LD. Gene expression and internalization following vector adsorption to immobilized proteins: dependence on protein identity and density. J Gene Med. 2007;9:668-78.
[188] Salvay DM, Zelivyanskaya M, Shea LD. Gene delivery by surface immobilization of plasmid to tissue-engineering scaffolds. Gene Therapy. 2010;17:1134-41.
[189] Jang JH, Rives CB, Shea LD. Plasmid delivery in vivo from porous tissue-engineering scaffolds: transgene expression and cellular transfection. Mol Ther. 2005;12:475-83.
[190] Thanik VD, Greives MR, Lerman OZ, Seiser N, Dec W, Chang CC, et al. Topical matrix-based siRNA silences local gene expression in a murine wound model. Gene Ther. 2007;14:1305-8.
[191] Han HD, Mora EM, Roh JW, Nishimura M, Lee SJ, Stone RL, et al. Chitosan hydrogel for localized gene silencing. Cancer Biol Ther. 2011;11:839-45.
[192] Manaka T, Suzuki A, Takayama K, Imai Y, Nakamura H, Takaoka K. Local delivery of siRNA using a biodegradable polymer application to enhance BMP-induced bone formation. Biomaterials. 2011;32:9642-8.
[193] Rujitanaroj PO, Wang YC, Wang J, Chew SY. Nanofiber-mediated controlled release of siRNA complexes for long term gene-silencing applications. Biomaterials. 2011;32:5915-23.
[194] Chen ML, Gao S, Dong MD, Song J, Yang CX, Howard KA, et al. Chitosan/siRNA Nanoparticles Encapsulated in PLGA Nanofibers for siRNA Delivery. Acs Nano. 2012;6:4835-44.

[195] Takahashi H, Wang Y, Grainger DW. Device-based local delivery of siRNA against mammalian target of rapamycin (mTOR) in a murine subcutaneous implant model to inhibit fibrous encapsulation. J Control Release. 2010;147:400-7.
[196] Cheema SK, Chen E, Shea LD, Mathur AB. Regulation and guidance of cell behavior for tissue regeneration via the siRNA mechanism. Wound Repair Regen. 2007;15:286-95.
[197] Palliser D, Chowdhury D, Wang QY, Lee SJ, Bronson RT, Knipe DM, et al. An siRNA-based microbicide protects mice from lethal herpes simplex virus 2 infection. Nature. 2006;439:89-94.
[198] Zhang W, Yang H, Kong X, Mohapatra S, San Juan-Vergara H, Hellermann G, et al. Inhibition of respiratory syncytial virus infection with intranasal siRNA nanoparticles targeting the viral NS1 gene. Nat Med. 2005;11:56-62.
[199] Andersen MO, Nygaard JV, Burns JS, Raarup MK, Nyengaard JR, Bunger C, et al. siRNA nanoparticle functionalization of nanostructured scaffolds enables controlled multilineage differentiation of stem cells. Mol Ther. 2010;18:2018-27.
[200] Jakobsen M, Stenderup K, Rosada C, Moldt B, Kamp S, Dam TN, et al. Amelioration of psoriasis by anti-TNF-alpha RNAi in the xenograft transplantation model. Mol Ther. 2009;17:1743-53.
[201] Zhang Y, Cristofaro P, Silbermann R, Pusch O, Boden D, Konkin T, et al. Engineering mucosal RNA interference in vivo. Mol Ther. 2006;14:336-42.
[202] Nakamura M, Jo JI, Tabata Y, Ishikawa O. Controlled delivery of T-box21 small interfering RNA ameliorates autoimmune alopecia (alopecia areata) in a C3H/HeJ mouse model. Am J Pathol. 2008;172:650-8.
[203] Ritprajak P, Hashiguchi M, Azuma M. Topical application of cream-emulsified CD86 siRNA ameliorates allergic skin disease by targeting cutaneous dendritic cells. Molecular Therapy. 2008;16:1323-30.
[204] Kawakami E, Kawai N, Kinouchi N, Mori H, Ohsawa Y, Ishimaru N, et al. Local Applications of Myostatin-siRNA with Atelocollagen Increase Skeletal Muscle Mass and Recovery of Muscle Function. Plos One. 2013;8.
[205] Lu P, Zhang GR, Song XH, Zou XH, Wang LL, Ouyang HW. Col V siRNA Engineered Tenocytes for Tendon Tissue Engineering. Plos One. 2011;6.
[206] Abraham D. Connective tissue growth factor: growth factor, matricellular organizer, fibrotic biomarker or molecular target for anti-fibrotic therapy in SSc. Rheumatology. 2008;47:V8-V9.
[207] Takahashi H, Wang YW, Grainger DW. Device-based local delivery of siRNA against mammalian target of rapamycin (mTOR) in a murine subcutaneous implant model to inhibit fibrous encapsulation. Journal of Controlled Release. 2010;147:400-7.
[208] Huang JS, Wang YH, Ling TY, Chuang SS, Johnson FE, Huang SS. Synthetic TGF-beta antagonist accelerates wound healing and reduces scarring. Faseb J. 2002;16:1269-70.
[209] Nakamura H, Siddiqui SS, Shen X, Malik AB, Pulido JS, Kumar NM, et al. RNA interference targeting transforming growth factor-beta type II receptor suppresses ocular inflammation and fibrosis. Molecular vision. 2004;10:703-11.
[210] Wang Z, Gao Z, Shi Y, Sun Y, Lin Z, Jiang H, et al. Inhibition of Smad3 expression decreases collagen synthesis in keloid disease fibroblasts. Journal of plastic, reconstructive & aesthetic surgery : JPRAS. 2007;60:1193-9.
[211] Zhang C, Kong X, Liu C, Liang Z, Zhao H, Tong W, et al. ERK2 small interfering RNAs prevent epidural fibrosis via the efficient inhibition of collagen expression and inflammation in laminectomy rats. Biochem Biophys Res Commun. 2014.
[212] Bedelbaeva K, Snyder A, Gourevitch D, Clark L, Zhang XM, Leferovich J, et al. Lack of p21 expression links cell cycle control and appendage regeneration in mice. Proc Natl Acad Sci U S A. 2010;107:5845-50.
[213] Brem H, Tomic-Canic M. Cellular and molecular basis of wound healing in diabetes. Journal of Clinical Investigation. 2007;117:1219-22.

[214] Ivan M, Kondo K, Yang H, Kim W, Valiando J, Ohh M, et al. HIFalpha targeted for VHL-mediated destruction by proline hydroxylation: implications for O2 sensing. Science. 2001;292:464-8.
[215] Jaakkola P, Mole DR, Tian YM, Wilson MI, Gielbert J, Gaskell SJ, et al. Targeting of HIF-alpha to the von Hippel-Lindau ubiquitylation complex by O2-regulated prolyl hydroxylation. Science. 2001;292:468-72.
[216] Epstein ACR, Gleadle JM, McNeill LA, Hewitson KS, O'Rourke J, Mole DR, et al. C-elegans EGL-9 and mammalian homologs define a family of dioxygenases that regulate HIF by prolyl hydroxylation. Cell. 2001;107:43-54.
[217] Semenza GL. Regulation of Oxygen Homeostasis by Hypoxia-Inducible Factor 1. Physiology. 2009;24:97-106.
[218] Agis H, Watzek G, Gruber R. Prolyl hydroxylase inhibitors increase the production of vascular endothelial growth factor by periodontal fibroblasts. Journal of Periodontal Research. 2012;47:165-73.
[219] Ceradini DJ, Kulkarni AR, Callaghan MJ, Tepper OM, Bastidas N, Kleinman ME, et al. Progenitor cell trafficking is regulated by hypoxic gradients through HIF-1 induction of SDF-1. Nat Med. 2004;10:858-64.
[220] Alfranca A. VEGF therapy: a timely retreat. Cardiovascular Research. 2009;83:611-2.
[221] Brudno Y, Ennett-Shepard AB, Chen RR, Aizenberg M, Mooney DJ. Enhancing microvascular formation and vessel maturation through temporal control over multiple pro-angiogenic and pro-maturation factors. Biomaterials. 2013;34:9201-9.
[222] Loinard C, Ginouvès A, Vilar J, Cochain C, Zouggari Y, Recalde A, et al. Inhibition of Prolyl Hydroxylase Domain Proteins Promotes Therapeutic Revascularization. Circulation. 2009;120:50-9.
[223] Shen X, Wan C, Ramaswamy G, Mavalli M, Wang Y, Duvall CL, et al. Prolyl hydroxylase inhibitors increase neoangiogenesis and callus formation following femur fracture in mice. Journal of Orthopaedic Research. 2009;27:1298-305.
[224] Nelson CE, Kim AJ, Adolph EJ, Gupta MK, Yu F, Hocking KM, et al. Tunable Delivery of siRNA from a Biodegradable Scaffold to Promote Angiogenesis In Vivo. Advanced Materials. In Press.
[225] Botusan IR, Sunkari VG, Savu O, Catrina AI, Grunler J, Lindberg S, et al. Stabilization of HIF-1alpha is critical to improve wound healing in diabetic mice. Proc Natl Acad Sci U S A. 2008;105:19426-31.
[226] Kaiser PK, Symons RC, Shah SM, Quinlan EJ, Tabandeh H, Do DV, et al. RNAi-based treatment for neovascular age-related macular degeneration by Sirna-027. Am J Ophthalmol. 2010;150:33-9 e2.
[227] Leachman SA, Hickerson RP, Schwartz ME, Bullough EE, Hutcherson SL, Boucher KM, et al. First-in-human mutation-targeted siRNA phase Ib trial of an inherited skin disorder. Mol Ther. 2010;18:442-6.
[228] Davis ME. The first targeted delivery of siRNA in humans via a self-assembling, cyclodextrin polymer-based nanoparticle: from concept to clinic. Mol Pharm. 2009;6:659-68.
[229] Ribas A, Zuckerman JE, Hsueh T, Koya RC, Davis ME. siRNA Knockdown of Ribonucleotide Reductase Inhibits Melanoma Cell Line Proliferation Alone or Synergistically with Temozolomide. Journal of Investigative Dermatology. 2011;131:453-60.
[230] White PJ. Barriers to successful delivery of short interfering RNA after systemic administration. Clin Exp Pharmacol Physiol. 2008;35:1371-6.
[231] Gao K, Huang L. Nonviral methods for siRNA delivery. Mol Pharm. 2009;6:651-8.
[232] Agrawal A, Min DH, Singh N, Zhu H, Birjiniuk A, von Maltzahn G, et al. Functional delivery of siRNA in mice using dendriworms. ACS Nano. 2009;3:2495-504.
[233] Convertine AJ, Benoit DS, Duvall CL, Hoffman AS, Stayton PS. Development of a novel endosomolytic diblock copolymer for siRNA delivery. J Control Release. 2009;133:221-9.
[234] Jafari M, Chen P. Peptide mediated siRNA delivery. Curr Top Med Chem. 2009;9:1088-97.
[235] Lee JS, Green JJ, Love KT, Sunshine J, Langer R, Anderson DG. Gold, poly(beta-amino ester) nanoparticles for small interfering RNA delivery. Nano Lett. 2009;9:2402-6.
[236] Qi L, Gao X. Quantum dot-amphipol nanocomplex for intracellular delivery and real-time imaging of siRNA. ACS Nano. 2008;2:1403-10.

[237] Watanabe K, Harada-Shiba M, Suzuki A, Gokuden R, Kurihara R, Sugao Y, et al. In vivo siRNA delivery with dendritic poly(L-lysine) for the treatment of hypercholesterolemia. Mol Biosyst. 2009;5:1306-10.
[238] Wu SY, McMillan NA. Lipidic systems for in vivo siRNA delivery. AAPS J. 2009;11:639-52.
[239] Xia CF, Boado RJ, Pardridge WM. Antibody-mediated targeting of siRNA via the human insulin receptor using avidin-biotin technology. Mol Pharm. 2009;6:747-51.
[240] Ghosn B, Kasturi SP, Roy K. Enhancing polysaccharide-mediated delivery of nucleic acids through functionalization with secondary and tertiary amines. Curr Top Med Chem. 2008;8:331-40.
[241] Moad G, Chiefari J, Chong YK, Ercole F, Krstina J, Jeffery J, et al. Living free-radical polymerization by reversible addition-fragmentation chain transfer: The RAFT process. Macromolecules. 1998;31:5559-62.
[242] Boyer C, Bulmus V, Davis TP, Ladmiral V, Liu J, Perrier S. Bioapplications of RAFT polymerization. Chem Rev. 2009;109:5402-36.
[243] Moad G, Chong YK, Postma A, Rizzardo E, Thang SH. Advances in RAFT polymerization: the synthesis of polymers with defined end-groups. Polymer. 2005;46:8458-68.
[244] Ferrito M, Tirrell DA. Poly(2-ethylacrylic acid). Macromol Synth. 1992;11:59-62.
[245] Guelcher SA, Patel V, Gallagher KM, Connolly S, Didier JE, Doctor JS, et al. Synthesis and in vitro biocompatibility of injectable polyurethane foam scaffolds. Tissue Eng. 2006;12:1247-59.
[246] Guelcher S, Srinivasan A, Hafeman A, Gallagher K, Doctor J, Khetan S, et al. Synthesis, in vitro degradation, and mechanical properties of two-component poly(ester urethane)urea scaffolds: effects of water and polyol composition. Tissue Eng. 2007;13:2321-33.
[247] Papadopoulou V, Kosmidis K, Vlachou M, Macheras P. On the use of the Weibull function for the discernment of drug release mechanisms. International Journal of Pharmaceutics. 2006;309:44-50.
[248] Duvall CL, Convertine AJ, Benoit DS, Hoffman AS, Stayton PS. Intracellular delivery of a proapoptotic peptide via conjugation to a RAFT synthesized endosomolytic polymer. Mol Pharm. 2010;7:468-76.
[249] Siepmann J, Peppas NA. Higuchi equation: Derivation, applications, use and misuse. Int J Pharm. 2011;418:6-12.
[250] Barone F, Cellai L, Matzeu M, Mazzei F, Pedone F. DNA, RNA and hybrid RNA-DNA oligomers of identical sequence: structural and dynamic differences. Biophys Chem. 2000;86:37-47.
[251] Akhtar S, Benter IF. Nonviral delivery of synthetic siRNAs in vivo. J Clin Invest. 2007;117:3623-32.
[252] Medina-Kauwe LK, Xie J, Hamm-Alvarez S. Intracellular trafficking of nonviral vectors. Gene Ther. 2005;12:1734-51.
[253] Cho YW, Kim JD, Park K. Polycation gene delivery systems: escape from endosomes to cytosol. J Pharm Pharmacol. 2003;55:721-34.
[254] van der Aa MA, Huth US, Hafele SY, Schubert R, Oosting RS, Mastrobattista E, et al. Cellular uptake of cationic polymer-DNA complexes via caveolae plays a pivotal role in gene transfection in COS-7 cells. Pharm Res. 2007;24:1590-8.
[255] Jones RA, Cheung CY, Black FE, Zia JK, Stayton PS, Hoffman AS, et al. Poly(2-alkylacrylic acid) polymers deliver molecules to the cytosol by pH-sensitive disruption of endosomal vesicles. Biochem J. 2003;372:65-75.
[256] El-Sayed ME, Hoffman AS, Stayton PS. Rational design of composition and activity correlations for pH-sensitive and glutathione-reactive polymer therapeutics. J Control Release. 2005;101:47-58.
[257] Thomas JL, Barton SW, Tirrell DA. Membrane solubilization by a hydrophobic polyelectrolyte: surface activity and membrane binding. Biophys J. 1994;67:1101-6.
[258] Hoffman AS, Lackey CA, Press OW, Stayton PS. A biomimetic pH-responsive polymer directs endosomal release and intracellular delivery of an endocytosed antibody complex. Bioconjugate Chem. 2002;13:996-1001.
[259] Krebs MD, Alsberg E. Localized, Targeted, and Sustained siRNA Delivery. Chem-Eur J. 2011;17:3054-62.

[260] Lei Y, Rahim M, Ng Q, Segura T. Hyaluronic acid and fibrin hydrogels with concentrated DNA/PEI polyplexes for local gene delivery. J Control Release. 2011.
[261] Dominska M, Dykxhoorn DM. Breaking down the barriers: siRNA delivery and endosome escape. Journal of Cell Science.123:1183-9.
[262] Tabernero J, Shapiro GI, Lorusso PM, Cervantes A, Schwartz GK, Weiss GJ, et al. First-in-Man Trial of an RNA Interference Therapeutic Targeting VEGF and KSP in Cancer Patients with Liver Involvement. Cancer discovery. 2013.
[263] Adolph EJ, Hafeman A, Davidson J, Nanney L, Guelcher S. Injectable Polyurethane Composite Scaffolds Delay Wound Contraction and Support Cellular Infiltration and Remodeling in Rat Excisional Wounds. Journal of Biomedical Materials Research: Part A. 2012;100A:450-61.
[264] Li HM, Yu SS, Miteva M, Nelson CE, Giorgio TD, Duvall CL. Matrix Metalloproteinase Responsive, Proximity-Activated Targeting Polymeric Nanoparticles for siRNA Delivery to Tumor Metastases. Molecular Therapy. 2012;20:S266-S.
[265] Boyer C, Teo J, Phillips P, Erlich RB, Sagnella S, Sharbeen G, et al. Effective delivery of siRNA into cancer cells and tumors using well-defined biodegradable cationic star polymers. Mol Pharm. 2013;10:2435-44.
[266] Kaushik JK, Bhat R. Why is trehalose an exceptional protein stabilizer? An analysis of the thermal stability of proteins in the presence of the compatible osmolyte trehalose. Journal of Biological Chemistry. 2003;278:26458-65.
[267] Nugent M, McLaren A, Vernon B, McLemore R. Strength of antimicrobial bone cement decreases with increased poragen fraction. Clinical orthopaedics and related research. 2010;468:2101-6.
[268] Bou-Gharios G, Garrett LA, Rossert J, Niederreither K, Eberspaecher H, Smith C, et al. A potent far-upstream enhancer in the mouse pro alpha 2(I) collagen gene regulates expression of reporter genes in transgenic mice. J Cell Biol. 1996;134:1333-44.
[269] Wu N, Jansen ED, Davidson JM. Comparison of mouse matrix metalloproteinase 13 expression in free-electron laser and scalpel incisions during wound healing. The Journal of investigative dermatology. 2003;121:926-32.
[270] Larange A, Antonios D, Pallardy M, Kerdine-Romer S. TLR7 and TLR8 agonists trigger different signaling pathways for human dendritic cell maturation. J Leukocyte Biol. 2009;85:673-83.
[271] Shen X, Wan C, Ramaswamy G, Mavalli M, Wang Y, Duvall CL, et al. Prolyl hydroxylase inhibitors increase neoangiogenesis and callus formation following femur fracture in mice. Journal of orthopaedic research : official publication of the Orthopaedic Research Society. 2009;27:1298-305.
[272] Duvall CL, Taylor WR, Weiss D, Guldberg RE. Quantitative microcomputed tomography analysis of collateral vessel development after ischemic injury. Am J Physiol-Heart C. 2004;287:H302-H10.
[273] van Weel V, van Tongeren RB, van Hinsbergh VW, van Bockel JH, Quax PH. Vascular growth in ischemic limbs: a review of mechanisms and possible therapeutic stimulation. Annals of vascular surgery. 2008;22:582-97.
[274] Guldberg RE, Duvall CL, Peister A, Oest ME, Lin AS, Palmer AW, et al. 3D imaging of tissue integration with porous biomaterials. Biomaterials. 2008;29:3757-61.
[275] Duvall CL, Weiss D, Robinson ST, Alameddine FMF, Guldberg RE, Taylor WR. The role of osteopontin in recovery from hind limb ischemia. Arterioscl Throm Vas. 2008;28:290-5.
[276] Phelps EA, Landazuri N, Thule PM, Taylor WR, Garcia AJ. Bioartificial matrices for therapeutic vascularization. P Natl Acad Sci USA. 2010;107:3323-8.
[277] Mislick KA, Baldeschwieler JD. Evidence for the role of proteoglycans in cation-mediated gene transfer. Proc Natl Acad Sci U S A. 1996;93:12349-54.
[278] Petersen H, Fechner PM, Martin AL, Kunath K, Stolnik S, Roberts CJ, et al. Polyethylenimine-graft-poly(ethylene glycol) copolymers: Influence of copolymer block structure on DNA complexation and biological activities as gene delivery system. Bioconjugate Chem. 2002;13:845-54.

[279] Rungsardthong U, Deshpande M, Bailey L, Vamvakaki M, Armes SP, Garnett MC, et al. Copolymers of amine methacrylate with poly(ethylene glycol) as vectors for gene therapy. J Control Release. 2001;73:359-80.
[280] Venkataraman S, Ong WL, Ong ZY, Joachim Loo SC, Ee PL, Yang YY. The role of PEG architecture and molecular weight in the gene transfection performance of PEGylated poly(dimethylaminoethyl methacrylate) based cationic polymers. Biomaterials. 2011;32:2369-78.
[281] Mishra S, Webster P, Davis ME. PEGylation significantly affects cellular uptake and intracellular trafficking of non-viral gene delivery particles. Eur J Cell Biol. 2004;83:97-111.
[282] Sato A, Choi SW, Hirai M, Yamayoshi A, Moriyarna R, Yamano T, et al. Polymer brush-stabilized polyplex for a siRNA carrier with long circulatory half-life. Journal of Controlled Release. 2007;122:209-16.
[283] Verbaan FJ, Oussoren C, Snel CJ, Crommelin DJ, Hennink WE, Storm G. Steric stabilization of poly(2-(dimethylamino)ethyl methacrylate)-based polyplexes mediates prolonged circulation and tumor targeting in mice. J Gene Med. 2004;6:64-75.
[284] Behr JP. The proton sponge, a means to enter cells viruses never thought of. M S-Med Sci. 1996;12:56-8.
[285] Behr JP. The proton sponge: A trick to enter cells the viruses did not exploit. Chimia. 1997;51:34-6.
[286] Lee H, Jeong JH, Park TG. A new gene delivery formulation of polyethylenimine/DNA complexes coated with PEG conjugated fusogenic peptide. J Control Release. 2001;76:183-92.
[287] Manganiello MJ, Cheng C, Convertine AJ, Bryers JD, Stayton PS. Diblock copolymers with tunable pH transitions for gene delivery. Biomaterials. 2012;33:2301-9.
[288] Cheng C, Convertine AJ, Stayton PS, Bryers JD. Multifunctional triblock copolymers for intracellular messenger RNA delivery. Biomaterials. 2012;33:6868-76.
[289] Liu Z, Zhang Z, Zhou C, Jiao Y. Hydrophobic modifications of cationic polymers for gene delivery. Progress in Polymer Science. 2010;35:1144-62.
[290] Gary DJ, Lee H, Sharma R, Lee JS, Kim Y, Cui ZY, et al. Influence of nano-carrier architecture on in vitro siRNA delivery performance and in vivo biodistribution: polyplexes vs micelleplexes. ACS Nano. 2011;5:3493-505.
[291] Xiao K, Li Y, Luo J, Lee JS, Xiao W, Gonik AM, et al. The effect of surface charge on in vivo biodistribution of PEG-oligocholic acid based micellar nanoparticles. Biomaterials. 2011;32:3435-46.
[292] Arvizo RR, Rana S, Miranda OR, Bhattacharya R, Rotello VM, Mukherjee P. Mechanism of anti-angiogenic property of gold nanoparticles: role of nanoparticle size and surface charge. Nanomedicine : nanotechnology, biology, and medicine. 2011;7:580-7.
[293] Evans BC, Nelson CE, Yu SS, Beavers KR, J. KA, Li H, et al. Ex Vivo Red Blood Cell Hemolysis Assay for the Evaluation Of PH-responsive Endosomolytic Agents for Cytosolic Delivery of Biomacromolecular Drugs. J Vis Exp. 2012:e50166, doi:10.3791/.
[294] Bartlett DW, Davis ME. Physicochemical and biological characterization of targeted, nucleic acid-containing nanoparticles. Bioconjug Chem. 2007;18:456-68.
[295] Gupta MK, Meyer TA, Nelson CE, Duvall CL. Poly(PS-b-DMA) micelles for reactive oxygen species triggered drug release. J Control Release. 2012;162:591-8.
[296] Naeye B, Deschout H, Caveliers V, Descamps B, Braeckmans K, Vanhove C, et al. In vivo disassembly of IV administered siRNA matrix nanoparticles at the renal filtration barrier. Biomaterials. 2013;34:2350-8.
[297] Chong YK, Le TPT, Moad G, Rizzardo E, Thang SH. A more versatile route to block copolymers and other polymers of complex architecture by living radical polymerization: The RAFT process. Macromolecules. 1999;32:2071-4.
[298] Joshi RV, Nelson CE, Poole KM, Skala MC, Duvall CL. Dual pH- and temperature-responsive microparticles for protein delivery to ischemic tissues. Acta Biomaterialia. 2013;9:6526-34.

[299] Bolte S, Cordelieres FP. A guided tour into subcellular colocalization analysis in light microscopy. J Microsc-Oxford. 2006;224:213-32.
[300] Liu L, Marti GP, Wei X, Zhang X, Zhang H, Liu YV, et al. Age-dependent impairment of HIF-1α expression in diabetic mice: Correction with electroporation-facilitated gene therapy increases wound healing, angiogenesis, and circulating angiogenic cells. Journal of Cellular Physiology. 2008;217:319-27.
[301] Sledz CA, Holko M, de Veer MJ, Silverman RH, Williams BRG. Activation of the interferon system by short-interfering RNAs. Nat Cell Biol. 2003;5:834-9.
[302] Akhtar S, Benter I. Toxicogenomics of non-viral drug delivery systems for RNAi: potential impact on siRNA-mediated gene silencing activity and specificity. Adv Drug Deliv Rev. 2007;59:164-82.
[303] Kastelein JJ, Ross CJ, Hayden MR. From mutation identification to therapy: discovery and origins of the first approved gene therapy in the Western world. Hum Gene Ther. 2013;24:472-8.
[304] Roy S, Biswas S, Khanna S, Gordillo G, Bergdall V, Green J, et al. Characterization of a preclinical model of chronic ischemic wound. Physiological Genomics. 2009;37:211-24.

Appendix A - Supplementary Information for Chapter 3

Supplemental Information

Sustained local delivery of siRNA from an injectable scaffold

Christopher E. Nelson[#], Mukesh K. Gupta, Elizabeth J. Adolph, Joshua M. Shannon, Scott A. Guelcher, Craig L. Duvall.

Contents of Supplemental Methods

A.1. Polymer Synthesis and Characterization

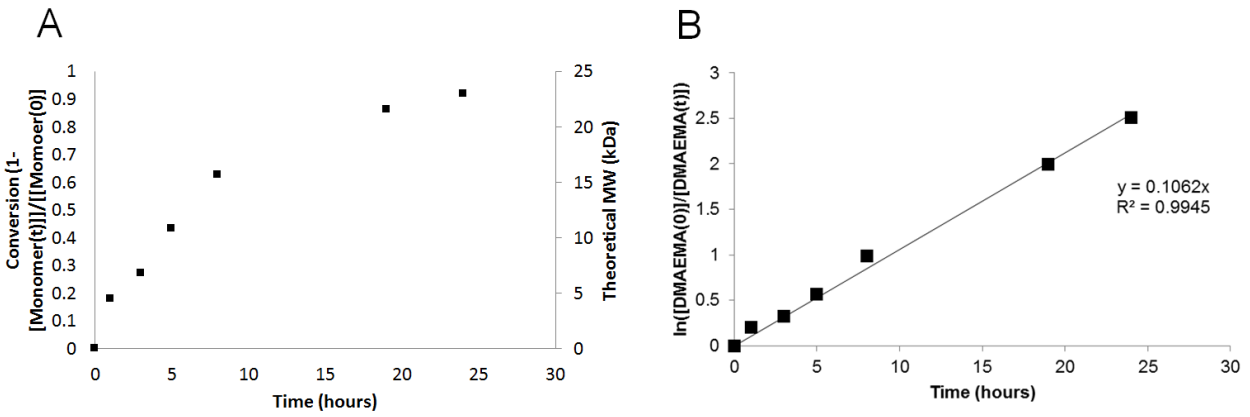

Figure A1: RAFT kinetics study on polymerization of pDMAEMA mCTA. A) Conversion is initially linear and then begins to plateau. B) The log plot of the kinetics shows a linear first order polymerization kinetics. Eight hour polymerization time was selected for the desired block length and %conversion.

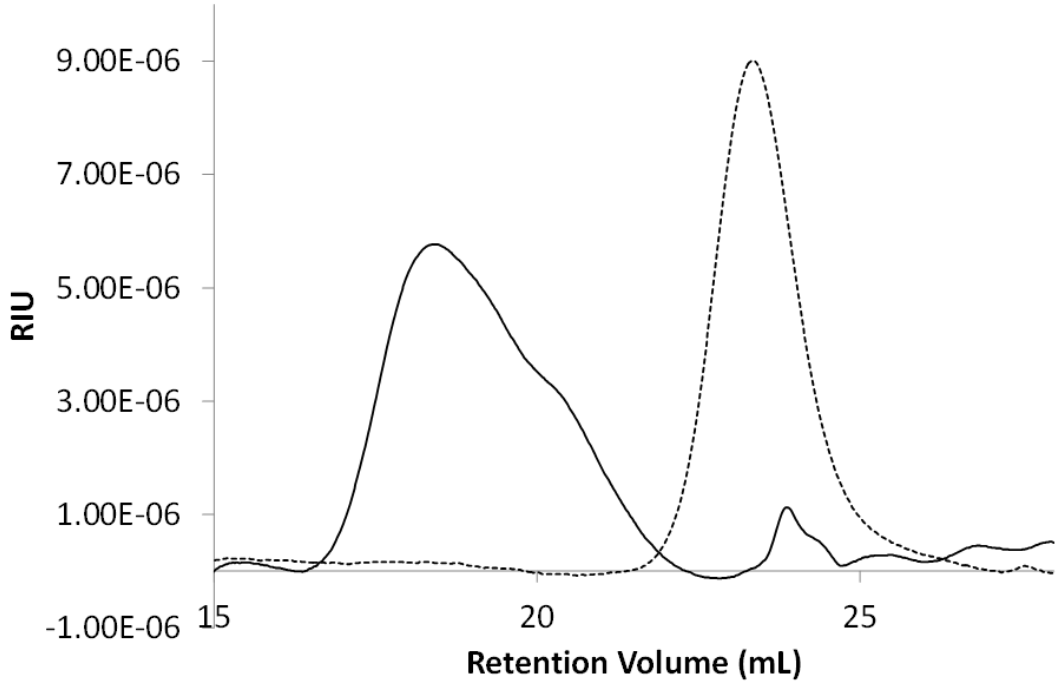

Figure A2: Refractive Index traces from Gel Permeation Chromatography for macro CTA of DMAEMA (dotted line) and diblock copolymer (solid line)

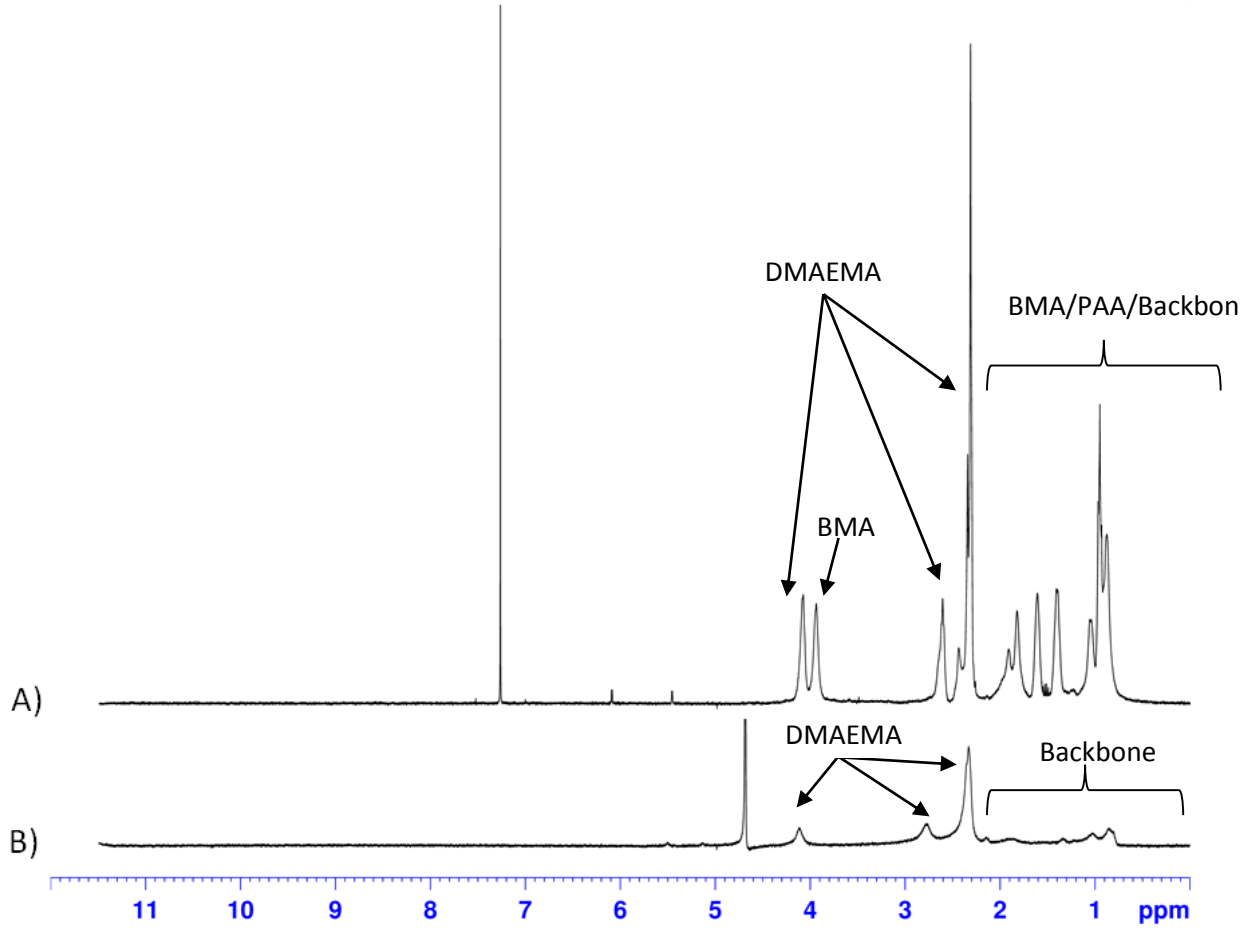

Figure A3: ^{1}H NMR in $CDCL_3$ (A) and D_2O (B) demonstrates micelle formation. A) $CDCL_3$ spectrum has all peaks due to the good solvation of both blocks. B) Peaks in the hydrophobic block are suppressed due to the poor solvation. Peaks in the DMAEMA block show up the strongest.

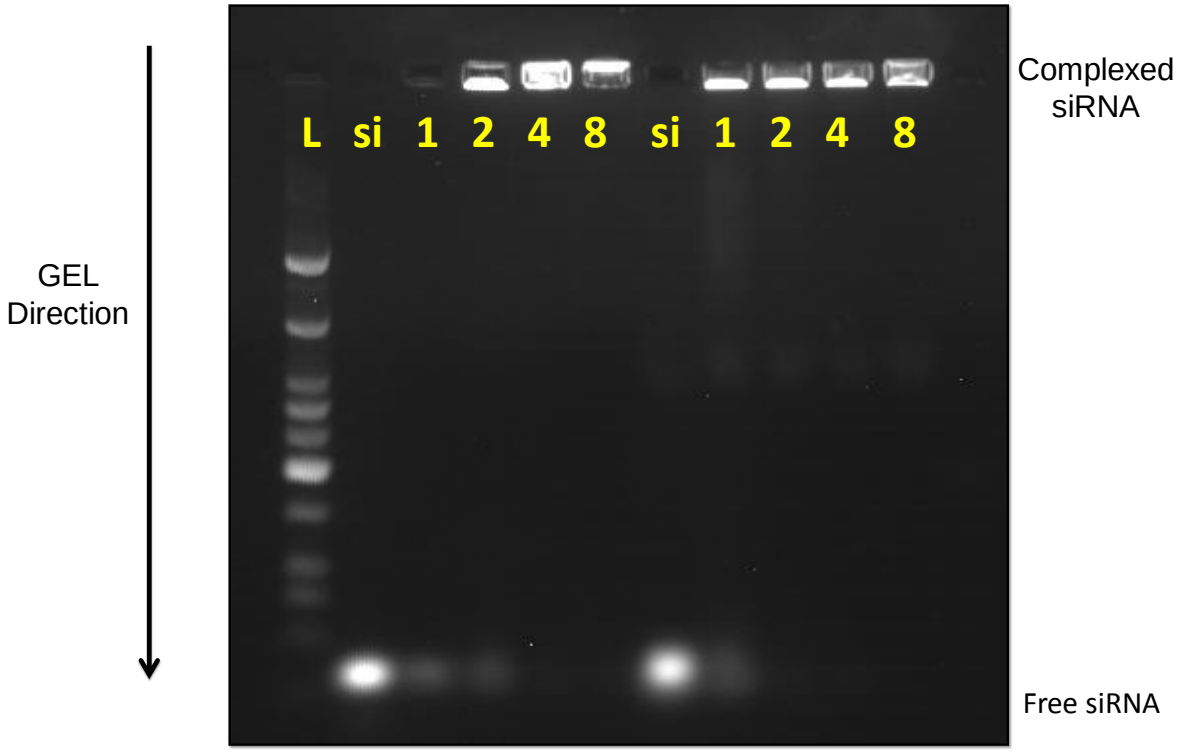

Figure A4: si-NPs effectively complex siRNA and are serum stable. Gel electrophoresis of si-NPs formulated at varying charge ratios shown in yellow letters. The left half of the gel is in nuclease free water. The right half is completed in 50% Bovine Calf Serum proving stability to serum proteins. A charge ratio of 4:1 was utilized for further experimentation.

A.2. NP Cytotoxicity Measurement

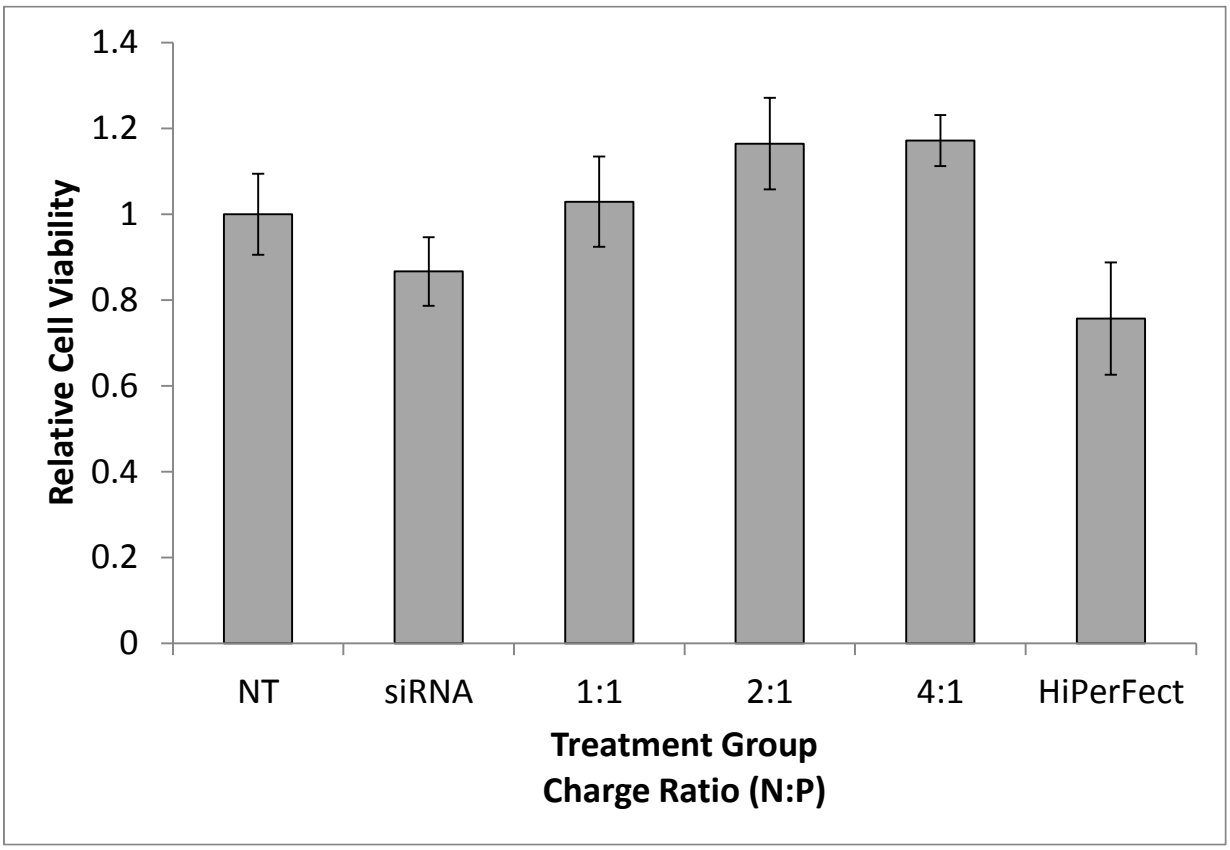

Figure A5: Cytotoxicity profile of treatment groups shows minimal toxicity at the charge ratios used during this study.

Appendix B - Supplementary Information for Chapter 4

Supplemental Information

Tunable Delivery of siRNA from a Biodegradable Scaffold to Promote Angiogenesis In Vivo

Christopher E. Nelson[#], Arnold J. Kim, Elizabeth J. Adolph, Mukesh K. Gupta, Fang Yu, Kyle M. Hocking, Jeffrey M. Davidson, Scott A. Guelcher, Craig L. Duvall.

Contents of Supplemental Methods

B.1 siRNA and primer sequences

Nucleic Acids were purchased from Integrated DNA Technologies (IDT, Coralville, IA, USA) based on the design principle that dsRNAs that contain a 27-mer antisense strand and a 25-mer sense strand have up to a 10-fold increased potency compared to 21-mer siRNA counterparts[1]. In addition, 2'-O-methyl (2-OMe) nucleotides were incorporated to improve duplex stability and nuclease resistance without affecting silencing activity or producing toxicity [2]. Minimal 2-OMe modifications on the backbone of the dsRNA were made to eliminate toll-like receptor activation and an immune response, with negligible effects on the potency of gene silencing [3, 4]. All listed siRNAs were screened *in vitro* before use *in vivo* (**Table A1**). Fluorescent labels were used in portions of the manuscript including 6-FAM and cy5. These labels were obtained from IDT which are purified by HPLC.

Table A1 – Nucleic acid sequences

Name	Sequence	mRNA Target Location	Silencing (in vitro 50nM)	Reference
dsDNA	S: 5′-FAM-GTCAGAAATAGAAACTGGTCATC-3′ AS:5′-GATGACCAGTTTCTATTTCTGAC-3′	N/A	N/A	[5]
PPIB#1 NM_011149	S: 5′-GCCUUAGCUACAGGAGAGAAAGG[dA][dT]-3′ AS:5′-AUCCUUUCUCUCCUGUAGCUAAGGCUA-3′	329	10%	N/A
PPIB#2 NM_011149	S: 5′-GCAUGGAUGUGGUACGGAAGGUG[dG][dA]-3′ AS:5′-UCCACCUUCCGUACCACAUCCAUGCCC-3′	621	95%	N/A
PPIB#3 NM_011149	S: 5′-CGAUAAGAAGAAGGGACCUAAAG[dT][dC]-3′ AS:5′-GACUUUAGGUCCCUUCUUCUUAUCGUU-3′	199	30%	N/A
Anti-Luciferase pGL2	S: 5′-CGUACGCGGAAUACUUCGAAAUG[dT][dC]-3′ AS:5′-GACAUUUCGAAGUAUUCCGCGUACGUG-3′	230	55%	[6, 7]
Scrambled	DS Scrambled Neg – from IDT	N/A	N/A	
PHD2 #1	S: 5′-ACAUAGUUACAAGAGGAAACAAGCC – 3′ AS: 5′-GGCUUGUUUCCUCUUGUAACUAUGUUG – 3′	2094	78%	
PHD2 #2	S: 5′-ACCUAACAGUAGAUGGUUGCCACTG – 3′ AS: 5′-CAGUGGCAACCAUCUACUGUUAGGUCG – 3′	2053	67%	
PHD2 #3	S: 5′ – GGUACGCAAUAACUGUUUGGUAUTT –3′ AS: 5′-AAAUACCAAACAGUUAUUGCGUACCUU – 3′	1278	8.2%	
PPIB Primers	FWD: 5′-TTCCATCGTGTCATCAAG-3′ REV: 5′-GAAGAACTGTGAGCCATT-3′			
GAPDH Primers	FWD: 5′-CTCACTCAAGATTGTCAGCAATG-3′ REV: 5′-GAGGGAGATGCTCAGTGTTGG-3′			
STAT-1 Primers	FWD: 5′-GCAACTGGCATATAACTT-3′ REV: 5′-GTGACATCCTTGAGATTC-3′			
TNFα Primers	FWD: 5′-CAAAGGGATGAGAAGTTC-3′ REV: 5′-TGAGAAGATGATCTGAGT-3′			
PHD2 Primers	FWD: 5′-ATCTAACAGGTGAGAAAGGT-3′ REV: 5′-ACAGAAGGCAACTGAGAG-3′			
VEGF Primers	FWD: 5'-CCTGGTGGACATCTTCCAGGAGTA-3' REV: 5'-CTCACCGCCTTGGCTTGTCACA-3'			
FGF-2 Primers	FWD: 5'-CTCCAGTTGGTATGTGGCACT-3' REV: 5'-CAGTATGGCCTTCTGTCCAGG-3'			

B.2. Poly[DMAEMA$_{71}$-b-(BMA$_{103}$-co-PAA$_{68}$-co-DMAEMA$_{57}$)]and nanoparticle (NP) characterization

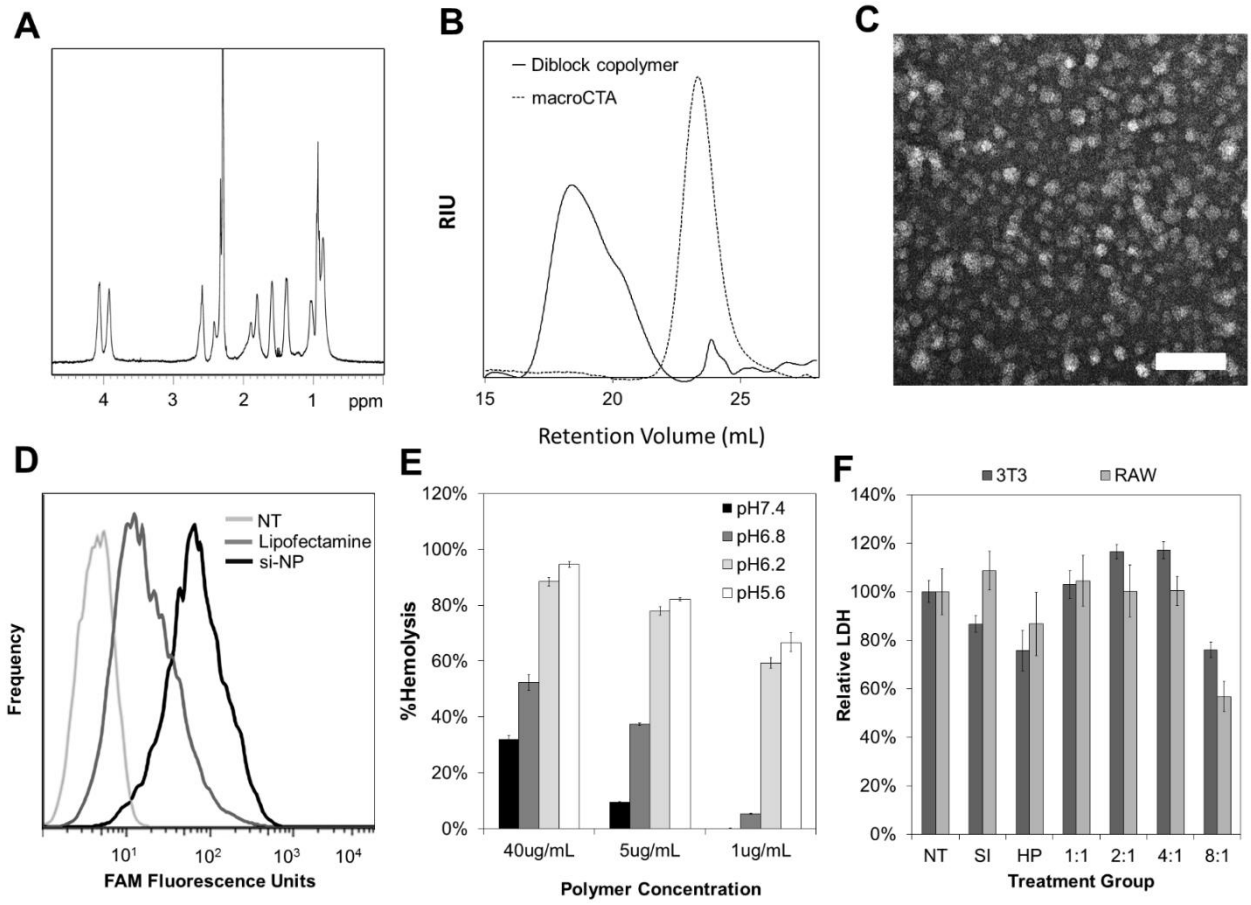

Figure A6: Characterization of Poly[DMAEMA$_{71}$-b-(BMA$_{103}$-co-PAA$_{68}$-co-DMAEMA$_{57}$)] and self-assembled nanoparticles. These data are representative of the polymer and the NPs used in this study. The formulations are similar to those characterized in previous publications [8-10]. **A**) H^1 NMR of the polymer was used to determine percent composition of each monomer. **B)** GPC for the DMAEMA macroCTA and the diblock copolymer were utilized to determine molecular weight and polydispersity. **C)** TEM of the NPs after micellar assembly of poly[DMAEMA$_{71}$-b-(BMA$_{103}$-co-PAA$_{68}$-co-DMAEMA$_{57}$)] shows a uniform structure of the particles(Scale = 100 nm). **D)** Flow cytometry of NIH3T3 mouse fibroblast uptake of fluorescently labeled dsDNA loaded into si-NPs and Lipofectamine 2000 relative to control cells with no treatment demonstrate a higher level of uptake for NPs. **E)** The hemolysis assay was used to demonstrate that the pH-dependent membrane disruptive activity of the NPs is appropriately tuned for endosomlytic behavior. **F)** All NP formulations used in this study were cytocompatible compared to a no treatment (NT) control, siRNA only (SI), and HiPerFect (HP) as shown by this LDH assay (note that 4:1 charge ratio (NH_3+/PO_4-) was utilized for all si-NPs formulations in these studies).

B.3. The Weibull model for release kinetics

Equation A.1: $$\frac{M_t}{M_\infty} = 1 - exp(-a \cdot t^b)$$

The Weibull model describes the % of mass of si-NPs released (M_t/M_∞) at time t, where *a* is a constant based on the system, and *b* is a constant based on the release kinetics. Previous reports suggest that values of b < 0.75 indicate that Fickian diffusion is the dominant release mechanism [11, 12].

Table A2. Weibull Model Analysis – In Vitro Release Data

Formulation	a	b	R^2
LTI – 0T	0.0273	0.5511	0.992
LTI – 1.25T	0.1582	0.3488	0.9183
LTI – 2.5T	0.4797	0.3648	0.869
LTI – 5T	1.729	0.4448	0.8736
HDIT – 0T	0.026	0.336	0.9792
HDIT – 1.25T	0.0399	0.3828	0.9764
HDIT – 2.5T	0.0691	0.4818	0.9689
HDIT – 5T	0.1451	0.4402	0.99

Table A3. Weibull Model Analysis – In Vivo Release Data

Formulation	a	b	R^2
LTI – 0T	0.433	0.3052	0.8912
LTI – 1.25T	0.9976	0.1599	0.8236
LTI – 5T	1.336	0.2436	0.7426
HDIT – 0T	0.2912	0.3707	0.8921
HDIT – 1.25T	0.4716	0.3591	0.9295
HDIT – 5T	0.867	0.317	0.8564

B.4. Representative release kinetics images

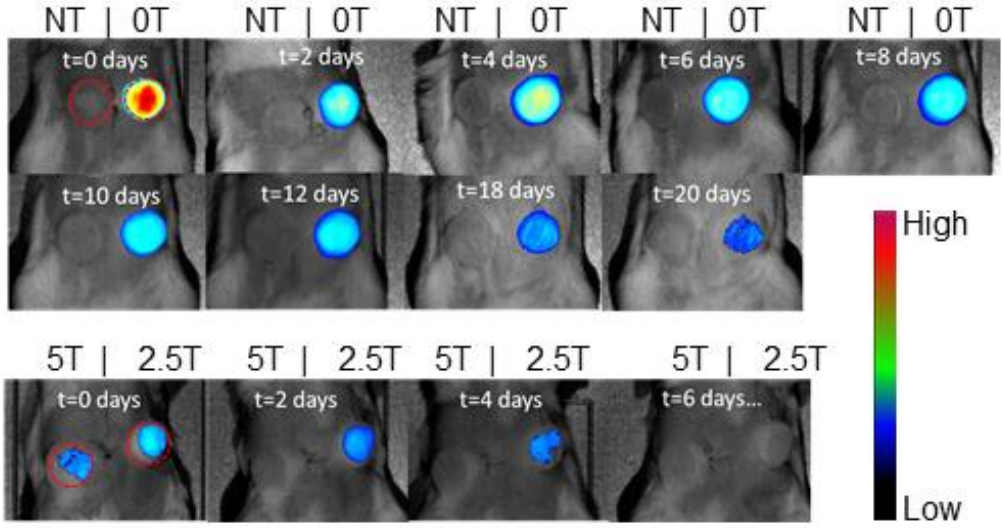

Figure A7. Visual Representation of Release Kinetics. The release kinetics data (Figure 2K, 2L) was calculated by loading the si-NPs with Cy5-labeled siRNA and measuring the change in fluorescence within the PEUR scaffolds with intravital imaging. In each case, a region of interest (shown in red) was defined that contained just the scaffold, and the average fluorescence was calculated and compared to the initial image of PUR before implantation (after compensating for loss of fluorescence from imaging through the tissue). The representative images above visually demonstrate the rate of loss of Cy5 fluorescence within the scaffold.

B.5. The 4 parameter logistic model used for IC_{50} and dose response analysis

Equation A.2:

$$\%\text{Expression} = \frac{-1}{\left(1+\left(\frac{x}{IC_{50}}\right)^{b}\right)} + 1$$

B.6. Temporal control of the gene silencing profile for scaffolds composed of HDIT PEUR

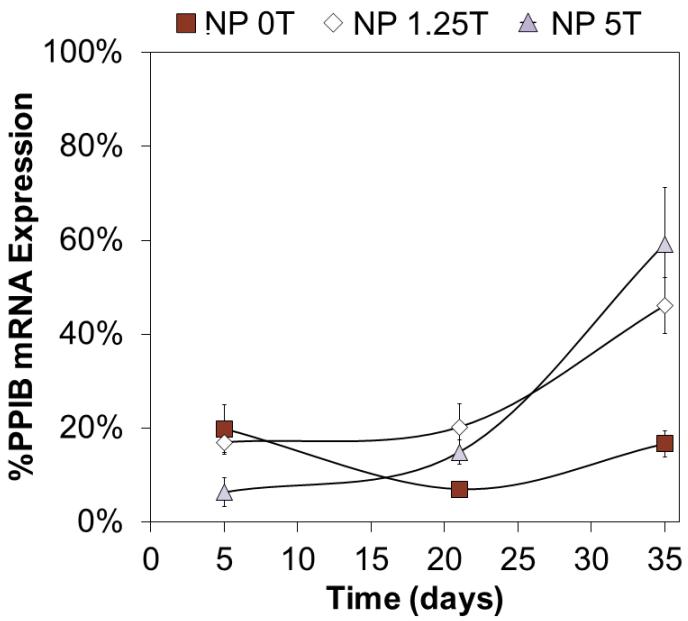

Figure A8: PCR for PPIB expression in the HDIt scaffolds using the same method described for the LTI data shown in Figure 3C. The temporal gene silencing profile was similar to that seen with the LTI based scaffolds.

B.7. Infiltration of PUR scaffolds. Effect of formulation

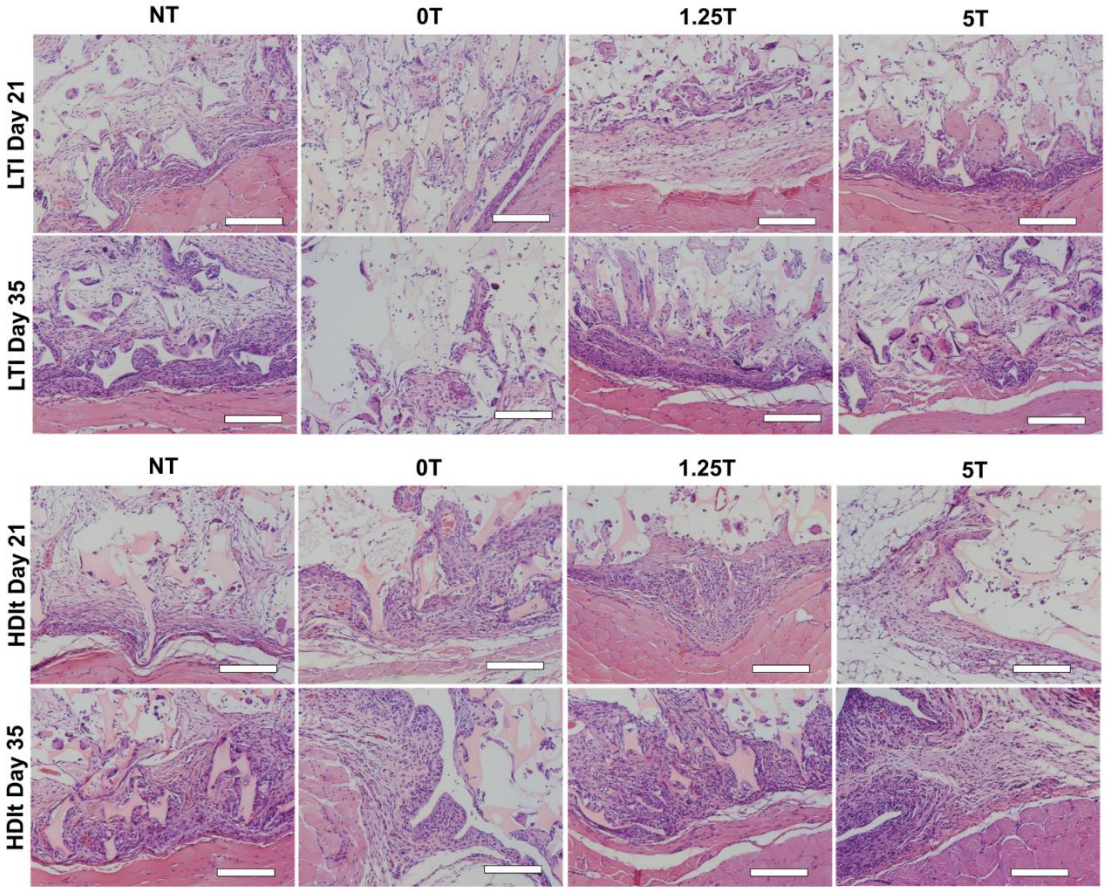

Figure A9: Microscopic view of Hematoxylin and eosin (H&E) stained sections shows the morphology and the degree of infiltration at day 21 and day 35 in LTI and HDIt based scaffolds demonstrating similar levels of cellular infiltration. Scale bar = 200 um. (n=1)

B.8. PCR for TNFα and STAT-1 markers of inflammation and TLR activation

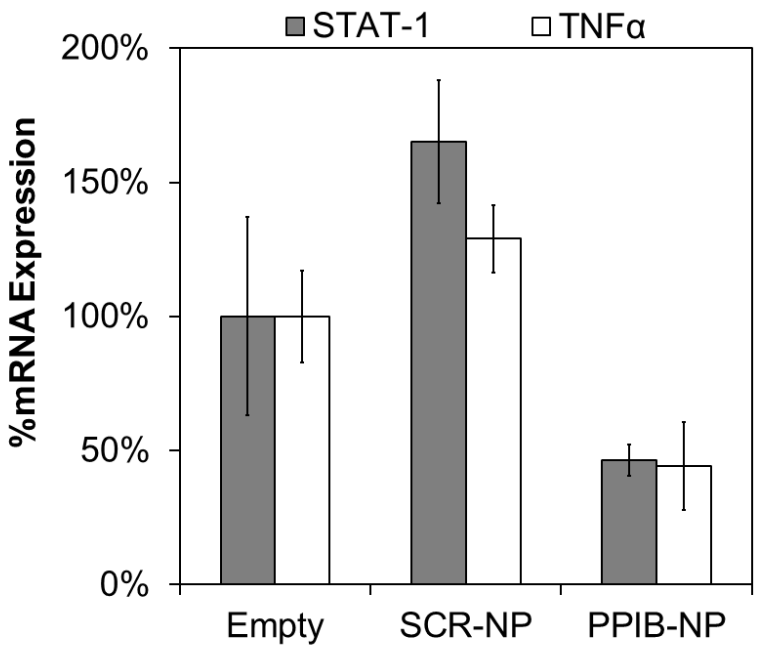

Figure A10: PCR for STAT-1 and TNFα normalized to GAPDH expression indicates that the delivery platform does not activate nonspecific inflammation or TLRs. A statistically insignificant increase in the scaffolds loaded with si-NPs containing scrambled siRNA may indicate a small non-specific inflammatory response to either the scrambled siRNA or the polymer, but is not indicative of the orders of magnitude increase in STAT-1 produced by TLR activation [13]. In the scaffolds containing si-NPs loaded with PPIB siRNA (PPIB-NP), there was a significant decrease in both STAT-1 and TNFα, suggesting anti-inflammatory activity was produced by silencing the model gene PPIB. This aligns with the known functions of PPIB as a pro-inflammatory secretory product of macrophages [14] that is increased in response to inflammatory stimuli [15] and that plays a role in adhesion of T-lymphocytes [16]. It has also been previously identified that inhibition of CD147 and PPIB interactions is a viable therapeutic strategy for reduction in inflammation [17]. Although it is outside the scope of the current report, this result indicates that potent PPIB silencing has the potential to be used as an anti-inflammatory therapy.

B.9. Supplemental methods

NP characterization

The diblock copolymer used in this study is from the same synthesis previously reported [10]. The polymers were characterized by gel permeation chromatography (GPC, Shimadzu Corp., Kyoto, Japan) in DMF with 0.1 M LiBr using an inline Wyatt miniDAWN TREOS light scattering detector (Wyatt Technology Corp., Santa Barabara, CA) and H^1 NMR (Bruker 400 MHz Spectrometer equipped with a 9.4 T Oxford magnet) for molecular weight and composition. Transmission Electron Microscopy (TEM, Philips CM20 Transmission Electron Microscope, EO, Netherlands) was used to evaluate micelle diameter and morphology. A gel retardation assay was used to select the charge ratio (NH_3+/PO_4-), and 4:1 was used for all experiments. Flow cytometry was performed on NIH3T3 fibroblasts treated with a concentration of 50nM FAM labeled dsDNA (**Supplemental Table 1**) and measured with a BD FACSCalibur flow cytometer (San Jose, CA). The data was analyzed using FlowJo software (version 7.6.4 Ashland, OR). A pH-dependent hemolysis assay was performed using a standardized protocol [18] to characterize pH-dependent membrane disruption of the polymer at concentrations of 40 µg/mL, 5µg/mL, and 1µg/mL in buffers of pHs 7.4, 6.8, 6.2, and 5.8. The percent hemolysis was calculated using data collected using a plate reader (Infinite F500, Tecan Group Ltd., Mannedorf, Switzerland) to measure absorbance at 541 nm. Cellular toxicity was analyzed at a concentration of 50nM siRNA with varying charge ratios up to N:P of 8:1 using an LDH cytotoxicity kit (Roche, Basal, Switzerland).

Western blot

Frozen samples were extracted with UDC buffer (8 M urea, 10 mM dithiothreitol (DTT), 4% CHAPS containing Phosphatase I and II protease inhibitor cocktail (Sigma, St. Louis, MO)) by vortexing at room temperature overnight and centrifugation at 14,000 rpm for 15 min at 4°C. Soluble protein concentrations were determined using the Bradford assay (Pierce Chemical, Rockfort, IL). Equal amounts (30 µg) of proteins were added to Laemmli sample buffer (Bio-Rad

laboratories, Inc. Hercules, CA), heated for 5 min at 100°C, and separated on 12% SDS polyacrylamide gels. Proteins from the gels were transferred onto nitrocellulose membranes (Li-COR Biosciences, Lincoln, NE) and blocked with blocking buffer for 1 hour at room temperature(Li-COR Biosciences, Lincoln, NE) prior to incubation overnight at 4°C with antisera against PPIB (1:2000,Sigma) and ß-actin (1:250,Santa Cruz Biotechnology). Membranes were washed three times with TBS containing Tween 20 (0.1%) (TBST) and incubated with 680 nm and 800 nm infrared-labeled secondary antibodies (Li-Cor, Lincoln, NE) for 1h at room temperature. The membranes were subsequently washed with TBST, and protein-antibody complexes were visualized and quantified using the Odyssey direct infrared fluorescence imaging system (Li-Cor Biosciences NE).

Cardiac Perfusion and microCT

Mice were sacrificed by CO_2 inhalation and perfused with normal PBS containing 4 mg/mL papaverine hydrochloride (Sigma) and 100 U/mL Heparin followed by 10% neutral buffered formalin, followed by PBS with papaverine hydrodhloride and Heparin. Next, 30 mL of the lead chromate based contrast agent Microfil® (Flowtec) was injected into the left ventricle and allowed to cure overnight at 4°C. Implants were retrieved and scanned using a microCT (uCT 50, Scanco Medical AG, Brüttisellen Switzerland) for vessel morphology, vascular volume and vascular thickness. Regions of Interest were selected by each slice selecting area inside the scaffold.

Appendix C - Supplementary Information for Chapter 5

Supplemental Information

Balancing Cationic and Hydrophobic Content of PEGylated siRNA Polyplexes Enhances Endosome Escape, Stability, Blood Circulation Time, and Bioactivity In Vivo

Christopher E. Nelson[#], James R. Kintzing[#], Ann Hanna, Joshua M. Shannon, Mukesh K. Gupta, Craig L. Duvall[*]

Contents of Supplemental Methods

C.1 Supplemental Methods

Luciferase Cell Line Derivation

Mouse Embryonic Fibroblasts (NIH3T3, ATC) or Human epithelial breast cancer cells (MDA-MB-231, ATCC) were plated into a 24 well plate and transfected with Lentiviral Expression particles for firefly luciferase, Red Fluorescent Protein (RFP), Blasticidin resistance, and a Bsd promoter (GenTarget Inc, San Diego, CA) at a multiplicity of infection (MOI) of 10. The cells were then incubated for 72 h, changing the media every 24 h, and monitored for RFP with fluorescent microscopy. Cells were trypsinized and transferred into 75 cm^2 flasks and treated with blasticidin (10 ug/mL, based on predetermined kill curves).The luciferase signal and the cell number are linearly related in the range tested such that the cell line may be used to determine cell number longitudinally. See Supplemental Information from [19].

C.2 siRNA Sequences

siRNAs were purchased from integrated DNA technologies (IDT, Coralivlle, IA, USA). 27-mer antisense strand and 25-mer sense strand were used due to the increase potency relative to 21-mer siRNAs[1]. Also, 2'-O-methyl (2-OMe) -modified nucleotides were used to improve stability, increase nuclease resistance, and eliminate toll-like receptor activation, with negligible effects on the level of gene silencing [2-4].

Table A4 – siRNA sequences

Name	Sequence	Reference
Scrambled	S: 5' – CGUUAAUCGCGUAUAAUACGCGUAT – 3' AS: 5' – AUACGCGUAUUAUACGCGAUUAACGAC – 3'	IDT
PPIB	S: 5'-GCAUGGAUGUGGUACGGAAGGUGGA – 3' AS: 5'- UCCACCUUCCGUACCACAUCCAUGCCC – 3'	[20]
dsDNA	S: 5'-Fl-GTCAGAAATAGAAACTGGTCATC-3' AS: 5'-GATGACCAGTTTCTATTTCTGAC-3' Where Fl = FAM, cy5, IRDye800, or Alexa488	[5]
Luciferase	Proprietary by Supplier	Ambion

C.3 PEG-ECT Conjugation

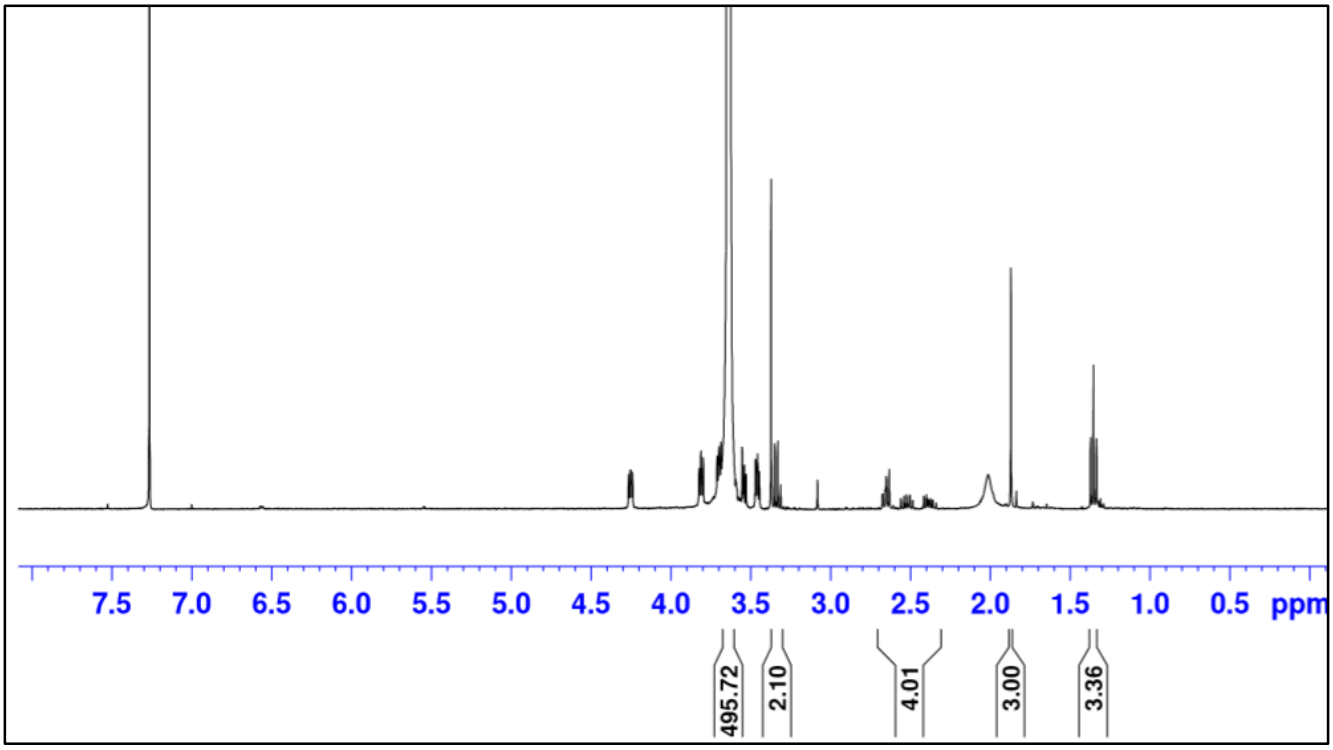

Figure A11 - Integration of the *δ* 1.88 s (CCNC**H**$_3$) ECT peak and the *δ* 3.65s (-OC**H**$_2$C**H**$_2$-) PEG peak reveals the %conjugation as shown in **Eqn. 1**. This batch of PEG-ECT was used in all of the polymerizations.

$$Equation\ A.3 \qquad \%conjugation = \frac{\int 1.88s}{3proton} \Big/ \frac{\int (3.65s)}{4proton \cdot 113repeats} = 91.2\%$$

C.4 NMR of polymer panel

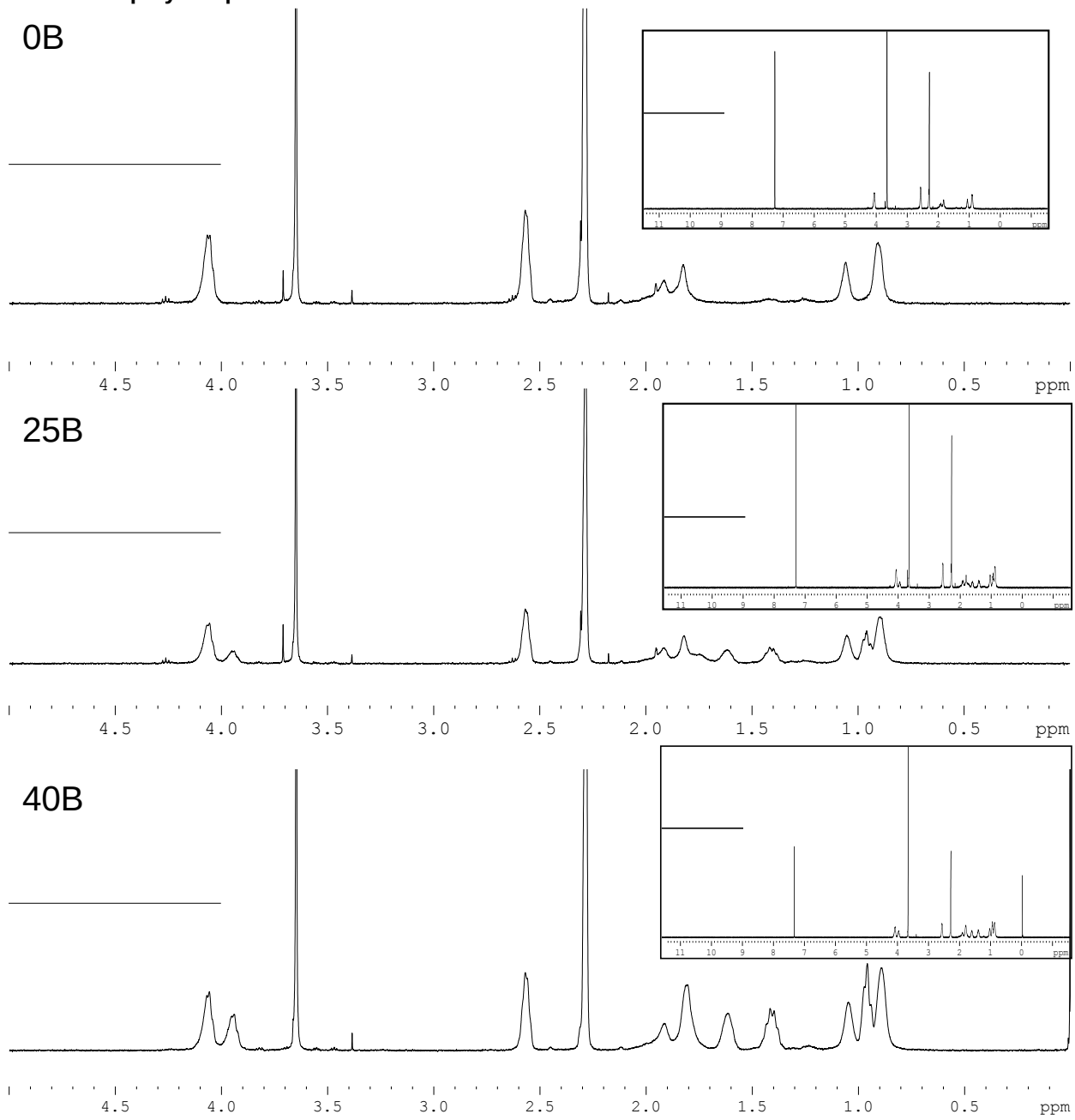

Figure A12 – NMR of polymer panel – *continued on next page*

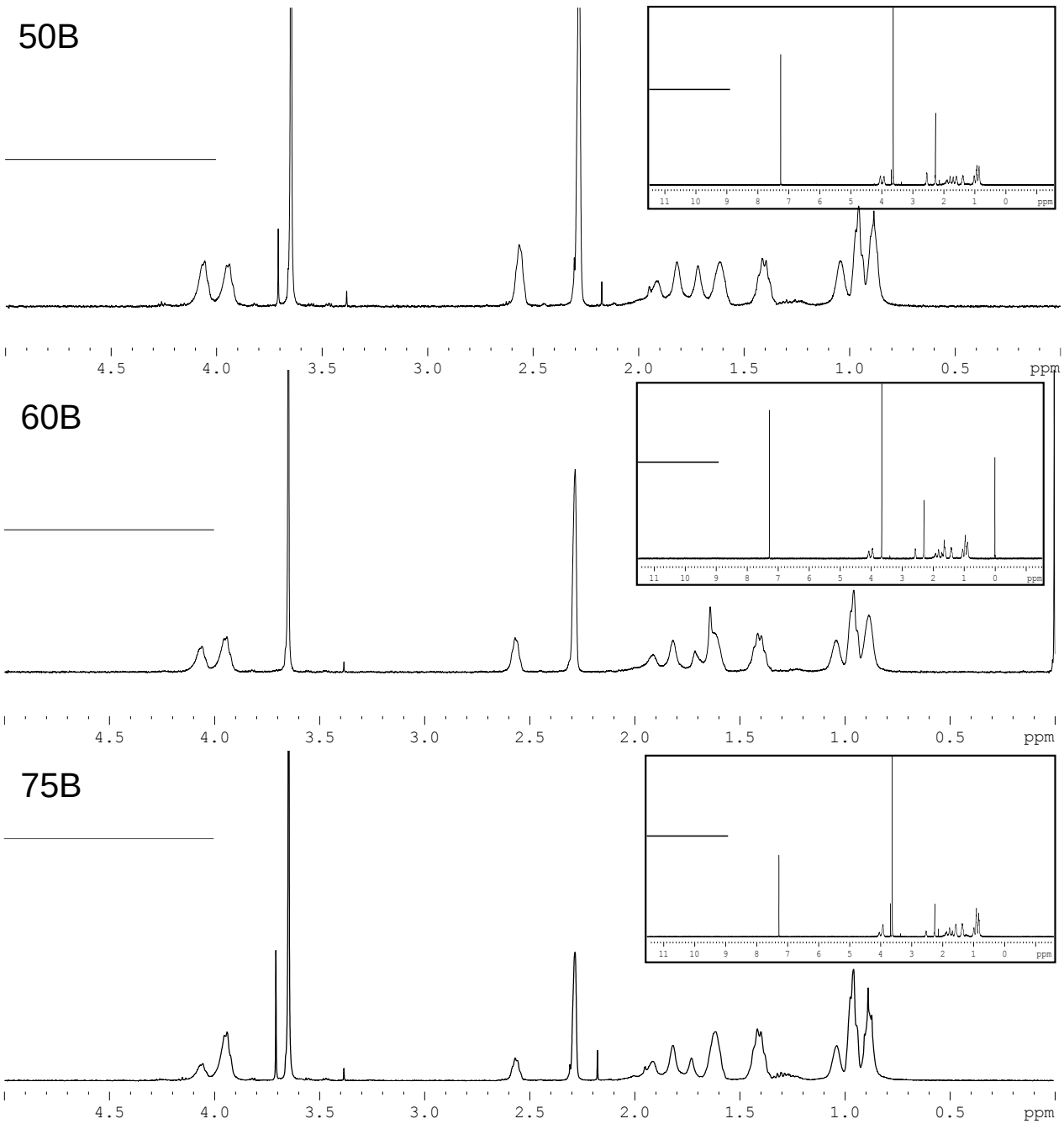

Figure A12 – NMR of polymer panel. Polymers were analyzed by ^{1}H NMR (400 MHz, $CDCl_3$) which were used to quantify molecular weight by integrating the δ 3.65s (-OC**H₂**C**H₂**-) PEG peak and comparing to the δ 2.58s (-CH_2N**H₂**) of the DMAEMA, the δ 4.05s(-O-C**H₂**CH_2-) of the DMAEMA and the δ 3.95s(-O-C**H₂**CH_2-) of the BMA. This method could also be used to quantify %composition by comparing the molar content of DMAEMA monomers and BMA monomers. The results are listed in **Table 1** in the manuscript.

C.5 GPC of Polymer Panel

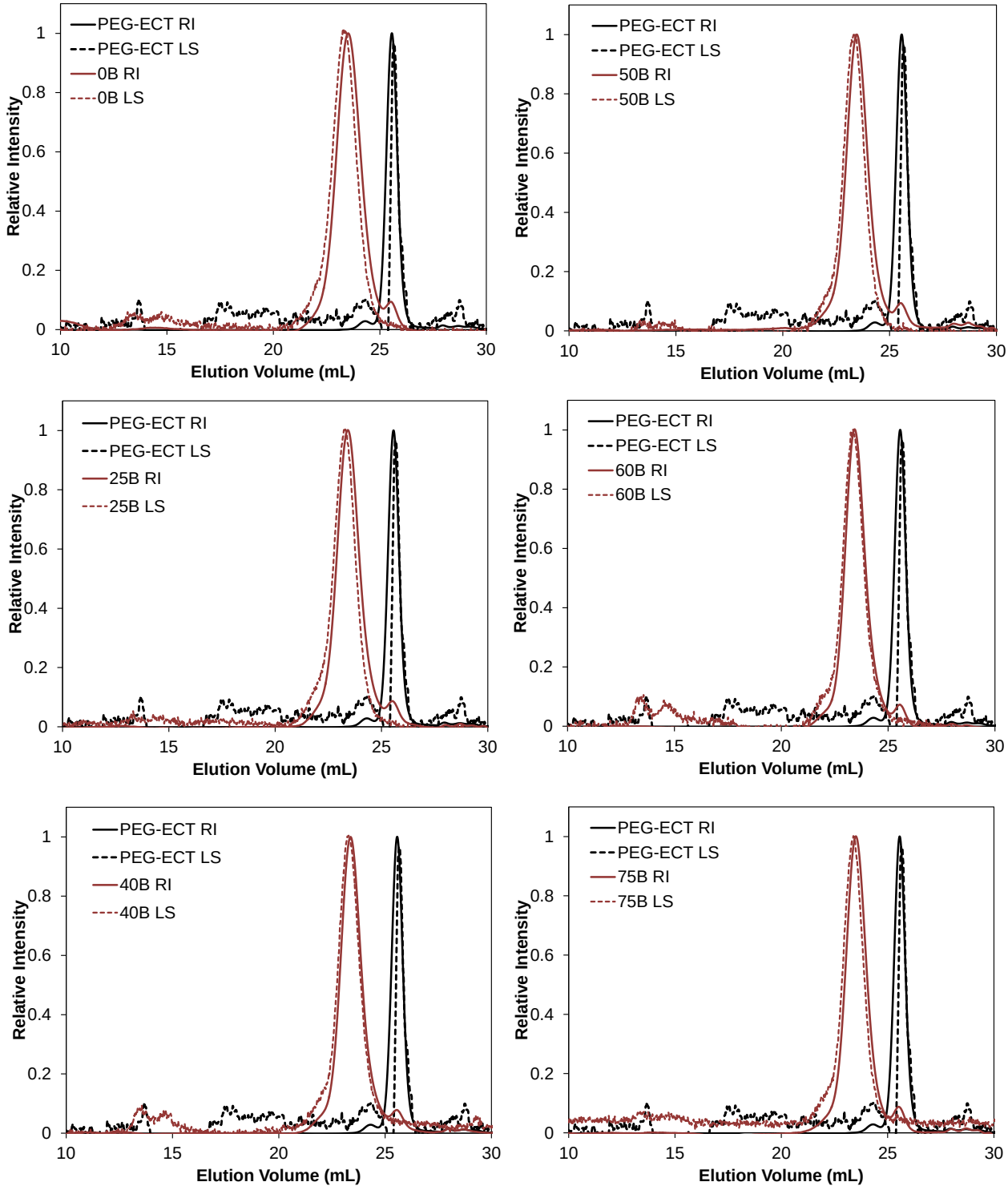

Figure A13 – Molecular weight and polydispersity obtained by GPC – GPC using DMF with 0.1M LiBr as the mobile phase was used to analyze the molecular weight and polydispersity of the synthesized polymers. Molecular weights were quantified with an inline light scattering (dotted lines) and refractive index (solid lines) detectors using calculated dn/dc values determined offline. All results are listed in **Table 1** in the manuscript.

C.6 Extended DLS and Zeta Potential Characterization

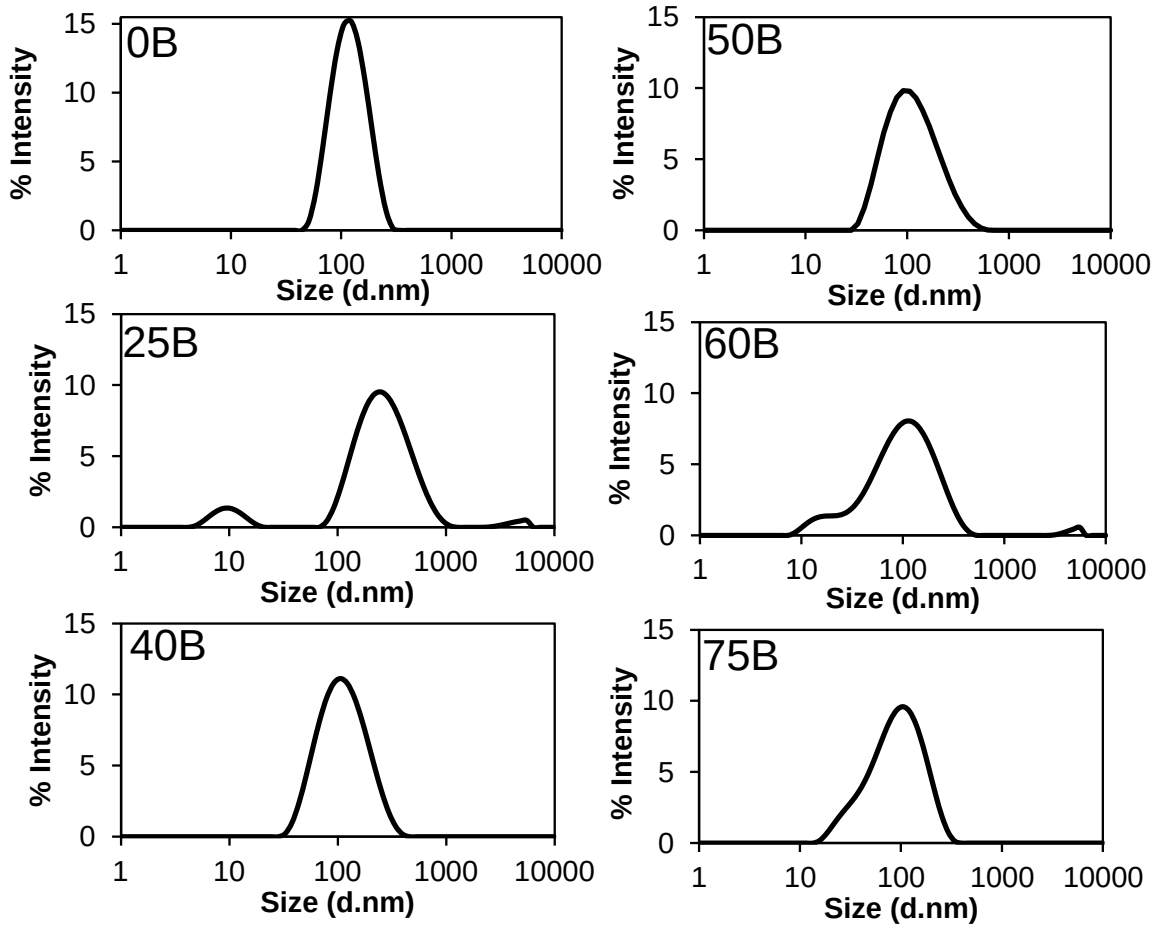

Figure A14 – DLS for each polymer-siRNA polyplex at a charge ratio of 10:1. Polyplexes are relatively monodispersed and centered around ~100 nm. Zeta potential measurements for 40B and 50B were -1.05 ±6.1 mV and -0.9 ±6.6 mV respectively.

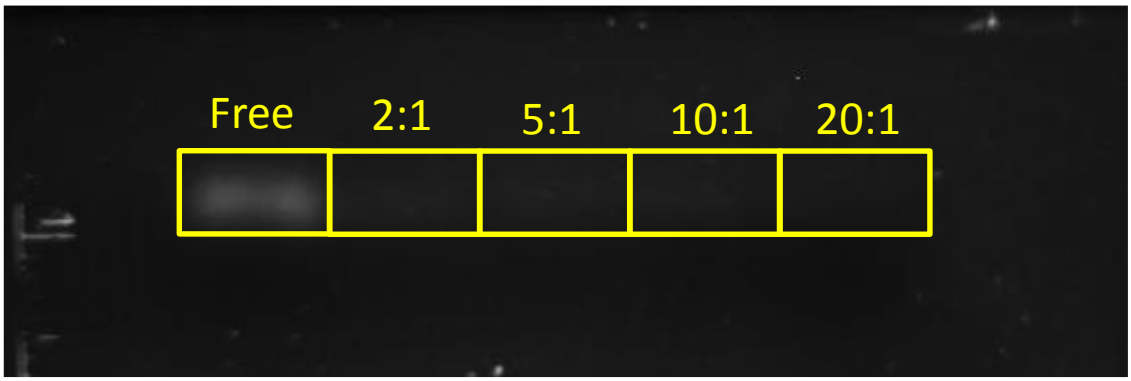

Figure A15 – Formulation of polyplexes at pH 4.0 improved siRNA encapsulation as shown in the gel for 50B. When quantified 82%, 88%, 93% and 97% are complexed by 2:1, 5:1, 10:1, and 20: 1 respectively.

C.7 pH Dependence of Polymers and Polyplexes

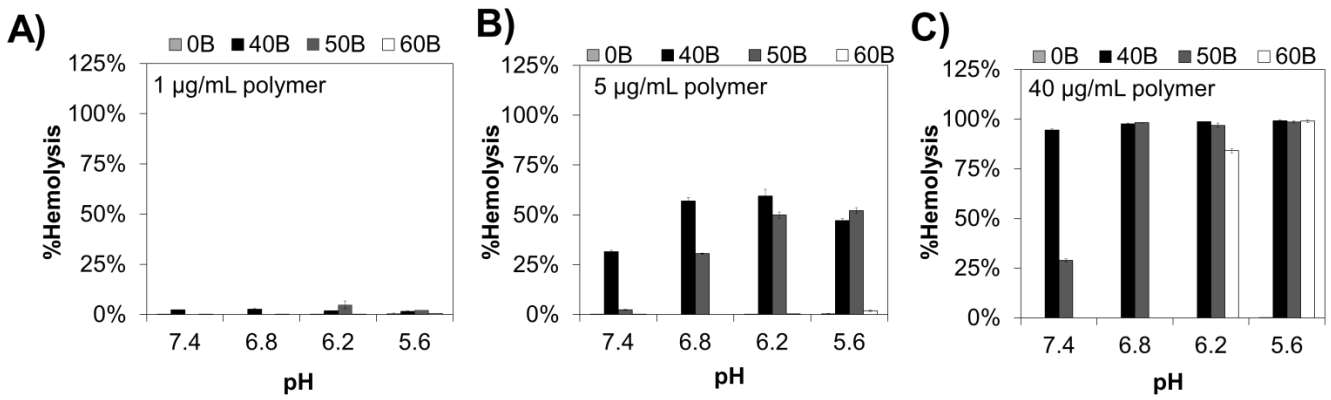

Figure A16 –RBCs incubated with polymer alone show a similar level of lysis as the data reported in the manuscript. This provides strong evidence that at the charge ratio used (NH_3/PO_4 = 10/1) the addition of siRNA does not significantly alter the pH dependent lysis.

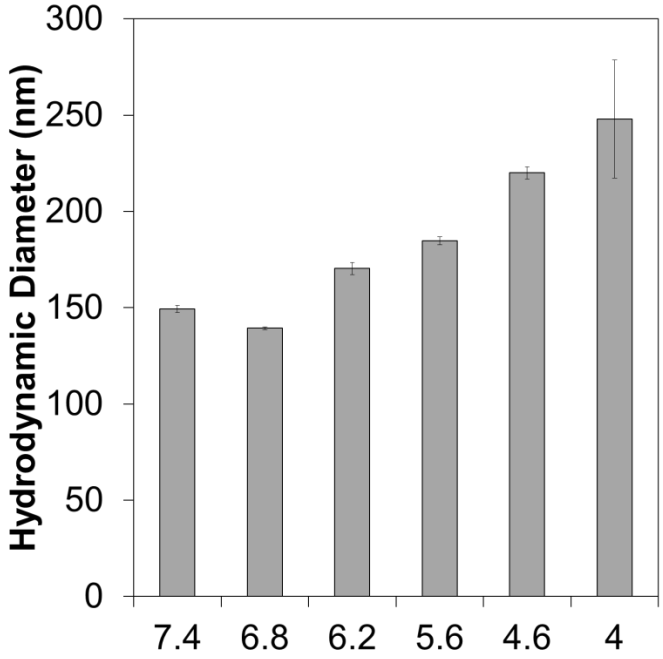

Figure A17 –pH dependent DLS of 50B polyplexes (NH_3/PO_4 = 10/1) indicates a pH responsive destabilization and which indicates a stability loss similar to that reported in Figure 2.

C.8 Comprehensive in vitro data

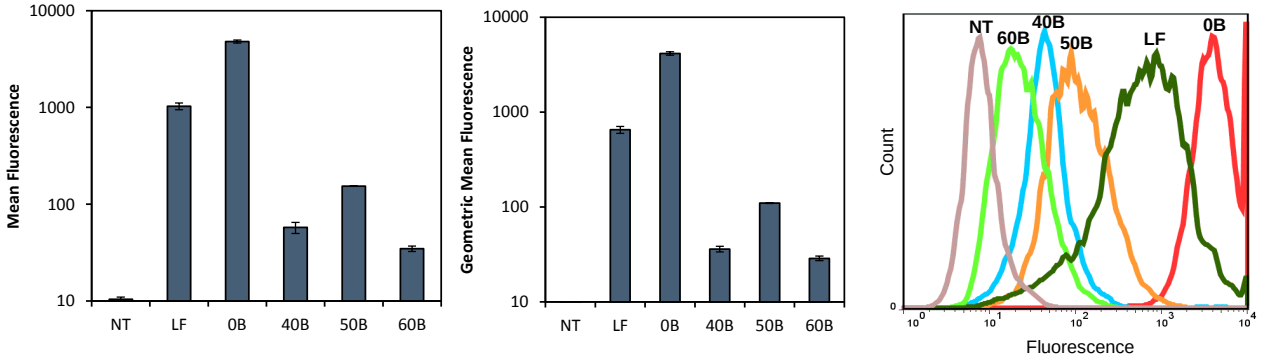

Figure A18 – Flow cytometry demonstrates a strong dependence of the polymer chemistry on cellular uptake. As demonstrated above, 0B had the highest fluorescence of any of the polymer formulations. 50B delivered more than 40B or 60B. (n=3)

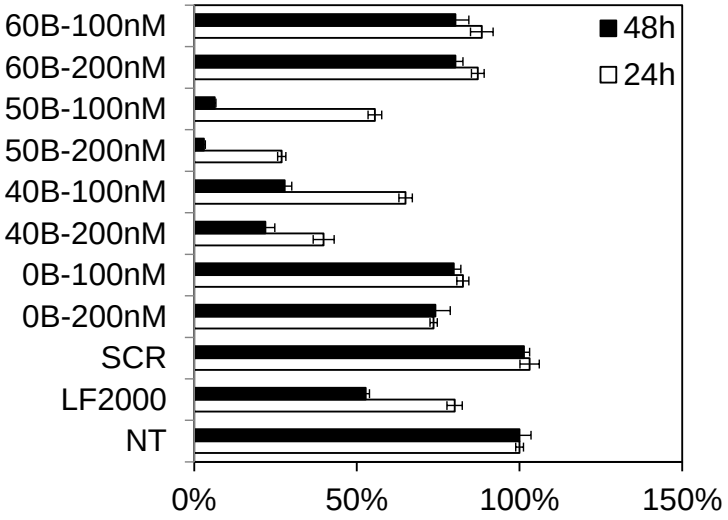

Figure A19 – Luciferase protein level silencing - L231 cells treated with polyplexes show varying levels of gene silencing with 50B being the highest. Additional data presented here indicate a dose dependent decrease in luciferase readings.

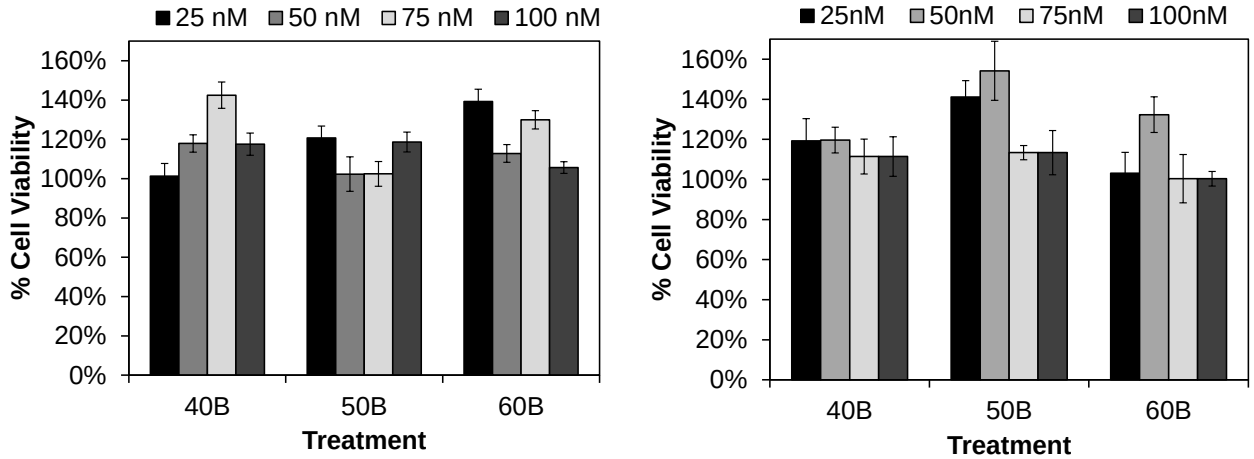

Figure A20 –The full panel of cytotoxicity measurements on LR3T3 cells indicate low levels of toxicity at all measured doses in the polymers 40B, 50B, and 60B at 24h (left panel) and 48h (right panel)

C.9 Micelle Stability

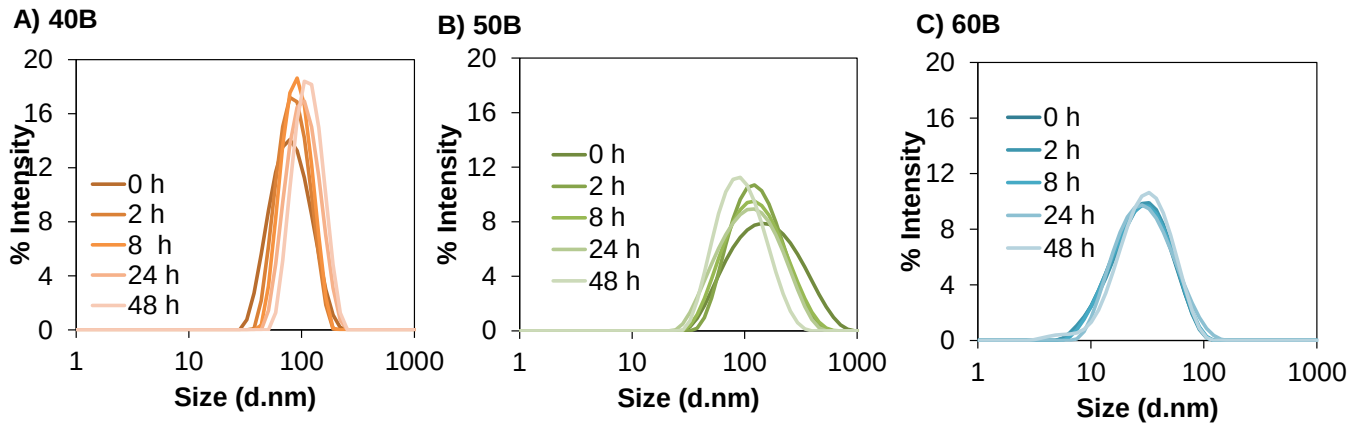

Figure A21 – Polyplexes were evaluated for stability by incubating in PBS and measuring the size over 48h. As Fig. S7 demonstrates, polyplexes were stable in PBS maintain a similar size and PDI over the time course measured. In addition, FRET was measured at 48h revealing 88% retention of the FRET signal suggesting polyplexes retained the siRNA cargo in the core of the micelle over 48h.

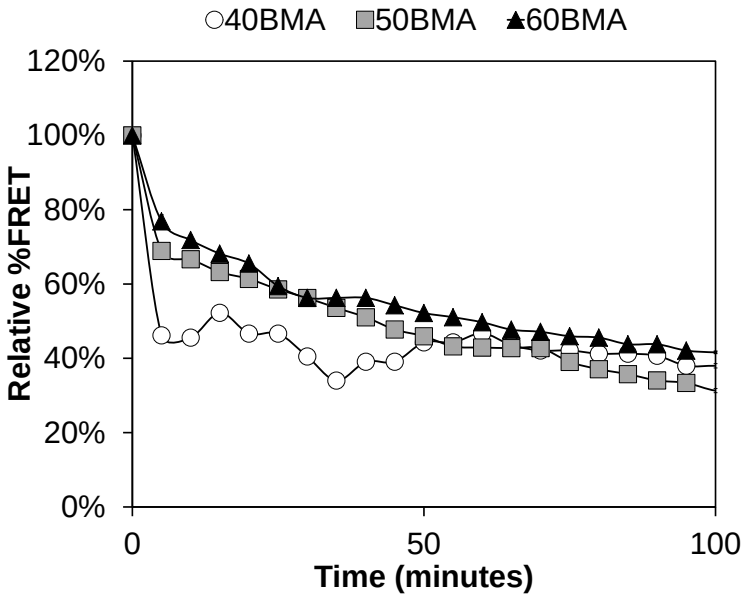

Figure A22 – Hydrophobic stabilized micelles are still susceptible to high concentrations of Heparin - When treated at 10U heparin / mL, polyplexes formulated from 40B, 50B, and 60B were no longer stable over the 100 min time course as demonstrated by the decrease in FRET. Also note that during this experiment, 0B and 25B were instantly destabilized to ~0% remaining FRET.

C.10. Full Biodistribution Panel

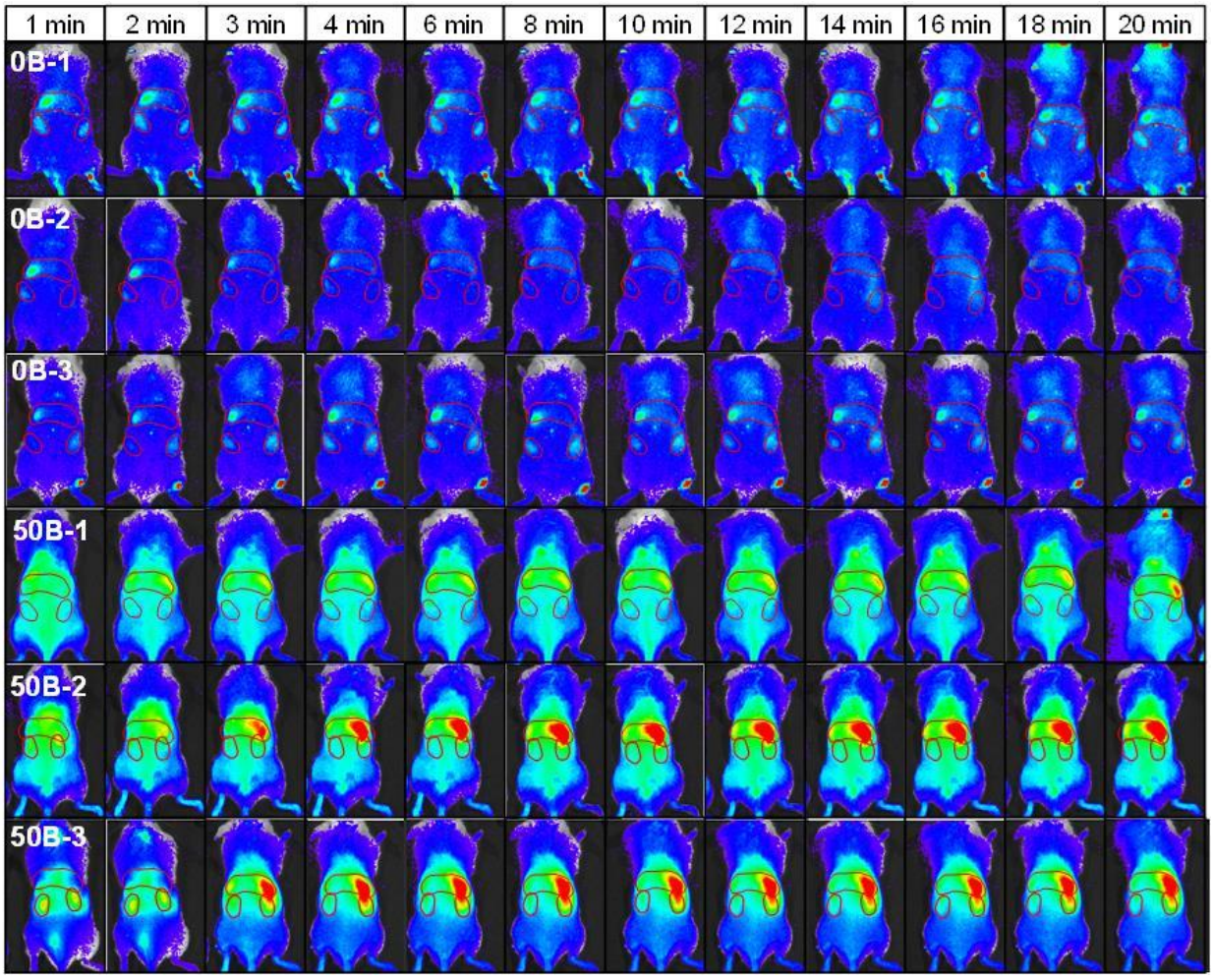

Figure A23 – Intravital imaging of intravenous administered polyplexes reveal renal clearance and pronounced liver uptake in mice. 0B mice showed a lower level of biodistribution to the tissue which suggests rapid renal clearance. 0B mice also had a high level of %biodistribution in the kidney. 50B polyplexes showed better biodistribution throughout the body with highest localization to the liver after ~3min.

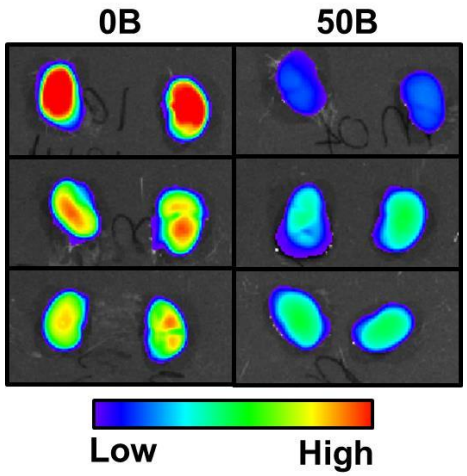

Figure A24 – An acute (5 minute) terminal study demonstrated rapid renal filtration of siRNA delivered via 0B polyplexes relative to 50B polyplexes

C.11 Liver Compatibility of Polyplexes

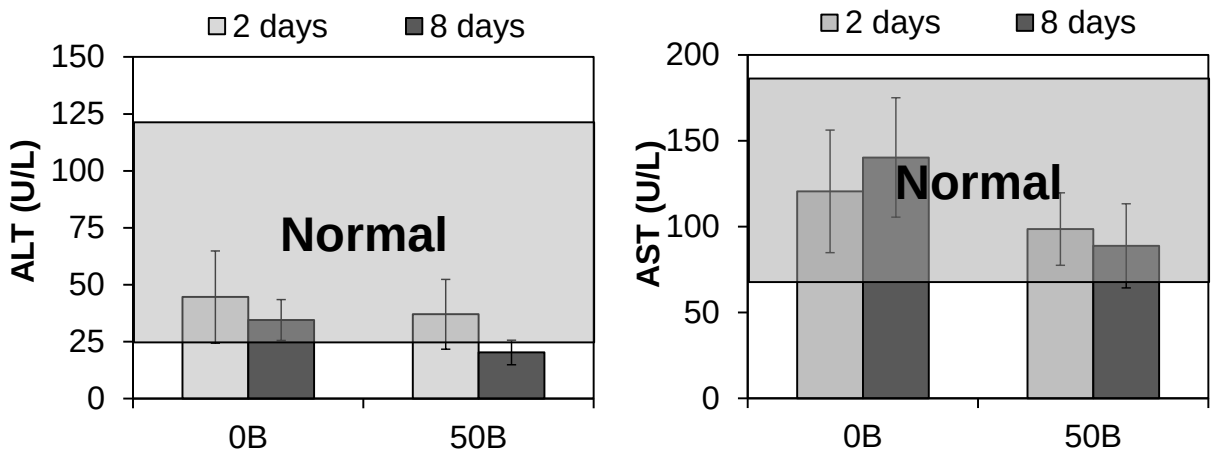

Figure A25 – Alanine aminotransferase (ALT) and aspartate aminotransferase (AST) measurements indicated that levels were normal at both 2 days and 8 days post treatment with intravenously injected 0B and 50B polyplexes. This is a good indication that polyplexes were well tolerated by the liver where the majority of the injected dose distributes.

Appendix D - Supplementary Information for Chapter 6

Contents of Supplemental Methods

D.1 NP Inflammatory Profile

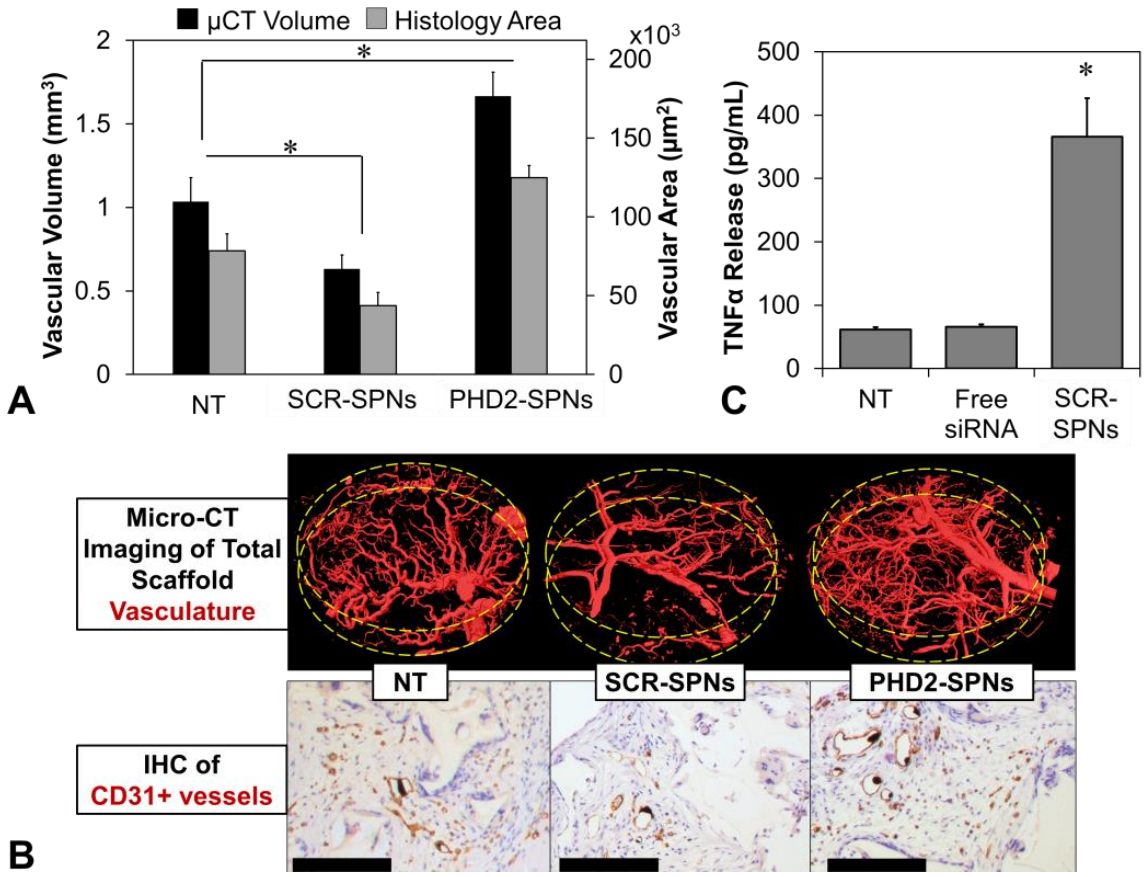

Figure A26 – PHD2 knockdown generates significant pro-angiogenic response, however, SPNs create a pro-inflammatory response that may inhibit angiogenesis. A) Quantification of vessel density by histology and μCT revealed a significant decrease in the PUR loaded with SCR-SPNs but an increase in vessel density in the PHD2-SPN group. B) Representative μCT and CD31 IHC. C) Primary mouse bone marrow derived macrophages increase TNFα production when exposed to SPNs.

D.2. Pro-Angiogenic Effects of PHD2 Silencing in Diabetic Rat Excisional Wounds

Methods

To investigate the PHD2 siRNA platform for improved wound healing, an excisional wound healing model that has been used extensively was adapted. Male 350-375g Sprague-Dawley rats were obtained and fasted overnight. Streptozotocin (STZ) was injected at 50mg/kg and hyperglycemia was monitored for 10 days (>300mg/dL). The wound site was shaved and full thickness excisional wounds were made in the dorsal skin. PUR with either no NPs (Empty), scrambled si-NPs (SCR), or PHD2 si-NPs (PHD2) were implanted in the wound bed and covered with NU-gel and Tegaderm. Ketoprofen was administered daily for 4 days. The rats were kept for 7 and 14 days then sacrificed by CO_2 inhalation and tissue was extracted and analyzed for gene expression changes by qRT-PCR and for vessel density by H&E. The same treatments were also examined using PTK-UR chemistry which has been shown to improve tissue regeneration by better matching the degradation rate with the cell infiltration rate [21].

Results and Discussion

We recently showed that PTK-UR scaffolds more effectively stented subcutaneous pockets in rats than PEUR materials [21]. This stenting behavior of PTK-URs was noted in the more mechanically challenging excisional rat wound model. This stenting effects retains the open scaffold pore morphology and enhances the quantity and quality of granulation tissue formation within the wound site (**Fig. A.27 A,C**). Using H&E sections, this effect was quantified, and PTK-UR scaffolds were both thicker and had a higher relative percentage of scaffold interior filled with granulation tissue relative to PEUR materials (**Fig. A.27 B,C**).

At day 14, wound areas were evaluated for vascular density and it was found that loading of PEUR and PTK scaffolds with PHD2 si-NPs increased vascular density relative to their respective SCR controls by 1.6 fold and 1.8 fold respectively (**Fig. A.28**).

At these later time points (day 7 and day 14), there was no detectable level of gene silencing or increase in HIF-1α regulated genes (not shown). Due to the increased rate of scaffold infiltration and healing in the rat model compared to the mouse model, the silencing effect may disappear more rapidly. Future work will investigate an earlier time point and investigate tissue sections by immunohistochemistry for improvements in wound healing.

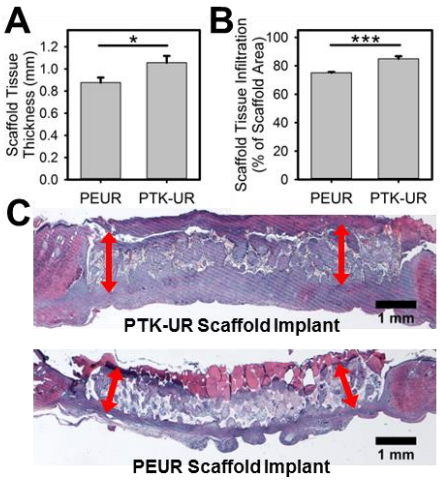

Figure A27 – PTK-UR more effectively stent the wound area and promote tissue infiltration at day 7. A) Wound size is reported showing that PTK-UR more effectively stent the wound area (*p<0.05). B) PTK-UR more effectively promote tissue ingrowth than the PEUR (***p<0.005)

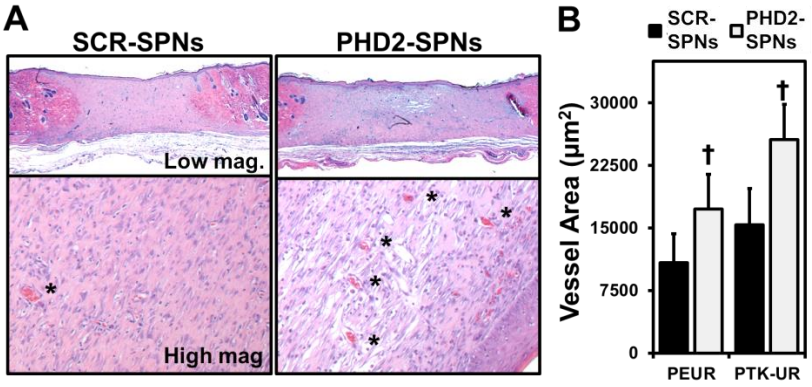

Figure A28 – PHD2 knockdown in diabetic rat excisional wounds generates a significant increase in blood vessel area in polyester urethanes and polythioketal based polyurethanes at day 14. A) Representative macro and micro histology shows the excisional wound by H&E. B) Quantified histology slides reveal a significant increase in blood vessel area by treatment with PHD2 siRNA compared to scrambled siRNA.(p<0.05)

D.3. Broader Impact: Cost Analysis and Clinical Viability

One of the biggest hindrance to siRNA therapy is the cost of RNA synthesis. Currently, 1 µmol of DsiRNA cost $981 from IDT (idtdna.com) which is roughly $1 per nmol. We are currently using around 500pmol per animal or about 0.50c per implant. If this technology were adapted for human use, the volume of the implant and thus the dose would increase. The average chronic wound volume is about 35 cm^3 [22] which would require ~$115 worth of DsiRNA. Currently, a dosing regimen of Regranex® costs $586 [23] making this technology competitive with the price. The cost of DsiRNA of the same sequence will also decrease in bulk quantities, and the dose may be reduce by ½ or ¼ for therapy reducing the price more. Overall, this technology should be price competitive with competing biologic delivery technologies. With the increase in medical costs, technologies should strive to decrease prices of medical care. Technologies like these should decrease costly amputations and the subsequent human cost of a long-term disability by reducing the number of amputations and improving the quality of life for diabetic patients.

Appendix E - Supplemental References

[1] Kim DH, Behlke MA, Rose SD, Chang MS, Choi S, Rossi JJ. Synthetic dsRNA Dicer substrates enhance RNAi potency and efficacy. Nat Biotechnol. 2005;23:222-6.
[2] Behlke MA. Chemical modification of siRNAs for in vivo use. Oligonucleotides. 2008;18:305-19.
[3] Judge A, MacLachlan I. Overcoming the innate immune response to small interfering RNA. Hum Gene Ther. 2008;19:111-24.
[4] Judge AD, Bola G, Lee AC, MacLachlan I. Design of noninflammatory synthetic siRNA mediating potent gene silencing in vivo. Mol Ther. 2006;13:494-505.
[5] Truong NP, Jia Z, Burgess M, Payne L, McMillan NA, Monteiro MJ. Self-catalyzed degradable cationic polymer for release of DNA. Biomacromolecules. 2011;12:3540-8.
[6] de Wet JR, Wood KV, DeLuca M, Helinski DR, Subramani S. Firefly luciferase gene: structure and expression in mammalian cells. Molecular and cellular biology. 1987;7:725-37.
[7] Elbashir SM, Harborth J, Lendeckel W, Yalcin A, Weber K, Tuschl T. Duplexes of 21-nucleotide RNAs mediate RNA interference in cultured mammalian cells. Nature. 2001;411:494-8.
[8] Convertine A, Benoit D, Duvall C, Hoffman A, Stayton P. Development of a novel endosomolytic diblock copolymer for siRNA delivery. Journal of Controlled Release. 2009;133:221-9.
[9] Convertine AJ, Diab C, Prieve M, Paschal A, Hoffman AS, Johnson PH, et al. pH-Responsive Polymeric Micelle Carriers for siRNA Drugs. Biomacromolecules. 2010.
[10] Nelson CE, Gupta MK, Adolph EJ, Shannon JM, Guelcher SA, Duvall CL. Sustained local delivery of siRNA from an injectable scaffold. Biomaterials. 2012;33:1154-61.
[11] Li B, Brown KV, Wenke JC, Guelcher SA. Sustained release of vancomycin from polyurethane scaffolds inhibits infection of bone wounds in a rat femoral segmental defect model. Journal of Controlled Release. 2010;145:221-30.
[12] Papadopoulou V, Kosmidis K, Vlachou M, Macheras P. On the use of the Weibull function for the discernment of drug release mechanisms. International Journal of Pharmaceutics. 2006;309:44-50.
[13] Sledz CA, Holko M, de Veer MJ, Silverman RH, Williams BRG. Activation of the interferon system by short-interfering RNAs. Nat Cell Biol. 2003;5:834-9.
[14] Sherry B, Yarlett N, Strupp A, Cerami A. Identification of Cyclophilin as a Proinflammatory Secretory Product of Lipopolysaccharide-Activated Macrophages. P Natl Acad Sci USA. 1992;89:3511-5.
[15] Melchior A, Denys A, Deligny A, Mazurier J, Allain F. Cyclophilin B induces integrin-mediated cell adhesion by a mechanism involving CD98-dependent activation of protein kinase C-delta and p44/42 mitogen-activated protein kinases. Exp Cell Res. 2008;314:616-28.
[16] Allain F, Vanpouille C, Carpentier M, Slomianny M-C, Durieux S, Spik G. Interaction with glycosaminoglycans is required for cyclophilin B to trigger integrin-mediated adhesion of peripheral blood T lymphocytes to extracellular matrix. Proceedings of the National Academy of Sciences. 2002;99:2714-9.
[17] Yurchenko V, Constant S, Eisenmesser E, Bukrinsky M. Cyclophilin-CD147 interactions: a new target for anti-inflammatory therapeutics. Clinical and experimental immunology. 2010;160:305-17.
[18] Evans BC, Nelson CE, Yu SS, Beavers KR, J. KA, Li H, et al. Ex Vivo Red Blood Cell Hemolysis Assay for the Evaluation Of PH-responsive Endosomolytic Agents for Cytosolic Delivery of Biomacromolecular Drugs. J Vis Exp. 2012:e50166, doi:10.3791/.
[19] Joshi RV, Nelson CE, Poole KM, Skala MC, Duvall CL. Dual pH- and temperature-responsive microparticles for protein delivery to ischemic tissues. Acta Biomaterialia. 2013;9:6526-34.
[20] Nelson CE, Kim AJ, Yu F, Hannah A, Adolph EJ, Gupta MK, et al. In preperation. 2012.
[21] Martin JR, Gupta MK, Page JM, Yu F, Davidson JM, Guelcher SA, et al. A porous tissue engineering scaffold selectively degraded by cell-generated reactive oxygen species. Biomaterials. 2014.

[22] Frykberg RG, Driver VR, Carman D, Lucero B, Borris-Hale C, Fylling CP, et al. Chronic Wounds Treated With a Physiologically Relevant Concentration of Platelet-rich Plasma Gel: A Prospective Case Series. Ostomy Wound Manag. 2010;56:36-+.
[23] Jarvis CI. Becaplermin (Regranex) for diabetic foot ulcers. Am Fam Physician. 2008;78:255-6.